DYNAMIC BEHAVIOR OF BIOLOGICAL MEMBRANES

by

Ross Magi

A dissertation submitted to the faculty of
The University of Utah
in partial fulfillment of the requirements for the degree of

Doctor of Philosophy

Department of Mathematics

The University of Utah

December 2014

ProQuest LLC.
789 East Eisenhower Parkway
P.O. Box 1346
Ann Arbor, MI 48106 - 1346

The University of Utah Graduate School

STATEMENT OF DISSERTATION APPROVAL

The dissertation of **Ross Magi**

has been approved by the following supervisory committee members:

James Keener	, Chair	**July 14, 2014** Date Approved
Aaron Fogelson	, Member	**July 14, 2014** Date Approved
Christel Hohenegger	, Member	**July 14, 2014** Date Approved
Markus Babst	, Member	**July 14, 2014** Date Approved
Paul Bressloff	, Member	Date Approved

and by **Peter Trapa**, Chair/Dean of

the Department/College/School of **Mathematics**

and by David B. Kieda, Dean of The Graduate School.

ABSTRACT

Biological membranes are important structural units in the cell. Composed of a lipid bilayer with embedded proteins, most exploration of membranes has focused on the proteins. While proteins play a vital role in membrane function, the lipids themselves can behave in dynamic ways which affect membrane structure and function. Furthermore, the dynamic behavior of the lipids can affect and be affected by membrane geometry. A novel fluid membrane model is developed in which two different types of lipids flow in a deforming membrane, modelled as a two-dimensional Riemannian manifold that resists bending. The two lipids behave like viscous Newtonian fluids whose motion is determined by realistic physical forces. By examining the stability of various shapes, it is shown that instability may result if the two lipids forming the membrane possess biophysical qualities, which cause them to respond differently to membrane curvature. By means of numerical simulation of a simplified model, it is shown that this instability results in curvature induced phase separation. Applying the simplified model to the Golgi apparatus, it is hypothesized that curvature induced phase separation may occur in a Golgi cisterna, aiding in the process of protein sorting.

In addition to flowing tangentially in the membrane, lipids also flip back and forth between the two leaflets in the bilayer. While traditionally assumed to occur very slowly, recent experiments have indicated that lipid flip-flop may occur rapidly. Two models are developed that explore the effect of rapid flip-flop on membrane geometry and the effect of a pH gradient on the distribution of charged lipids in the leaflets of the bilayer. By means of a stochastic model, it is shown that even the rapid flip-flop rates observed are unlikely to be significant inducers of membrane curvature. By means of a nonlinear Poisson–Boltzmann model, it is shown that pH gradients are unlikely to be significant inducers of bilayer asymmetry under physiological conditions.

CONTENTS

CHAPTER 1

INTRODUCTION

Biological membranes are important structural units in the cell. They serve to separate the intracellular domain from the extracellular domain. Further, they serve to separate the intracellular domain into separate structures called organelles. Biomembranes are made up primarily of lipids, proteins, and cholesterol. The classic fluid mosaic model proposed by Singer and Nicolson in 1972 [59] describes the lipid bilayer as a two-dimensional viscous fluid in which proteins can diffuse relatively freely. Figure 1.1 shows a schematic drawing of a membrane as described by Singer and Nicolson. While the fluid mosaic model was quite popular and remains useful today, the focus was primarily on proteins, not lipids. To this day, lipids are often assumed to play a relatively passive role in cellular function [5]. On the contrary, the lipids themselves are being shown to have interesting and dynamic behaviors. In this dissertation, we explore how lipid motion can influence the dynamic behavior of biological membranes.

A lipid is a small biological molecule, generally cylindrical or cone shaped, with length on the order of nine nanometers [74] and head group area on the order of 40 square Angstroms [1]. A lipid usually has a hydrophilic head group and hydrophobic tail as shown in Figure 1.2.

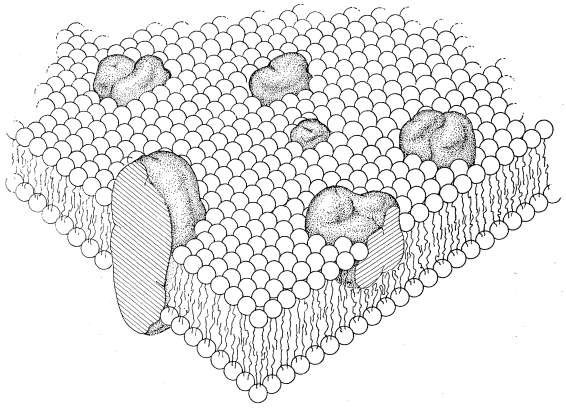

Figure 1.1. Schematic drawing of a membrane. The globular structures are protens. The balls with two tails are lipids. Adapted from [59].

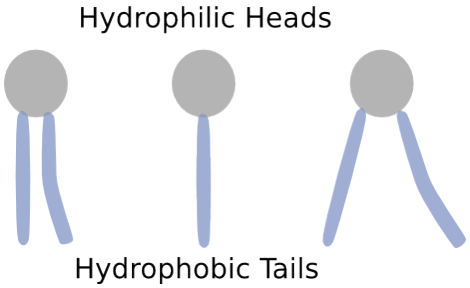

Figure 1.2. Various lipid shapes.

Individual lipids can have different geometries based on the number and shape of their hydrophobic tails and size of their head groups [48]. When dissolved in a polar solvent such as water, the hydrophilic head interacts favorably with the solvent, while the hydrophobic tail interacts unfavorably with the solvent. For low lipid concentrations, the positive effect of translational entropy on the free energy ensures that most of the lipid molecules remain as monomers in the solvent in spite of the negative interactions of the tails with the solvent. Above a specific concentration, often called the critical micellar concentration, the negative interactions between the hydrophobic tails and the polar solvent overcome the positive effects of translational entropy and cause the lipid molecules to spontaneously aggregate [14]. These aggregates are often in the form of bilayers or micelles, as shown in Figure 1.3, where the shape of the aggregate depends on the geometry and concentration of the individual lipids [48]. These shapes allow the hydrophobic tails to interact favorably with each other and the hydrophilic heads to interact favorably with the solvent.

There are three main classes of lipids in biological membranes, glycerolipids, sphingolipids, and sterols [20]. These main classes of lipids are shown schematically in Figure 1.4. Sphingolipids have a sphingoid base as their backbone, while glycerolipids have a glycerol backbone [28]. Cholesterol has a different shape and tends to associate with the tails of the other lipids in the interior or the bilayer. The different structures of sphingolipids and

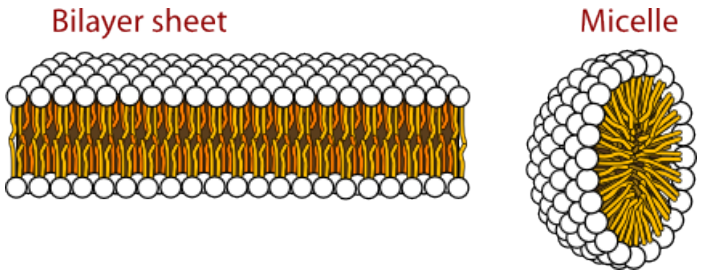

Figure 1.3. Various lipid structures. (Adapted from [66].)

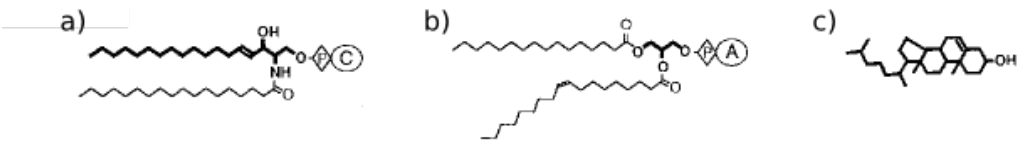

Figure 1.4. Schematic drawing of different classes of lipids. a) Sphingolipid. b) Glycerolipid. c) Cholesterol. (Adapted from [28].)

glycerolipids endows them with different physical properties. Sphingolipids tend to associate with cholesterol and form more tightly packed bilayers that are thicker and more resistant to bending than bilayers formed primarily of glycerolipids [28]. Further, model membranes made up of appropriate combinations of sphingolipids and glycerolipids exhibit the ability to spontaneously phase separate [24]. Phase separation means that certain areas of the membrane are enriched in sphingolipids and cholesterol while other areas of the membrane are enriched in glycerolipids. It occurs because lipid self interactions are energetically more favorably than mixed interactions between different types of lipids. Phase separation of the lipids which make up the membrane can result in interesting geometries as shown in Figure 1.5. Phase separation in membranes may also be relevant to the membrane raft hypothesis in which small transitory membrane patches enriched in sphingolipids, cholesterol, and associated proteins may play an important role in cellular signalling events [58]. The existence of different classes of lipids with different biophysical properties and the possibility of phase separation provides the motivation for the two phase fluid models developed in this dissertation.

A classical model widely used to study phase separation phenomena is called the Cahn–Hilliard (C–H) model [9]. Briefly, the C–H model is given by [36]

$$\frac{\partial c}{\partial t} = \nabla \cdot (M \nabla \mu) = M \Delta \mu, \tag{1.1}$$

where c is a phase variable usually scaled to range between 1 and -1, M is the constant mobility coefficient, and μ is the local chemical potential given by

$$\mu = F'(c) - k\Delta c. \tag{1.2}$$

In equation 1.2, F is the Helmholz free energy density, and k is a positive constant.

The C–H model is derived by assuming a free energy density of the form

$$F(c) + \frac{k}{2} |\nabla c|^2 . \tag{1.3}$$

The second term represents a free energy penalty for gradients in the phase variable c. From this point, one can either define the chemical potential via the variational derivative

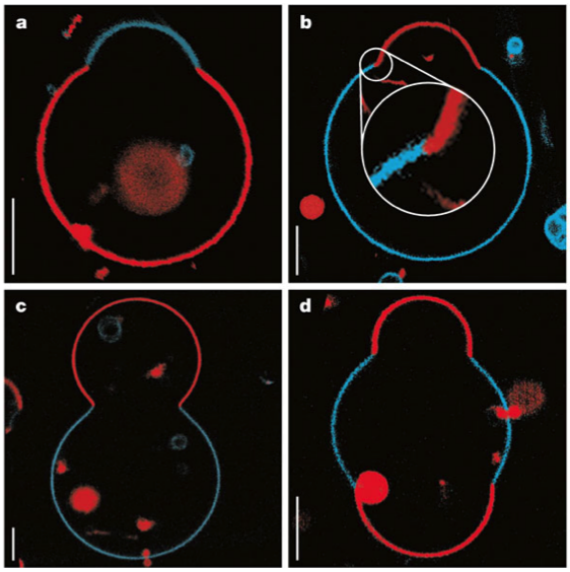

Figure 1.5. Interesting shapes caused by phase separation. The different colors indicate different phases. The scale bar is $5\mu m$. (Adapted from [6].)

and assume a conservation law with flux given via $J = -M\nabla c$ [36], or describe the time evolution via a gradient flow in a cleverly chosen inner product space [19, 32]. Either way, one ends up with the C–H model.

The squared gradient term in equation 1.3 acts to penalize sharp gradients in the concentration c and leads to pattern formation as demonstrated in Figure 1.6. In the figure, we start the simulation with a random perturbation of the value $c = 0$. The value of the parameter k dictates the size of the channels formed and the width of the interface between phases.

While the C–H model describes phase separation, it lacks certain aspects necessary to study phase separation in a biological membrane. First, the model as presented can describe phase separating in two-dimensional or three-dimensional Euclidean space. The membrane, on the other hand, is described as a two-dimensional Riemannian manifold embedded in three-dimensional space, so the C–H model must be reformulated accordingly. Second, biological membranes are resistant to bending [48]. We will see in Chapter 2 that our free energy density includes bending energy terms in addition to the homogeneous free energy and gradient penalty terms present in the classical C–H model. Finally, the fluid mosaic model describes the membrane as a two-dimension viscous fluid [59]. The classical C–H model neglects the viscosity of the species undergoing phase separation.

Other attempts to study phase separation involve so called multiphase fluid models. Two phase fluid models have been used previously to describe the swelling of polyelectrolyte gels

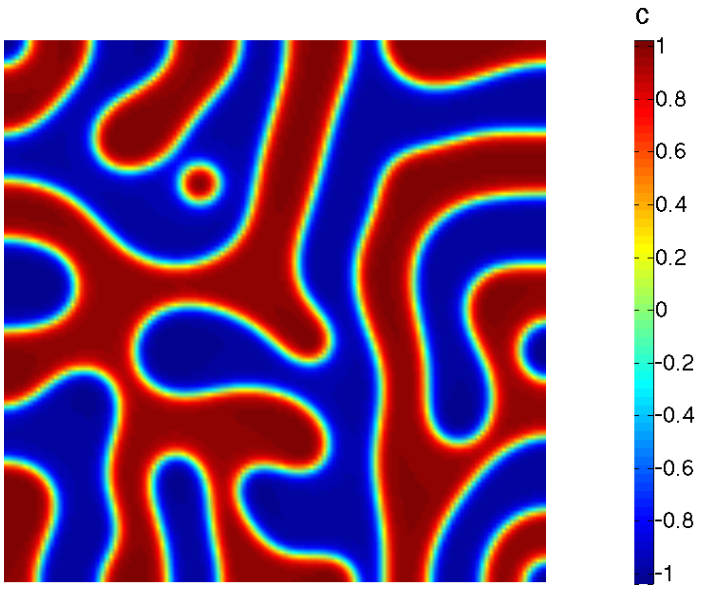

Figure 1.6. The result of a Cahn–Hilliard result. The colors indicate concentration, showing clear phase separation and pattern formation.

[68, 17], but those models do not treat both phases as viscous fluids. A later model [69] expanded upon the earlier work to treat each phase as an incompressible viscous fluid. More recently, authors have developed a two phase fluid model where each phase behaves as a compressible viscous or viscoelastic fluid [33, 60]. The model can describe phase separation [71], but is formulated for Euclidean space using Cartesian coordinates. It also does not include terms in the free energy to penalize sharp gradients. In this dissertation, we extend previous models to describe two phase flow on a two-dimensional Reimannian manifold.

Returning to our discussion of biological membranes and the lipids therein, the main location of sphingolipid synthesis is the Golgi apparatus [21], a cellular organelle important in the exocytic and endocytic pathways [28]. The main job of the Golgi is to package and sort proteins for transport to different parts of the cell [28]. The Golgi is usually described as a sequence of flattened membranous sacks called cisternae, possibly connected by tubules [23] as shown in Figure 1.7. While protein sorting in the Golgi is not fully understood, it has been hypothesized that phase separation in the Golgi may be influential to the protein sorting processes essential to cellular transport [47, 63] and that this phase separation may be influenced by membrane curvature [12, 61, 31, 54, 42]. This hypothesis provides the motivation for the model of curvature-induced phase separation explored in Chapter 4 of this dissertation. While there has been some mathematical treatment of this phenomenon [12, 31, 42], those treatments all differ significantly from our model. The

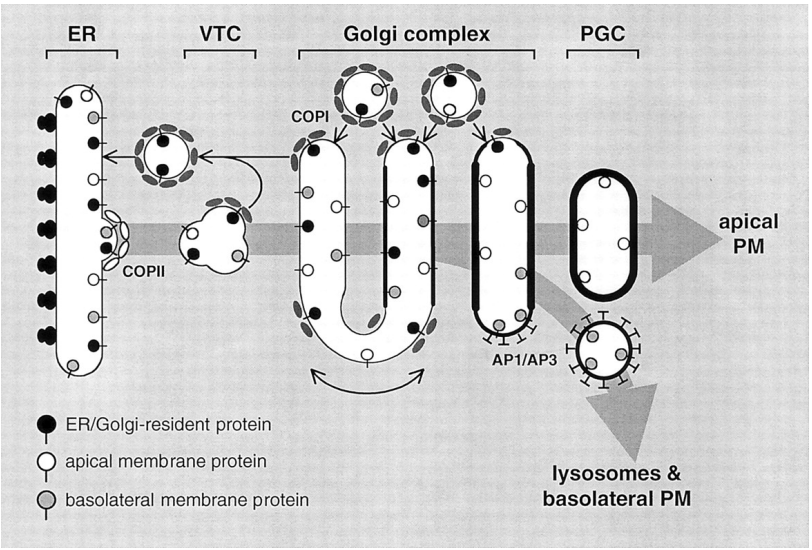

Figure 1.7. A schematic drawing of the Golgi apparatus. The thicker membranes indicate areas enriched in sphingolipids, while the thinner membranes indicate areas enriched in glycerolipids. (Adapted from [28].)

models in [12] and [31] are both equilibrium models. The model in [42] describes dynamic phase separation, but uses a level set method to describe the membrane instead of modelling it as a two-dimensional Riemannian manifold.

One of the earliest attempts to describe a membrane mathematically was by Canham in 1970 [11], where he undertook to explain the biconcave shape of the red blood cell. A few years later in 1973, Helfrich proposed a similar model describing the elastic properties of bilayers [27]. Briefly, the Helfrich (or Helfrich–Canham) model treats the membrane as an elastic surface and describes a functional for the energy of the membrane. Energetic contributions come through two terms, the mean curvature of the surface with associated bending modulus and the Gaussian curvature of the surface with associated Gaussian bending modulus. The free energy density in the Helfrich model is given by

$$f = \frac{\kappa}{2}(2H - C_0)^2 + \kappa_g G, \tag{1.4}$$

where H is the mean curvature of the membrane and G is the Gaussian curvature. These quantites are defined mathematically in Chapter 2. The bending moduli κ and κ_g have units of energy. The constant C_0 is called the spontaneous or preferred curvature, has units of curvature, and reflects the possibility that the preferred state of a membrane is not flat. The Helfrich model is derived via writing the free energy density as a function of curvature, Taylor expanding, and keeping only lowest order terms [55].

The original Helfrich model shown in equation 1.4 has a contribution to the energy from the Gaussian curvature of the surface. According to the Gauss–Bonnet theorem, the Guassian curvature is constant for a closed surface that does not change genus [55]. As a result, many authors neglect the Gaussian curvature contribution to the free energy, a pattern we follow in this dissertation.

The Helfrich model has had a dramatic impact on later membrane studies, being cited thousands of times since its original publication. Using the Helfrich model and its variants, authors have had much success describing the shapes of fluid membranes, especially the shapes of vesicles. The review [55] provides an in depth description of membrane models and results. Though much work has been done, the majority of models have been static, describing the equilibrium shapes of vesicles. Other models have undertaken to model fluctuations around steady states, but still have not attempted a complete fluid model.

While the majority of membrane models are static, there has been some work to model the membrane as a viscous fluid. One of the earliest attempts to describe flow on a surface is described in [53] where the author derives flow equations for a fluid interface. The book [2] makes significant use of these ideas in its chapter on surface flow. In both [53] and [2], the equations describing flow are described first using a purely intrinsic formulation and then using an extrinsic formulation in terms of the basis of the three-dimensional Euclidean embedding space. In more recent work [3, 10, 29, 46, 49, 50, 51, 72], authors have formulated the fluid equations in terms of the local basis formed by the two tangent vectors to the surface and the associated normal vector. These models describe flow and bending resistance, but do not incorporate the existence of multiple types of lipids in the membrane.

As has been mentioned, certain combinations of lipids exhibit the ability to spontaneously phase separate. It has been shown experimentally that giant unilamellar vesicles made up of different lipid compositions exhibit the ability to phase separate and that this phase separation can result in interesting geometrical shapes [6]. This phenomenon has be explored mathematically by various authors [39, 42, 54, 57] with the basis of most models being the Helfrich model. Existing models have had some success in reproducing experimental shapes, but again most of the existing models examine only equilibrium shapes. In other words, the shapes predicted by the models come from minimizing a free energy functional, but do not treat the lipids as dynamic fluids. Essential to most of these models is the inclusion of line tension [39]. Line tension is a phenomenological force to minimize the length of an interface between two lipid phases. It is based on the

idea that interfaces between two phases are energetically unfavorable due to unfavorable interactions with water resulting from the two phases having different thicknesses. Line tension is most often expressed as an energy contribution proportional to the length of the interface between the phases [39]. An implicit assumption in this formulation is that the membrane already exists in a phase separated state. In the model we present in Chapter 2, we use a Cahn-Hilliard type penalty term [36], similar to the treatment in [42] and [31], in an attempt to model line tension during dynamic phase separation. The model in [31] uses a Cahn–Hiliard penalty term, but is still a static model, only looking at equilibrium membrane configurations. To our knowledge, the model in [42] is the most similar to the model presented in Chapter 2 of this dissertation. The authors of [42] describe a model of dynamic phase separation, incorporating fluid viscosity, bending rigidity, and Cahn–Hilliard penalty terms. The fundamental difference from the current model is that the authors in [42] use a diffuse interface technique to describe the membrane surface, while we leverage the tools of differential geometry to describe the membrane shape and fluid flow equations. We demonstrate in Chapter 3 that our treatment is amenable to mathematical analyses such as linear stability analysis.

A simplification in the Helfrich model is the treatment of the membrane as a thin elastic sheet. Biological membranes are in fact made up of two lipid monolayers. It has been shown that different types of lipids are enriched in different membranes of the cell [65], and that lipids are asymmetrically distributed between different leaflets in the bilayer [64], with an important example being the location of phosphatidylserine in the plasma membrane of platelets [37]. It has long been believed that lipid motion within a specific leaflet is quick, while flip-flop between leaflets of the bilayer is very slow [45] and that the maintenance and loss of membrane asymmetry is primarily a protein-mediated process [35, 64]. Work in John Conboy's lab at the University of Utah has cast doubt on this conventional belief. Their experiments have measured lipid flip-flop rates much faster than those measured previously, and they hypothesize that flip rates may be even faster under physiological conditions [41]. Based on these findings, we develop and explore two models in Chapter 5 to investigate the effects of rapid flip-flop between leaflets of the bilayer. In the first model, we explore a stochastic description of the membrane to see if lipid flip-flop can significantly deform a membrane and possibly serve as an initiator of vesicle budding. In the second, we use the Poisson–Boltzmann equation to explore a model of bilayer asymmetry to see whether an asymmetric distribution of negatively charged lipids can be maintained by a pH gradient rather than by an active protein-mediated process.

Chapters 2–4 of this dissertation present the derivation and analysis of two phase fluid models of a membrane. In Chapter 2, we treat the membrane as a two-dimensional viscous fluid which resists bending. Using the tools of differential geometry, we derive the equations of motion governing the behavior of the membrane. In Chapter 3, we explore two specific parametrizations of the general model derived in Chapter 2. Using linear stability analysis, we highlight situations in which curvature induced instability occurs. In Chapter 4, we explore a one-dimensional simplification of the model with the goal of studying curvature induced phase separation in the Golgi apparatus. Chapter 5 addresses the bilayer nature of membranes. Specifically, we explore various implications of rapid flip-flop of lipids between the two leaflets of the bilayer with the goal to shed light on the process of vesicle formation in the multivesicular body. We conclude the dissertation with a brief description of ideas for model extensions and future work.

CHAPTER 2

TWO PHASE FLUID FLOW ON A SURFACE

Phase separation has important impacts on the shape and functions of biological membranes. While much work has been done to understand the flow of a single lipid phase in a membrane, there has been little effort to describe multiphase flow on a membrane. That is the goal of the current work. Much of the subsequent notation follows [2]. Some of the logic, especially in the meaning of a surface fixed coordinate system follows [51]. The derivation was also influenced by [46]. A nice treatment of much of the differential geometry used in the derivation can be found in [49] and in the unpublished notes [13]. Our goal in the current work is not to describe new results in the fields of differential geometry or to describe flow on a surface in a completely new way. Rather, we seek to combine existing theories of two phase fluid flow and flow on a deforming surface in a new and novel way. By using a realistic free energy density developed in this chapter, we provide a description of a biological membrane that more accurately reflects the reality that a membrane is a surface composed of various lipid species with different biophysical properties.

In the following chapter, we first describe the differential geometry background necessary to derive the model. We then derive in detail the equations describing the flow of lipids on a surface along with the shape of the surface. We conclude by examining simplifications of the derived model to show that the model generalizes various published works in the fields of membrane shape and two phase fluid flow.

2.1 Basic Setup and Differential Geometry Background

Let $S(t)$ be a time varying surface in $\mathbb{R}^3$ upon which a fluid can flow. Let $\{u^\alpha\}$, $\alpha = 1, 2$ be some surface coordinates. Then $S(t)$ can be described parametrically by

$$\mathbf{r}(u^1, u^2, t) = (x(u^1, u^2, t), y(u^1, u^2, t), z(u^1, u^2, t))^T. \tag{2.1}$$

Any coordinate description of the surface yields a natural basis for vectors originating on the surface. Define two tangent vectors $\mathbf{t}_\alpha = \frac{\partial \mathbf{r}}{\partial u^\alpha}$ for $\alpha = 1, 2$. Note that in general, these tangent vectors are neither orthogonal nor unit vectors. Define the unit normal via

$$\mathbf{n} = \frac{\mathbf{t}_1 \times \mathbf{t}_2}{||\mathbf{t}_1 \times \mathbf{t}_2||}. \tag{2.2}$$

A schematic diagram showing the surface with the two tangent vectors and the normal vectors is shown in Figure 2.1.

Using the tangent vectors, define the surface metric tensor

$$a_{\alpha\beta} = \mathbf{t}_\alpha \cdot \mathbf{t}_\beta. \tag{2.3}$$

The metric tensor is symmetric with a nonzero determinant denoted

$$a = \det(a_{\alpha\beta}). \tag{2.4}$$

The local area element in the surface dA is given via the metric tensor as

$$dA = \sqrt{a} du^1 du^2. \tag{2.5}$$

The inverse metric tensor $a^{\alpha\beta}$ is defined via

$$a^{\alpha\gamma} a_{\gamma\beta} = \delta^\alpha_\beta, \tag{2.6}$$

where δ^α_β is the delta function, and the Einstein summation convention is used. Using the summation convention, a repeated index that appears as both a superscript and subscript is summed. A raised index indicates a contravariant component of a tensor, and a lowered index indicates a covariant component of a tensor. The words covariant and contravariant indicate that the tensor component follows a specific transformation rule under a change of coordinates. These rules are described in section A.7. Given a basis of covariant tangent

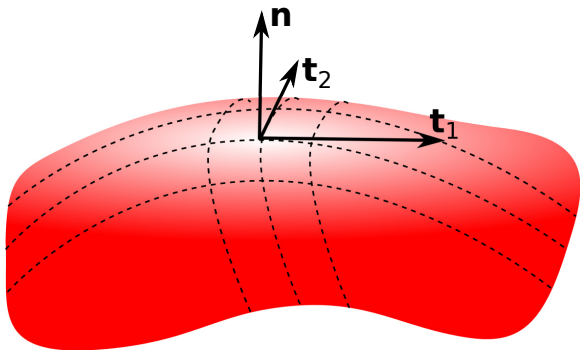

Figure 2.1. Schematic diagram of a surface.

vectors $\{\mathbf{t}_\alpha\}$ for the tangent space at a point P, the inverse metric tensor can be used to define a biorthogonal basis of contravariant tangent vectors $\{\mathbf{t}^\alpha\}$ at P via $\mathbf{t}^\alpha = a^{\alpha\beta}\mathbf{t}_\beta$ for $\alpha, \beta = 1, 2$ with the feature $\mathbf{t}_\alpha \cdot \mathbf{t}^\beta = \delta_\alpha^\beta$.

Any vector $\mathbf{w}$ in the tangent space to P can be expressed as a linear combination of either the covariant or contravariant tangent vectors, $\mathbf{w} = w^\alpha \mathbf{t}_\alpha$ or $\mathbf{w} = w_\beta \mathbf{t}^\beta$. The relationship between the contravariant components w^α and the covariant components w_β is given by $w^\alpha = a^{\alpha\beta} w_\beta$ and $w_\beta = a_{\alpha\beta} w^\alpha$. Thus, the metric tensor and its inverse can be used to raise or lower indices. In other words, they allow us to switch between a covariant or contravariant description of a vector or tensor quantity.

The metric tensor is also used to define the dot product of two surface vectors. Let $\mathbf{v}$ and $\mathbf{w}$ be two vectors in the tangent space to P. Write $\mathbf{v} = v_\alpha \mathbf{t}^\alpha$ and $\mathbf{w} = w^\beta \mathbf{t}_\beta$. Define

$$\mathbf{v} \cdot \mathbf{w} = v_\alpha w^\alpha = a_{\alpha\beta} v^\beta w^\alpha = a^{\alpha\beta} v_\alpha w_\beta. \tag{2.7}$$

Since $\mathbf{n}$ is a unit vector, it follows that $\frac{\partial \mathbf{n}}{\partial u^\alpha} \cdot \mathbf{n} = 0$. Thus, $\frac{\partial \mathbf{n}}{\partial u^\alpha}$ can be written as a linear combination of the tangent vectors $\{\mathbf{t}_\alpha\}$. This linear combination is given by the Weingarten equations [49] as

$$\frac{\partial \mathbf{n}}{\partial u^\alpha} = -b_{\alpha\beta} a^{\beta\gamma} \mathbf{t}_\gamma = -b_\alpha^\gamma \mathbf{t}_\gamma, \tag{2.8}$$

where $b_{\alpha\beta}$ is called the curvature tensor and describes how the normal to the surface varies due to movements along the coordinate lines. Since $\mathbf{n}$ and $\mathbf{t}_\beta$ are orthogonal, $\mathbf{n} \cdot \mathbf{t}_\beta = 0 \Rightarrow \frac{\partial \mathbf{n}}{\partial u^\alpha} \cdot \mathbf{t}_\beta = -\mathbf{n} \cdot \frac{\partial}{\partial u^\alpha} \mathbf{t}_\beta$, and equation 2.8 implies that

$$\begin{aligned} \frac{\partial \mathbf{n}}{\partial u^\alpha} \cdot \mathbf{t}_\beta &= -b_{\alpha\beta} \\ \Rightarrow \mathbf{n} \cdot \frac{\partial}{\partial u^\alpha} \mathbf{t}_\beta &= b_{\alpha\beta}, \end{aligned} \tag{2.9}$$

which provides a way to calculate the components of the curvature tensor. Since $\frac{\partial}{\partial u^\alpha} \mathbf{t}_\beta = \frac{\partial}{\partial u^\alpha} \frac{\partial}{\partial u^\beta} \mathbf{r} = \frac{\partial}{\partial u^\beta} \frac{\partial}{\partial u^\alpha} \mathbf{r} = \frac{\partial}{\partial u^\beta} \mathbf{t}_\alpha$, it follows that the curvature tensor is symmetric.

The curvature tensor also appears in the Gauss Equations [13], which describe the derivative of a tangent vector. Since the tangent vectors are not generally unit vectors, their partial derivatives have both tangential and normal components given by

$$\frac{\partial}{\partial u^\alpha} \mathbf{t}_\beta = \Gamma_{\alpha\beta}^\gamma \mathbf{t}_\gamma + b_{\alpha\beta} \mathbf{n}, \tag{2.10}$$

where the tangential coefficients $\Gamma_{\alpha\beta}^\gamma$, are Christoffel symbols discussed in section A.5, and the normal components are found to be the components of the curvature tensor as given by equation 2.9. Note that because the left hand side and $b_{\alpha\beta}$ are symmetric, it follows that

the Christoffel symbols are symmetric in the two lower indices.

The curvature tensor furnishes two concepts of curvature, both given by exploring $a^{\alpha\gamma}b_{\gamma\beta}$, sometimes referred to as the shape operator. The two eigenvalues of the shape operator at P are the two principal curvatures of the surface at the point P. The mean curvature, denoted H, is the average of the two principal curvatures, given by $1/2$ the trace of the shape operator,

$$H = \frac{1}{2}a^{\alpha\beta}b_{\alpha\beta} = \frac{1}{2}(C_1 + C_2), \tag{2.11}$$

where C_1 and C_2 are the principal curvatures. The Guassian curvature, denoted K, is the product of the two principal curvatures, given by the determinant of the shape operator,

$$K = \det(a^{\alpha\gamma}b_{\gamma\beta}) = C_1C_2. \tag{2.12}$$

The mean curvature H is an extrinsic quantity of the surface, meaning that knowledge of the embedding space is needed in order to define H. In other words, H could not be measured by an entity living on the surface with no knowledge of the embedding space. Gauss' Theorema Egregium states that K is an intrinsic quantity of the surface and can be expressed independently of the curvature tensor. K could be measured by an entity living on the surface and only making local measurements. In practice though, it is often easier to calculate K by making use of the curvature tensor.

In addition to appearing in the description of partial derivatives of the tangent vectors, the Christoffel symbols also allow for the definition of the covariant derivative. Consider the partial derivative of the purely tangential vector field $\mathbf{w} = w^\beta \mathbf{t}_\beta$ given by

$$\frac{\partial \mathbf{w}}{\partial u^\alpha} = \frac{\partial}{\partial u^\alpha}(w^\beta \mathbf{t}_\beta) = \frac{\partial w^\beta}{\partial u^\alpha}\mathbf{t}_\beta + w^\beta\left(\Gamma^\gamma_{\alpha\beta}\mathbf{t}_\gamma + b_{\alpha\beta}\mathbf{n}\right). \tag{2.13}$$

By permuting summed indices, this can be expressed as

$$\frac{\partial \mathbf{w}}{\partial u^\alpha} = \left(\frac{\partial w^\beta}{\partial u^\alpha} + w^\gamma\Gamma^\beta_{\alpha\gamma}\right)\mathbf{t}_\beta + w^\beta b_{\alpha\beta}\mathbf{n}. \tag{2.14}$$

The covariant derivative of the contravariant components of a vector field is defined as the tangential component of $\frac{\partial \mathbf{w}}{\partial u^\alpha}$ and is expressed as

$$\nabla_\alpha w^\beta = \frac{\partial w^\beta}{\partial u^\alpha} + w^\gamma\Gamma^\beta_{\alpha\gamma}. \tag{2.15}$$

The covariant derivative is a tensor quantity whose components change according to the transformation rules in section A.7 upon a change of coordinates. The partial derivative $\frac{\partial w^\beta}{\partial u^\alpha}$, on the other hand, does not transform like a tensor and thus does not give the components of a physical object. One can think of the first term in the covariant derivative as describing

the change in the component upon movement in the $\mathbf{t}_\alpha$ direction and the second term as describing the change in the component caused by changes in the basis vectors $\{\mathbf{t}_\beta\}$ upon movement in the $\mathbf{t}_\alpha$ direction.

The covariant derivative can be generalized to scalar functions on the surface, covariant vector fields, and higher order tensor fields. The covariant derivative of a scalar function is simply the partial derivative, $\nabla_\alpha f = \frac{\partial f}{\partial u^\alpha}$. Using the fact that the dot product of two surface vectors $\mathbf{v}$ and $\mathbf{w}$ is a scalar, $\nabla_\alpha(v^\beta w_\beta) = \frac{\partial}{\partial u^\alpha}(v^\beta w_\beta)$, one can use the product rule on both the partial derivative and the covariant derivative to define the covariant derivative of a covariant vector field,

$$\nabla_\alpha w_\beta = \frac{\partial w_\beta}{\partial u^\alpha} - w_\gamma \Gamma^\gamma_{\alpha\beta}. \tag{2.16}$$

In general, the covariant derivative of a tensor field is defined as the partial derivative with an added term with a Christoffel symbol for each raised index and a subtracted term with a Christoffel symbol for each lowered index,

$$\begin{aligned}\nabla_\xi T^{\alpha\beta\gamma\cdots}_{\lambda\mu\nu\cdots} = \frac{\partial T^{\alpha\beta\gamma\cdots}_{\lambda\mu\nu\cdots}}{\partial u^\xi} &+ T^{\delta\beta\gamma\cdots}_{\lambda\mu\nu\cdots}\Gamma^\alpha_{\delta\xi} + T^{\alpha\delta\gamma\cdots}_{\lambda\mu\nu\cdots}\Gamma^\beta_{\delta\xi} + T^{\alpha\beta\delta\cdots}_{\lambda\mu\nu\cdots}\Gamma^\gamma_{\delta\xi} + \cdots \\ &- T^{\alpha\beta\gamma\cdots}_{\delta\mu\nu\cdots}\Gamma^\delta_{\lambda\xi} - T^{\alpha\beta\gamma\cdots}_{\lambda\delta\nu\cdots}\Gamma^\delta_{\mu\xi} - T^{\alpha\beta\gamma\cdots}_{\lambda\mu\delta\cdots}\Gamma^\delta_{\nu\xi} - \cdots\end{aligned} \tag{2.17}$$

Further, note that $\nabla_\alpha w^\alpha$ is a scalar, often called the surface divergence, and it can be shown to be given by

$$\nabla_\alpha w^\alpha = \frac{1}{\sqrt{a}}\frac{\partial}{\partial u^\alpha}\left(\sqrt{a}w^\alpha\right). \tag{2.18}$$

As a final detail, we mention that the Lemma of Ricci states that covariant derivatives of the metric tensor, inverse metric tensor, and determinant of the metric tensor are all zero [13]. Thus, these quantities can freely cross the covariant derivative symbol.

2.2 Convected Coordinates

Parametrize the surface at time $t = 0$ using surface coordinates $\{u^\Gamma\}, \Gamma = 1, 2$ in such a way that a particular fluid particle retains its coordinate label. We denote these convected or material coordinates using capital Greek indices. The associated surface S_0 with representation $\mathbf{r}(u^\Gamma, 0)$ is fixed and serves as a reference surface. So for fixed $\{u^\Gamma\}$, the map $\mathbf{r}(u^\Gamma, t)$ describes the path through $\mathbb{R}^3$ of the particle labelled by $\{u^\Gamma\}$.

Assume there is an invertible transformation between the two coordinate descriptions given by

$$u^\alpha = u^\alpha(u^\Gamma, t), \qquad \alpha, \Gamma = 1, 2, \tag{2.19}$$

and

$$u^\Gamma = u^\Gamma(u^\alpha, t), \quad \alpha, \Gamma = 1, 2, \tag{2.20}$$

subject to $u^\alpha(u^\Gamma, t_0) = u^\Gamma$ and $u^\Gamma(u^\alpha, t_0) = u^\alpha$.

Any function $f(u^\alpha, t)$ defined on the surface can be expressed in convected coordinates as $f(u^\alpha(u^\Gamma, t), t)$. Denote the material derivative (derivative with fixed u^Γ) by $\frac{d}{dt}$ and the derivative with fixed u^α by $\frac{\partial}{\partial t}$. The material derivative of $f(u^\alpha, t)$ is given by

$$\frac{d}{dt} f(u^\alpha(u^\Gamma, t), t) = \frac{\partial f}{\partial u^\alpha}\frac{du^\alpha}{dt} + \frac{\partial f}{\partial t}, \tag{2.21}$$

where $\frac{du^\alpha}{dt}$ is the velocity of the particle labelled by fixed u^Γ with respect to the u^α coordinate system. Denote this velocity v^α.

2.3 Surface Fixed Coordinates

Consider the velocity $\mathbf{v} \in \mathbb{R}^3$ of a material particle on the surface,

$$\mathbf{v} = \frac{d\mathbf{r}}{dt} = \frac{\partial \mathbf{r}}{\partial u^\alpha}\frac{du^\alpha}{dt} + \frac{\partial \mathbf{r}}{\partial t} = v^\alpha \mathbf{t}_\alpha + \frac{\partial \mathbf{r}}{\partial t}. \tag{2.22}$$

The term $v^\alpha \mathbf{t}_\alpha$ describes the tangential velocity of the particle due to the particle's flow in the surface. The term $\frac{\partial \mathbf{r}}{\partial t}$ describes the velocity of the particle due to movement of the coordinate system. In general, $\frac{\partial \mathbf{r}}{\partial t}$ can have components both tangential and normal to the surface.

Another description of the velocity of a material particle can be given using the local basis induced by the u^α parametrization of the surface,

$$\mathbf{v} = \hat{v}^\alpha \mathbf{t}_\alpha + U_n \mathbf{n}. \tag{2.23}$$

In this description, $\hat{v}^\alpha$ are the contravariant components of a vector field, while U_n are the components of a scalar field. The n in the subscript denotes the normal direction, not covariant components. Note that in general $\hat{v}^\alpha$ is not the same as v^α, for $\hat{v}^\alpha$ describes the total tangential component of the velocity through the Euclidean embedding space, while v^α describes the velocity with respect to the u^α coordinates caused by the flow of the particle (which is necessarily tangential to the surface).

It is possible to choose the $\{u^\alpha\}$ coordinate system in a specific way, such that

$$v^\alpha = \frac{du^\alpha}{dt} = \hat{v}^\alpha \text{ with } u^\alpha(t_0) = u^\Gamma. \tag{2.24}$$

In other words, choose the u^α coordinate system so that the velocity of the particle with respect to the coordinate system is the same as the tangential component of the velocity

through the embedding space. This coordinate system has the feature that a fixed coordinate u^α moves entirely in a direction normal to the surface,

$$\frac{\partial \mathbf{r}}{\partial t} = U_n \mathbf{n}, \tag{2.25}$$

which is useful when deriving equations of motion for fluids on the surface. Following [2], we call this coordinate system the surface fixed coordinate system. For notational clarity, ξ^α for $\alpha = 1, 2$ is used to denote surface fixed coordinates.

An intuitive way to visualize this particular coordinate system is as follows: imagine the surface at time t with coordinates given by ξ^α for $\alpha = 1, 2$. Consider a specific coordinate $\tilde{\xi}^\alpha$. This coordinate has a specific spatial location $\tilde{\mathbf{x}}$ in the embedding space. Now imagine the surface at time $t + \Delta t$. The surface has deformed and no longer occupies the same locations in the embedding space. Find the point on the surface at time $t + \Delta t$ that has the smallest Euclidean distance from the point $\tilde{\mathbf{x}}$, and label the new point $\tilde{\xi}^\alpha$. Clearly, the new point lies along the normal $\mathbf{n}$. This provides a time dependent parametrization such that motion of a fixed ξ^α on the surface is always normal to the surface.

2.4 General Coordinates

The surface fixed coordinate system ξ^α will prove to be convenient when deriving equations of motion for fluids on a surface, but it is not always suitable to describe the motion of a surface. Consider a surface described using the Monge parametrization $\mathbf{r}(x, y) = (x, y, h(x, y))^T$. In this coordinate system, motion of a specific (x, y) on the surface is purely in the z direction, not normal to the surface. Thus it is useful to formulate equations of motion in terms of general coordinates in addition to surface fixed coordinates. Suppose $\frac{\partial \mathbf{r}}{\partial t}$ has components both tangential and normal to the surface,

$$\frac{\partial \mathbf{r}}{\partial t} = U^\alpha \mathbf{t}_\alpha + U_n \mathbf{n}. \tag{2.26}$$

Then the velocity of a material particle is given by

$$\mathbf{v} = v^\alpha \mathbf{t}_\alpha + U^\alpha \mathbf{t}_\alpha + U_n \mathbf{n}. \tag{2.27}$$

Note that the quantities v^α, U^α, and the tangent vectors $\mathbf{t}_\alpha$ depend on the specific coordinate description of the surface, but the quantity U_n and the normal vector $\mathbf{n}$ are indepenent of the coordinate system. (They depend on the description of the Euclidean embedding space, which is always assumed to be Cartesian.) For notational clarity, u^α for $\alpha = 1, 2$ will be used to denote any coordinate system that is not specifically a surface-fixed or convected coordinate system.

2.5 Continuity Equations

2.5.1 Continuity Equations for Concentrations

Consider a material patch inside the domain $\Omega(t)$ expressed in a general coordinate system, with concentration c_s of sphingolipid particles in the material patch. Note that concentration in this context means number of particles per unit area. Let Ω_0 be the corresponding fixed patch expressed in the convected coordinate system. Let $a' = \det(a_{\Gamma\Delta})$ denote the determinant of the metric tensor in the convected coordinates. From conservation of mass, it follows that

$$\frac{d}{dt}\int_{\Omega(t)} dA\ c_s = \frac{d}{dt}\int_{\Omega_0} du^I du^{II}\sqrt{a'}c_s = \int_{\Omega_0} du^I du^{II}\sqrt{a'}\left(\frac{dc_s}{dt} + \frac{c_s}{2a'}\frac{da'}{dt}\right) = 0. \tag{2.28}$$

Since $\Omega(t)$ is arbitrary, the convected coordinated description of the continuity equation is

$$\frac{dc_s}{dt} + \frac{c_s}{2a'}\frac{da'}{dt} = 0. \tag{2.29}$$

The first term is simply the material derivative defined in equation (2.21). Thus in both surface fixed and general coordinates

$$\frac{dc_s}{dt} = \frac{\partial c_s}{\partial t} + v^\alpha \nabla_\alpha c_s, \tag{2.30}$$

where v^α is the tangential component of the velocity of a sphingolipid particle. We show in section A.3 that

$$\frac{1}{2a'}\frac{da'}{dt} = \nabla_\alpha v^\alpha - 2HU_n, \tag{2.31}$$

in surface fixed coordinates, and

$$\frac{1}{2a'}\frac{da'}{dt} = \nabla_\alpha v^\alpha + \nabla_\alpha U^\alpha - 2HU_n, \tag{2.32}$$

in general coordinates.

This yields the surface fixed coordinate version of the continuity equation for c_s,

$$\frac{\partial c_s}{\partial t} + \nabla_\alpha(c_s v^\alpha) - 2c_s HU_n = 0, \tag{2.33}$$

and general coordinate version,

$$\frac{\partial c_s}{\partial t} + \nabla_\alpha(c_s v^\alpha) + c_s(\nabla_\alpha U^\alpha - 2HU_n) = 0. \tag{2.34}$$

Similar expressions exist for the glycerlipid concentration c_g:

$$\frac{\partial c_g}{\partial t} + \nabla_\alpha(c_g w^\alpha) - 2c_g HU_n = 0, \tag{2.35}$$

for surface fixed coordinates, and

$$\frac{\partial c_g}{\partial t} + \nabla_\alpha(c_g w^\alpha) + c_g(\nabla_\alpha U^\alpha - 2HU_n) = 0, \tag{2.36}$$

for general coordinates, where w^α is the tangential component of the velocity of a glycerolipid particle. We wish to express these continuity equations in terms of volume fractions θ_s and θ_g.

2.5.2 Continuity Equations for Volume Fractions

Define the volume fractions

$$\theta_s = c_s \nu_s, \tag{2.37}$$

$$\theta_g = c_g \nu_g, \tag{2.38}$$

where ν_s and ν_g are constants giving the area of a sphingolipid and glycerolipid molecule, respectively. Upon substituting definitions 2.37 and 2.38 into the continuity equations for c_s and c_g, we find the continuity equations

$$\frac{\partial \theta_s}{\partial t} + \nabla_\alpha(\theta_s v^\alpha) - 2\theta_s HU_n = 0, \tag{2.39}$$

$$\frac{\partial \theta_g}{\partial t} + \nabla_\alpha(\theta_g w^\alpha) - 2\theta_g HU_n = 0, \tag{2.40}$$

for surface fixed coordinates, and

$$\frac{\partial \theta_s}{\partial t} + \nabla_\alpha(\theta_s v^\alpha) + \theta_s\left(\nabla_\alpha U^\alpha - 2HU_n\right) = 0, \tag{2.41}$$

$$\frac{\partial \theta_g}{\partial t} + \nabla_\alpha(\theta_g w^\alpha) + \theta_g\left(\nabla_\alpha U^\alpha - 2HU_n\right) = 0, \tag{2.42}$$

for general coordinates.

Let us assume that the membrane is a closed surface. Then the total number of lipid particles must be fixed. If we think of the lipid particles as forming the membrane, we should assume that particles fill all space in the membrane. This space filling assumption is equivalent to the assumption that

$$\theta_s + \theta_g = 1. \tag{2.43}$$

Using the conservation laws, we can restate the space filling assumption as the coincompressibilty condition

$$\nabla_\alpha\left(\theta_s v^\alpha + \theta_g w^\alpha\right) - 2HU_n = 0, \tag{2.44}$$

for surface fixed coordinates, and

$$\nabla_\alpha\left(\theta_s v^\alpha + \theta_g w^\alpha\right) + \nabla_\alpha U^\alpha - 2HU_n = 0, \tag{2.45}$$

for general coordinates. We note that flows that satisfy the space filling assumption conserve the total area of the membrane since the total number of particles is fixed, and particles do not change size.

2.6 Equations of Motion

To find the equations of motion for our two-phase fluid, we first make the assumption that intertia is negligible in the system. Then the conservation of linear momentum equations become force balance equations. Many analyses simply write down equations that account for all the forces at this point. The current system, however, has forces from viscosity, from drag between the two phases, from gradients in the chemical potential, and from bending of the membrane. It is not straightforward to simply write down equations that balance all the forces in the tangential and normal directions. To mitigate this difficulty, we follow the method presented in [16] of minimizing what the author calls the Rayleighian over all admissible velocities. The method is based on Onsager's reciprocal relation, which is an extension of Rayleigh's principle of least energy dissipation [16]. The main idea is that the system evolves in such a way that the rate of energy dissipation is minimized, i.e. in the most efficient way possible. In [16], the author derives various classical models using the Rayleighian. Other authors [50, 3] have used the same technique, but refer to it as the principle of virtual power.

The Rayleighian is defined as the sum of one half the total viscous dissipation and the rate of change of the free energy of the system,

$$R = \frac{1}{2}\Phi + \frac{\partial}{\partial t}F. \tag{2.46}$$

Since the system evolves via velocities that minimize the Rayleighian, its first variation respect to velocity is set to zero, yielding the appropriate force balance equations.

In the following sections, we describe the different components of the Rayleighian and how to take their first variation. All of the calculations that follow are carried out in the surface fixed coordinates. The reason for this is that in surface fixed coordinates, the tangential components of the velocity of a particle are given by the velocity of that particle with respect to the coordinate system. Thus there is no need to try to disentangle components in the velocity due to flow of the particles from components in the velocity due to motion of the coordinate system. Further, calculations are simpler in the surface fixed coordinates due to the simpler form of $\frac{\partial \mathbf{r}}{\partial t}$.

2.6.1 Viscous Dissipation

We assume viscous dissipation occurs via two mechanisms, internal viscosity in each phase and drag between the two phases. The internal viscosity dissipation rate for each phase is given by the doubly contracted product of the stress tensor for that phase with the rate of strain tensor for that phase. This term is scaled by the volume fraction. The rate of dissipation from drag between the two phases is taken to be proportional to the squared magnitude of the difference in their velocities. The frictional coefficient is taken to be $\theta_s\theta_g\xi$, where ξ is a constant. Putting all these contributions together, the rate of the viscous dissipation is given by

$$\Phi = \int_S d\xi^1 d\xi^2 \sqrt{a} \left[{}_sT^{\alpha\beta} {}_sS_{\alpha\beta}\theta_s + {}_gT^{\alpha\beta} {}_gS_{\alpha\beta}\theta_g + \theta_s\theta_g\xi a^{\alpha\beta}(v_\alpha - w_\alpha)(v_\beta - w_\beta) \right], \quad (2.47)$$

where ${}_sT^{\alpha\beta}$, ${}_gT^{\alpha\beta}$, ${}_sS_{\alpha\beta}$, and ${}_gS_{\alpha\beta}$ are the stress and rate of strain tensors for the sphingolipid and gylcerolipid phases, respectively. The integration is taken over the entire surface S. Note that the expression $a^{\alpha\beta}(v_\alpha - w_\alpha)(v_\beta - w_\beta)$ is the surface generalization of the expression $(\mathbf{v} - \mathbf{w}) \cdot (\mathbf{v} - \mathbf{w})$.

Under the assumption that both phases behave as compressible Newtonian fluids, each has a stress tensor of the form [2]

$$T^{\alpha\beta} = \eta a^{\alpha\beta} a^{\lambda\mu} S_{\lambda\mu} + \epsilon(a^{\alpha\lambda}a^{\beta\mu} + a^{\alpha\mu}a^{\beta\lambda} - a^{\alpha\beta}a^{\lambda\mu})S_{\lambda\mu}, \quad (2.48)$$

where η and ϵ describe the bulk and shear moduli of the phase. Note that these could be different for the different phases, and are subscripted accordingly. We show in section A.2 that the rates of strain for the two phases in surface fixed coordinates are given by

$${}_sS_{\alpha\beta} = \frac{1}{2}(\nabla_\alpha v_\beta + \nabla_\beta v_\alpha - 2b_{\alpha\beta}U_n), \quad (2.49)$$

$${}_gS_{\alpha\beta} = \frac{1}{2}(\nabla_\alpha w_\beta + \nabla_\beta w_\alpha - 2b_{\alpha\beta}U_n). \quad (2.50)$$

The first variation of the viscous dissipation is worked out explicitly in section A.4. We find that

$$\begin{aligned} \frac{1}{2}\delta\Phi = \int_S d\xi^1 d\xi^2 \sqrt{a} \Big[& \left\{ -\nabla_\alpha({}_sT^{\alpha\beta}\theta_s) + \theta_s\theta_g\xi a^{\alpha\beta}(v_\alpha - w_\alpha) \right\} \delta v_\beta \\ & + \left\{ -\nabla_\alpha({}_gT^{\alpha\beta}\theta_g) + \theta_s\theta_g\xi a^{\alpha\beta}(w_\alpha - v_\alpha) \right\} \delta w_\beta \\ & + \left\{ -{}_sT^{\alpha\beta}b_{\alpha\beta}\theta_s - {}_gT^{\alpha\beta}b_{\alpha\beta}\theta_g \right\} \delta U_n \Big]. \end{aligned} \quad (2.51)$$

2.6.2 Free Energy and Its Time Derivative

The second term that appears in the Rayleighian is the time derivative of the free energy of the system. We assume that the free energy has three distinct parts, a homogeneous part, a curvature dependent part, and a part which penalizes sharp gradients in the volume fraction. The derivation of the homogeneous part of the free energy comes from a typical lattice model as described in [14]. We suppose that each point in space is made up of N lattice sites, N_s of them filled with sphingolipids, and N_g of them filled with glycerolipids. Let $F = U - TS$ be the Helmholtz free energy, where U is the internal energy, T is the absolute temperature, and S is the entropy. Using Boltzmann's equation, we have $S = k_b \ln(W)$, where k_b is Boltzmann's constant and W is the number of arrangements of molecules. In our case $W = N!/(N_s!N_g!)$. Using Stirling's approximation, we get after simplification that $S = -k_b\left(N_s \ln(N_s/N) + N_g \ln(N_g/N)\right)$. For internal energy U, we count the number of interactions between molecules using the Bragg–Williams approximation, essentially an assumption that things are well mixed. This gives $U = (zw_{ss}/2)N_s + (zw_{gg}/2)N_g + k_bT\chi N_sN_g/N$, where $\chi = (z/k_bT)(w_{sg} - (w_{ss}+w_{gg})/2)$ is the unitless Flory interaction parameter, z is the coordination number of the lattice, and w_{ij} is the interaction energy between two lipids of type i and j, respectively. Then

$$F = \left(\frac{zw_{ss}}{2}\right) N_s + \left(\frac{zw_{gg}}{2}\right) N_g + k_bT\chi\frac{N_sN_g}{N} + k_bT\left(N_s \ln\left(\frac{N_s}{N}\right) + N_g \ln\left(\frac{N_g}{N}\right)\right). \quad (2.52)$$

Suppose that $\nu_s = \nu_g = \nu$ so that both types of lipids have the same area per lipid. In the analysis that follows, we use the free energy density, $f = F/(N\nu)$. Under the assumption that both types of lipids have the same area per lipid, N_s/N and N_g/N, though technically particle fractions, are also equal to the volume fractions θ_s and θ_g. It follows that the homogeneous free energy density is given by

$$f^h(\theta_s, \theta_g) = \epsilon_{ss}\theta_s + \epsilon_{gg}\theta_g + \frac{k_bT}{\nu}\left(\chi\theta_s\theta_g + \theta_s \ln\theta_s + \theta_g \ln\theta_g\right), \quad (2.53)$$

where $\epsilon_{ij} = zw_{ij}/2\nu$ for $i, j = s, g$ are energy densities, and the unitless parameter χ is now $\chi = [(2\nu)/(K_bT)](\epsilon_{sg} - (\epsilon_{ss} + \epsilon_{gg})/2)$.

For the curvature dependent part of the free energy density, we follow the Helfrich model [27] and take the bending free energy density to be

$$f^b(\theta_s, \theta_g, H) = \frac{\theta_s\kappa_s}{2}(2H - C_s)^2 + \frac{\theta_g\kappa_g}{2}(2H - C_g)^2, \quad (2.54)$$

where κ_s and κ_b are bending moduli with units of energy, H is the mean curvature of the surface, and C_s and C_g are the preferred curvatures of the sphingolipid and glycerolipid phases. Nonzero C_s or C_g reflect the preference for the lipids to be in a curved instead of

flat state. Though often a result of inhomogeneities between the two leaflets of the bilayer [55], different types of lipids also have different basic shapes which could contribute to the spontaneous curvatures of the two phases [18, 25].

For the third part of the free energy density, we include two Cahn–Hilliard type terms,

$$\frac{\alpha_s^2}{2}a^{\alpha\beta}\nabla_\alpha\theta_s\nabla_\beta\theta_s \text{ and } \frac{\alpha_g^2}{2}a^{\alpha\beta}\nabla_\alpha\theta_g\nabla_\beta\theta_g, \tag{2.55}$$

where α_s and α_g are constants with units of the square root of energy and characterize the resistance to sharp gradients in the volume fractions. These terms may play a similar role to the phenomenological line tension terms that appear in various models of phase separation and penalize boundaries between phases [39]. They are also the usual terms appearing in the free energy density used to derive the Cahn–Hilliard equation [36], formulated for a surface.

Define

$$f(\theta_s,\theta_g,H) = f^h(\theta_s,\theta_g) + f^b(\theta_s,\theta_g,H). \tag{2.56}$$

Define the total free energy density to be

$$f^T(\theta_s,\theta_g,H) = f(\theta_s,\theta_g,H) + \frac{\alpha_s^2}{2}a^{\alpha\beta}\nabla_\alpha\theta_s\nabla_\beta\theta_s + \frac{\alpha_g^2}{2}a^{\alpha\beta}\nabla_\alpha\theta_g\nabla_\beta\theta_g. \tag{2.57}$$

The total free energy of the system is given by

$$F = \int_S d\xi^1 d\xi^2 \sqrt{a} f^T(\theta_s,\theta_g,H), \tag{2.58}$$

with time derivative

$$\frac{\partial}{\partial t}F = \int_S d\xi^1 d\xi^2 \sqrt{a}\left(\frac{\delta f^T}{\delta\theta_s}\frac{\partial\theta_s}{\partial t} + \frac{\delta f^T}{\delta\theta_g}\frac{\partial\theta_g}{\partial t} + \frac{\partial f^T}{\partial H}\frac{\partial H}{\partial t} + \frac{f^T}{2a}\frac{\partial a}{\partial t}\right), \tag{2.59}$$

where the δ notation indicates a functional derivative. The functional derivative of f is simply the partial derivative. For the functional derivative of the Cahn–Hilliard penalty terms (shown only for the sphingolipid phase here), we have the first variation

$$\begin{aligned}
&\int d\xi^1 d\xi^2 \sqrt{a}\left[\frac{\alpha_s^2}{2}a^{\alpha\beta}(\nabla_\alpha\theta_s\nabla_\beta\delta\theta_s + \nabla_\alpha\delta\theta_s\nabla_\beta\theta_s)\right] \\
&= \int d\xi^1 d\xi^2 \sqrt{a}\left[\alpha_s^2 a^{\alpha\beta}\nabla_\alpha\delta\theta_s\nabla_\beta\theta_s\right] \\
&= -\int d\xi^1 d\xi^2 \sqrt{a}\left[\alpha_s^2 a^{\alpha\beta}\nabla_\alpha\nabla_\beta\theta_s\right]\delta\theta_s,
\end{aligned} \tag{2.60}$$

so that $\frac{\delta f^T}{\delta\theta_s} = \frac{\partial f}{\partial\theta_s} - \alpha_s^2 a^{\alpha\beta}\nabla_\alpha\nabla_\beta\theta_s$ and similarly for the glycerolipid phase.

Using the continuity equations for θ_s and θ_g given in equations 2.39–2.40 and equations A.9 and A.3 for $\partial H/\partial t$ and $\partial a/\partial t$, we then have

$$\begin{aligned}\frac{\partial}{\partial t}F = \int_S d\xi^1 d\xi^2 \sqrt{a} \Bigg[& \left(\frac{\partial f}{\partial \theta_s} - \alpha_s^2 a^{\alpha\beta} \nabla_\alpha \nabla_\beta \theta_s \right) \left(-\nabla_\alpha (\theta_s v^\alpha) + 2\theta_s H U_n \right) \\ & + \left(\frac{\partial f}{\partial \theta_g} - \alpha_g^2 a^{\alpha\beta} \nabla_\alpha \nabla_\beta \theta_g \right) \left(-\nabla_\alpha (\theta_g w^\alpha) + 2\theta_g H U_n \right) \\ & + \frac{\partial f}{\partial H} \left((2H^2 - K) U_n + \frac{1}{2} a^{\alpha\beta} \nabla_\beta \nabla_\alpha U_n \right) \\ & - 2 \left(f + \frac{\alpha_s^2}{2} a^{\alpha\beta} \nabla_\alpha \theta_s \nabla_\beta \theta_s + \frac{\alpha_g^2}{2} a^{\alpha\beta} \nabla_\alpha \theta_g \nabla_\beta \theta_g \right) H U_n \Bigg] .\end{aligned} \tag{2.61}$$

2.6.3 Constrained Rayleighian

Combining equation 2.47 for the rate of viscous dissipation and equation 2.61 for the the time derivative of the free energy, we have the full Rayleighian

$$\begin{aligned} R = \int_S d\xi^1 d\xi^2 \sqrt{a} \Bigg\{ & \frac{1}{2} \left[{}_s T^{\alpha\beta}{}_s S_{\alpha\beta} \theta_s + {}_g T^{\alpha\beta}{}_g S_{\alpha\beta} \theta_g + \theta_s \theta_g \xi a^{\alpha\beta} (v_\alpha - w_\alpha)(v_\beta - w_\beta) \right] \\ & - \left(\frac{\partial f}{\partial \theta_s} - \alpha_s^2 a^{\alpha\beta} \nabla_\alpha \nabla_\beta \theta_s \right) \nabla_\alpha (\theta_s v^\alpha) - \left(\frac{\partial f}{\partial \theta_g} - \alpha_g^2 a^{\alpha\beta} \nabla_\alpha \nabla_\beta \theta_g \right) \nabla_\alpha (\theta_g w^\alpha) \\ & + \frac{\partial f}{\partial H} \left((2H^2 - K) U_n + \frac{1}{2} a^{\alpha\beta} \nabla_\beta \nabla_\alpha U_n \right) \\ & + 2 \Bigg[\theta_s \left(\frac{\partial f}{\partial \theta_s} - \alpha_s^2 a^{\alpha\beta} \nabla_\alpha \nabla_\beta \theta_s \right) + \theta_g \left(\frac{\partial f}{\partial \theta_g} - \alpha_g^2 a^{\alpha\beta} \nabla_\alpha \nabla_\beta \theta_g \right) \\ & - \left(f + \frac{\alpha_s^2}{2} a^{\alpha\beta} \nabla_\alpha \theta_s \nabla_\beta \theta_s + \frac{\alpha_g^2}{2} a^{\alpha\beta} \nabla_\alpha \theta_g \nabla_\beta \theta_g \right) \Bigg] H U_n \Bigg\} . \end{aligned} \tag{2.62}$$

We wish to minimize the Rayleighian over velocity, but only velocities that satisfy the coincompressiblity constraint (2.44). Using the Lagrange multiplier σ, we seek to minimize

$$R_c = R - \int_S d\xi^1 d\xi^2 \sigma \left(\nabla_\alpha (\theta_s v^\alpha + \theta_g w^\alpha) - 2 H U_n \right) . \tag{2.63}$$

The Lagrange multiplier σ acts as a surface pressure and affects both the tangential and normal force balance equations.

2.6.4 Full Force Balance Equations

Using equation (2.51) and integration by parts (section A.6), the variation of R_c with respect to velocity is given by

$$
\begin{aligned}
\delta R_c = \int_S d\xi^1 d\xi^2 \sqrt{a} \Big[\Big\{ & -\nabla_\alpha ({}_sT^{\alpha\beta}\theta_s) + \theta_s\theta_g \xi a^{\alpha\beta}(v_\alpha - w_\alpha) \\
& + a^{\alpha\beta}\theta_s \nabla_\alpha \left(\frac{\partial f}{\partial \theta_s} - \alpha_s^2 a^{\lambda\mu} \nabla_\lambda \nabla_\mu \theta_s + \sigma \right) \Big\} \delta v_\beta + \Big\{ -\nabla_\alpha ({}_gT^{\alpha\beta}\theta_g) \\
& + \theta_s\theta_g \xi a^{\alpha\beta}(w_\alpha - v_\alpha) + a^{\alpha\beta}\theta_g \nabla_\alpha \left(\frac{\partial f}{\partial \theta_g} - \alpha_g^2 a^{\lambda\mu} \nabla_\lambda \nabla_\mu \theta_g + \sigma \right) \Big\} \delta w_\beta \\
& + \Big\{ -{}_sT^{\alpha\beta} b_{\alpha\beta}\theta_s - {}_gT^{\alpha\beta} b_{\alpha\beta}\theta_g + (2H^2 - K)\frac{\partial f}{\partial H} + \frac{1}{2} a^{\alpha\beta}\nabla_\alpha \nabla_\beta \frac{\partial f}{\partial H} \\
& + 2 \left[\theta_s \left(\frac{\partial f}{\partial \theta_s} - \alpha_s^2 a^{\alpha\beta} \nabla_\alpha \nabla_\beta \theta_s \right) + \theta_g \left(\frac{\partial f}{\partial \theta_g} - \alpha_g^2 a^{\alpha\beta} \nabla_\alpha \nabla_\beta \theta_g \right) \right. \\
& \left. - \left(f + \frac{\alpha_s^2}{2} a^{\alpha\beta} \nabla_\alpha \theta_s \nabla_\beta \theta_s + \frac{\alpha_g^2}{2} a^{\alpha\beta} \nabla_\alpha \theta_g \nabla_\beta \theta_g \right) + \sigma \right] H \Big\} \delta U_n \Big] .
\end{aligned}
\tag{2.64}
$$

Using a Lagrange multiplier to constrain the variation allows us to treat $\delta v_\beta, \delta w_\beta$, and δU_n as independent and arbitrary variations. Thus, δR_c is zero when the following three equations are satisfied:

$$
\nabla_\alpha ({}_sT^{\alpha\beta}\theta_s) - \theta_s\theta_g \xi a^{\alpha\beta}(v_\alpha - w_\alpha) - a^{\alpha\beta}\theta_s \nabla_\alpha \left(\frac{\partial f}{\partial \theta_s} - \alpha_s^2 a^{\lambda\mu} \nabla_\lambda \nabla_\mu \theta_s + \sigma \right) = 0, \tag{2.65}
$$

$$
\nabla_\alpha ({}_gT^{\alpha\beta}\theta_g) - \theta_s\theta_g \xi a^{\alpha\beta}(w_\alpha - v_\alpha) - a^{\alpha\beta}\theta_g \nabla_\alpha \left(\frac{\partial f}{\partial \theta_g} - \alpha_g^2 a^{\lambda\mu} \nabla_\lambda \nabla_\mu \theta_g + \sigma \right) = 0, \tag{2.66}
$$

$$
\begin{aligned}
& {}_sT^{\alpha\beta} b_{\alpha\beta}\theta_s + {}_gT^{\alpha\beta} b_{\alpha\beta}\theta_g - (2H^2 - K)\frac{\partial f}{\partial H} - \frac{1}{2} a^{\alpha\beta}\nabla_\alpha \nabla_\beta \frac{\partial f}{\partial H} \\
& -2 \left[\theta_s \left(\frac{\partial f}{\partial \theta_s} - \alpha_s^2 a^{\alpha\beta} \nabla_\alpha \nabla_\beta \theta_s \right) + \theta_g \left(\frac{\partial f}{\partial \theta_g} - \alpha_g^2 a^{\alpha\beta} \nabla_\alpha \nabla_\beta \theta_g \right) \right. \\
& \left. - \left(f + \frac{\alpha_s^2}{2} a^{\alpha\beta} \nabla_\alpha \theta_s \nabla_\beta \theta_s + \frac{\alpha_g^2}{2} a^{\alpha\beta} \nabla_\alpha \theta_g \nabla_\beta \theta_g \right) + \sigma \right] H = 0.
\end{aligned}
\tag{2.67}
$$

Equation 2.65 is a tensor equation and describes the balance of tangential forces for the sphingolipid phase. Equation 2.66 is a tensor equation and describes the balance of tangential forces for the glycerolipid phase. Equation 2.67 is a scalar equation and describes the balance of forces in the normal direction.

2.7 Full System

2.7.1 Surface Fixed Coordinates

The full system of equations includes the continuity equations, the force balance equations, and the equation of motion for the membrane. These equations are given by

$$
\frac{\partial \theta_s}{\partial t} + \nabla_\alpha (\theta_s v^\alpha) - 2\theta_s H U_n = 0, \tag{2.68}
$$

$$
\frac{\partial \theta_g}{\partial t} + \nabla_\alpha (\theta_g w^\alpha) - 2\theta_g H U_n = 0, \tag{2.69}
$$

$$\nabla_\alpha({}_sT^{\alpha\beta}\theta_s) - \theta_s\theta_g\xi(v^\beta - w^\beta) - a^{\alpha\beta}\theta_s\nabla_\alpha\left(\frac{\partial f}{\partial\theta_s} - \alpha_s^2 a^{\lambda\mu}\nabla_\lambda\nabla_\mu\theta_s + \sigma\right) = 0, \tag{2.70}$$

$$\nabla_\alpha({}_gT^{\alpha\beta}\theta_g) - \theta_s\theta_g\xi(w^\beta - v^\beta) - a^{\alpha\beta}\theta_g\nabla_\alpha\left(\frac{\partial f}{\partial\theta_g} - \alpha_g^2 a^{\lambda\mu}\nabla_\lambda\nabla_\mu\theta_g + \sigma\right) = 0, \tag{2.71}$$

$$\begin{aligned} {}_sT^{\alpha\beta}b_{\alpha\beta}\theta_s + {}_gT^{\alpha\beta}b_{\alpha\beta}\theta_g - (2H^2 - K)\frac{\partial f}{\partial H} - \frac{1}{2}a^{\alpha\beta}\nabla_\alpha\nabla_\beta\frac{\partial f}{\partial H} \\ -2\left[\theta_s\left(\frac{\partial f}{\partial\theta_s} - \alpha_s^2 a^{\alpha\beta}\nabla_\alpha\nabla_\beta\theta_s\right) + \theta_g\left(\frac{\partial f}{\partial\theta_g} - \alpha_g^2 a^{\alpha\beta}\nabla_\alpha\nabla_\beta\theta_g\right)\right. \\ \left. - \left(f + \frac{\alpha_s^2}{2}a^{\alpha\beta}\nabla_\alpha\theta_s\nabla_\beta\theta_s + \frac{\alpha_g^2}{2}a^{\alpha\beta}\nabla_\alpha\theta_g\nabla_\beta\theta_g\right) + \sigma\right]H = 0, \end{aligned} \tag{2.72}$$

$$\frac{\partial\mathbf{r}}{\partial t} - U_n\mathbf{n} = 0. \tag{2.73}$$

This system of equations is supplemented by either of the following equations,

$$\nabla_\alpha(\theta_s v^\alpha + \theta_g w^\alpha) - 2HU_n = 0, \tag{2.74}$$

$$\theta_s + \theta_g = 1, \tag{2.75}$$

each of which expresses the space filling assumption.

2.7.2 General Coordinates

The continuity equations and coincompressibility condition for general coordinates have already been described in section 2.5. It is not necessary to repeat the derivation in section 2.6 for general coordinates. Because the force balance equations derived are valid tensor equations, they hold true in any coordinate system, and expressing them in general coordinates only involves a coordinate transformation from surface fixed to general coordinates. (See section A.7 for a description of coordinate transformations.) Though the components in the tensors depend on the coordinate system, the general form of the equations appears the same after transformation, with the only difference being the expression for the rate of strain tensor. We show in section A.2 that the rate of strain tensor in general coordinates for the sphingolipid phase is given by

$$S_{\alpha\beta} = \frac{1}{2}\left(\nabla_\alpha v_\beta + \nabla_\beta v_\alpha + \nabla_\alpha U_\beta + \nabla_\beta U_\alpha - 2b_{\alpha\beta}U_n\right). \tag{2.76}$$

The rate of strain tensor for the glycerolipid phase is identical with w substituted for v. Thus the full system of equations in general coordinates is given by

$$\frac{\partial\theta_s}{\partial t} + \nabla_\alpha(\theta_s v^\alpha) + \theta_s(\nabla_\alpha U^\alpha - 2HU_n) = 0, \tag{2.77}$$

$$\frac{\partial\theta_g}{\partial t} + \nabla_\alpha(\theta_g w^\alpha) + \theta_g(\nabla_\alpha U^\alpha - 2HU_n) = 0, \tag{2.78}$$

$$\nabla_\alpha({}_sT^{\alpha\beta}\theta_s) - \theta_s\theta_g\xi(v^\beta - w^\beta) - a^{\alpha\beta}\theta_s\nabla_\alpha\left(\frac{\partial f}{\partial\theta_s} - \alpha_s^2 a^{\lambda\mu}\nabla_\lambda\nabla_\mu\theta_s + \sigma\right) = 0, \tag{2.79}$$

$$\nabla_\alpha({}_gT^{\alpha\beta}\theta_g) - \theta_s\theta_g\xi(w^\beta - v^\beta) - a^{\alpha\beta}\theta_g\nabla_\alpha\left(\frac{\partial f}{\partial\theta_g} - \alpha_g^2 a^{\lambda\mu}\nabla_\lambda\nabla_\mu\theta_g + \sigma\right) = 0, \tag{2.80}$$

$$\begin{aligned} {}_sT^{\alpha\beta}b_{\alpha\beta}\theta_s + {}_gT^{\alpha\beta}b_{\alpha\beta}\theta_g - (2H^2 - K)\frac{\partial f}{\partial H} - \frac{1}{2}a^{\alpha\beta}\nabla_\alpha\nabla_\beta\frac{\partial f}{\partial H} \\ -2\left[\theta_s\left(\frac{\partial f}{\partial\theta_s} - \alpha_s^2 a^{\alpha\beta}\nabla_\alpha\nabla_\beta\theta_s\right) + \theta_g\left(\frac{\partial f}{\partial\theta_g} - \alpha_g^2 a^{\alpha\beta}\nabla_\alpha\nabla_\beta\theta_g\right)\right. \\ \left. - \left(f + \frac{\alpha_s^2}{2}a^{\alpha\beta}\nabla_\alpha\theta_s\nabla_\beta\theta_s + \frac{\alpha_g^2}{2}a^{\alpha\beta}\nabla_\alpha\theta_g\nabla_\beta\theta_g\right) + \sigma\right]H = 0, \end{aligned} \tag{2.81}$$

$$\frac{\partial\mathbf{r}}{\partial t} - U^\alpha\mathbf{t}_\alpha - U_n\mathbf{n} = 0. \tag{2.82}$$

supplemented by either of the following

$$\nabla_\alpha(\theta_s v^\alpha + \theta_g w^\alpha) + \nabla_\alpha U^\alpha - 2HU_n = 0, \tag{2.83}$$

$$\theta_s + \theta_g = 1. \tag{2.84}$$

2.8 Simplifications

In this section we explore three simplifications of the two phase model developed in the previous sections. First, we examine the equations under the assumption that there is only one phase and no flow. Second, we explore the simplification to the flat plane $\mathbb{R}^2$. Third, we explore the simplification to a single phase fluid on a moving surface.

2.8.1 Comparison with the Classical Shape Equations

Consider the system 2.68–2.75 when $\theta_s = 1$, $\theta_g = 0$, $\alpha = 0$, all the velocities are zero, and the free energy density is given by the Helfrich free energy density,

$$f = \frac{\kappa}{2}\left(2H - C_0\right)^2. \tag{2.85}$$

We see from the tangential force balance equations that σ is constant. Then with a short calculation, the normal force balance equation yields the classical shape equation [55, 73]

$$\kappa\left[\left(2H - C_0\right)\left(2H^2 - 2K + HC_0\right) + 2a^{\alpha\beta}\nabla_\alpha\nabla_\beta H\right] + 2H\sigma = 0. \tag{2.86}$$

This equation has been used extensively to describe the equilibrium shape of vesicles [55]. Thus our system generalizes the simpler situation of a single phase fluid membrane at equilibrium. We should note that the original derivation in [73] uses a different sign convention for mean curvature and includes a term to maintain constant volume inside the closed surface.

2.8.2 Simplification to $\mathbb{R}^2$

Suppose we use the system 2.68–2.75 to describe the flow of a two phase fluid in $\mathbb{R}^2$ using Cartesian coordinates. We briefly cover the current form of the geometric quantities described in section 2.1.

The surface in this case is simply given by $\mathbf{r}(x, y, t) = (x, y, 0)^T$, with no time dependence. The tangent vectors are $\mathbf{t}_x = (1, 0, 0)^T$ and $\mathbf{t}_y = (0, 1, 0)^T$. The normal velocity is $U_n = 0$ because the surface does not deform in time. The metric tensor is the identity tensor, and the curvature tensor is the zero tensor. The determinant of the metric tensor is one. Since Christoffel symbols are linear combinations of partial derivatives of the metric tensor (see section A.5), all components of the Christoffel symbols are zero, and covariant derivatives are simply partial derivatives. Because the curvature tensor is zero, both the mean and Gaussian curvatures are zero.

With the simple forms of the geometric quantities, we see that the rate of strain tensor for the sphingolipid phase is simply

$$S_s = \frac{1}{2}\left(\nabla \mathbf{v} + \nabla \mathbf{v}^T\right), \tag{2.87}$$

where ∇ is the typical cartesian gradient operator. The rate of strain tensor for the glycerolipid phase is identical, but with $\mathbf{w}$. The stress tensor for the sphingolipid phase is

$$T_s = (\eta_s - \epsilon_s) I \nabla \cdot \mathbf{v} + 2\epsilon_s S_s, \tag{2.88}$$

where I is the identity tensor, and the expression for the sphingolipid stress tensor is similar.

Combining all these aspects, we arrive at the system of equations

$$\frac{\partial \theta_s}{\partial t} + \nabla \cdot (\theta_s \mathbf{v}) = 0, \tag{2.89}$$

$$\frac{\partial \theta_g}{\partial t} + \nabla \cdot (\theta_g \mathbf{w}) = 0, \tag{2.90}$$

$$\nabla \cdot (\theta_s T_s) - \theta_s \theta_g \xi (\mathbf{v} - \mathbf{w}) - \theta_s \nabla \left(\frac{\partial f}{\partial \theta_s} - \alpha_s^2 \nabla^2 \theta_s + \sigma \right) = 0, \tag{2.91}$$

$$\nabla \cdot (\theta_g T_g) - \theta_s \theta_g \xi (\mathbf{w} - \mathbf{v}) - \theta_g \nabla \left(\frac{\partial f}{\partial \theta_g} - \alpha_g^2 \nabla^2 \theta_g + \sigma \right) = 0, \tag{2.92}$$

$$\nabla \cdot (\theta_s \mathbf{v} + \theta_g \mathbf{w}) = 0. \tag{2.93}$$

Except for a different form of the free energy (or chemical potential), this is the same two phase system used previously [33, 60, 70, 71], which has been used to study the kinetics of gels in 2- and three-dimensional Euclidean space. Thus we see that our system generalizes existing models of two phase fluid flow in Euclidean space.

2.8.3 Simplification to a Single Phase

Suppose that $\theta_s = 1$ and $\theta_g = 0$. Then the coincompressibility condition becomes

$$\nabla_\alpha(v^\alpha) - 2HU_n = a^{\alpha\beta}S_{\alpha\beta} = 0,$$

corresponding to an incompressible fluid [2, 49]. In this case, the stress tensor simplifies to

$$T^{\alpha\beta} = \epsilon(a^{\alpha\lambda}a^{\beta\mu} + a^{\alpha\mu}a^{\beta\lambda})S_{\lambda\mu}.$$

The surface fixed coordinate coordinate representation of the system of equations is now

$$\nabla_\alpha(T^{\alpha\beta}) - a^{\alpha\beta}\nabla_\alpha\sigma = 0, \tag{2.94}$$

$$T^{\alpha\beta}b_{\alpha\beta} - (2H^2 - K)\frac{\partial f}{\partial H} - \frac{1}{2}a^{\alpha\beta}\nabla_\alpha\nabla_\beta\frac{\partial f}{\partial H} + 2\,(f - \sigma)\,H = 0, \tag{2.95}$$

$$\nabla_\alpha v^\alpha - 2HU_n = 0, \tag{2.96}$$

$$\frac{\partial \mathbf{r}}{\partial t} - U_n\mathbf{n} = 0. \tag{2.97}$$

Except for possible differences in the form of the free energy density, this is a the same system presented in other published works describing flow on an evolving surface [3, 51, 49]. Thus our system generalizes incompressible Stokes' flow on an evolving surface.

2.9 Conclusion

Using the tools of differential geometry, we have derived the equations describing two phase flow on a two-dimensional Riemannian manifold. We explored two classes of coordinate systems, a surface fixed coordinate system where the motion of the surface is purely normal to the surface, and a more general coordinate system where motion is not normal to the surface. We found that the resulting systems of equations are different depending on the assumptions on the coordinate system. In deriving the equations of motion for the flows on our surface, we used a free energy density which combined Flory–Huggins theory, Helfrich bending theory, and Cahn–Hilliard theory. Using our free energy density, we made use of the Rayleighian to produce the force balance equations describing the motion of our two phase fluid.

Though we have specifically discussed two types of lipids, sphingolipids and glycerolipids, the model derivation is general and describes any two phase fluid which fills space. We have seen that the derived equations reproduce the classical shape equations, existing two phase models in two dimensional cartesian coordinates, and existing surface flow models under appropriate simplifying assumptions.

CHAPTER 3

EXPLORATION OF TWO SPECIFIC PARAMETRIZATIONS

In this chapter, we explore two specific parametrizations of the general system derived in Chapter 2. First, we explore the Monge parametrization, useful for describing perturbations of the flat sheet. In the Monge parametrization, the surface coordinates are the Cartesian coordinates x and y, and the surface is described by the height function $h(x, y)$. We note that motion is not expected to be normal to the surface in the Monge parametrization, so it is necessary to use the general coordinate version of the two phase fluid equations instead of the simpler surface fixed coordinate version.

Second, we explore a parametrization suitable for describing axisymmetric shapes. In the axisymmetric parametrization, the surface parameters are taken to be u and θ where u parametrizes the generating curve, and θ describes the azimuthal angle. For the axisymmetric perturbation, it is appropriate to use the surface fixed coordinate version of the system.

For each parametrization, we first derive the basic objects necessary to describe the system. We then derive the parametrization-specific version of the two phase fluid equations. Finally, we perform linear stability analysis to explore the interaction between curvature and phase separation.

3.1 Monge Parametrization

3.1.1 Basic Setup and Definitions

Suppose we have an infinite surface $S(t)$ described by the parametrization

$$\mathbf{r}(x, y, t) = (x, y, h(x, y, t))^T \tag{3.1}$$

for $x, y \in \mathbb{R}$. Note that because we are on in infinite surface, all boundary conditions that may have arisen from integrating by parts in the derivation presented in Chapter 2 are neglected. A schematic representation of the surface is shown in Figure 3.1.

The tangent vectors are given by

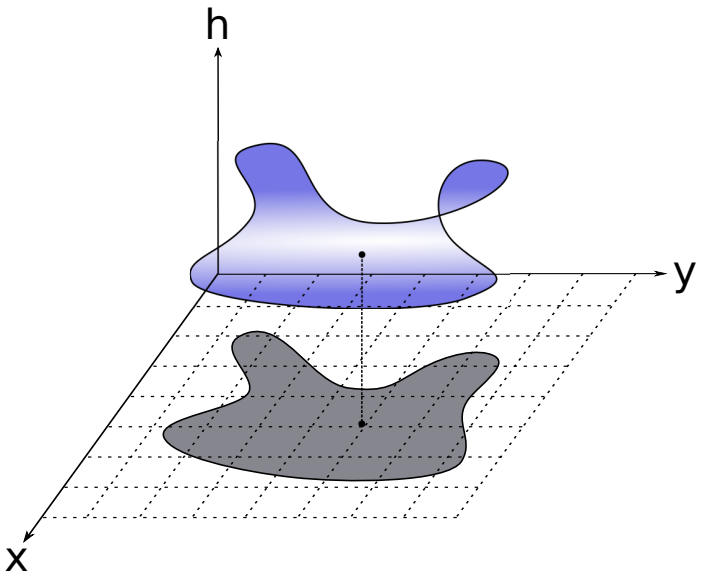

Figure 3.1. The Monge parametrization.

$$\mathbf{t}_x = (1, 0, h_x)^T \tag{3.2}$$

and

$$\mathbf{t}_y = (0, 1, h_y)^T, \tag{3.3}$$

where h_x and h_y indicate the partial derivatives of $h(x, y, t)$ with respect to x and y, respectively.

The metric tensor is given by

$$a_{\alpha\beta} = \begin{pmatrix} 1 + h_x^2 & h_x h_y \\ h_x h_y & 1 + h_y^2 \end{pmatrix}, \tag{3.4}$$

with determinant given by

$$a = 1 + h_x^2 + h_y^2. \tag{3.5}$$

The inverse metric tensor is given by

$$a^{\alpha\beta} = \frac{1}{a} \begin{pmatrix} 1 + h_y^2 & -h_x h_y \\ -h_x h_y & 1 + h_x^2 \end{pmatrix}, \tag{3.6}$$

and the outward unit normal vector is given by

$$\mathbf{n} = \frac{1}{\sqrt{a}}(-h_x, -h_y, 1)^T. \tag{3.7}$$

Using equation 2.9, we find that the curvature tensor is given by

$$b_{\alpha\beta} = \frac{1}{\sqrt{a}} \begin{pmatrix} h_{xx} & h_{xy} \\ h_{xy} & h_{yy} \end{pmatrix}. \tag{3.8}$$

The mean curvature is given by

$$\begin{aligned} H &= \frac{1}{2}\text{trace}\left(a^{\alpha\gamma}b_{\gamma\beta}\right) \\ &= \frac{h_{xx}\left(1+h_y^2\right)+h_{yy}\left(1+h_x^2\right)-2h_xh_yh_{xy}}{2a^{3/2}}, \end{aligned} \tag{3.9}$$

and the Gaussian curvature is given by

$$\begin{aligned} K &= \det\left(a^{\alpha\gamma}b_{\gamma\beta}\right) \\ &= \frac{h_{xx}h_{yy}-h_{xy}^2}{a^2}. \end{aligned} \tag{3.10}$$

Since we are working in a general coordinate system, we have

$$\frac{\partial \mathbf{r}}{\partial t} = U^\alpha \mathbf{t}_\alpha + U_n \mathbf{n}. \tag{3.11}$$

This can be written as

$$\begin{pmatrix} 0 \\ 0 \\ h_t \end{pmatrix} = U^x \begin{pmatrix} 1 \\ 0 \\ h_x \end{pmatrix} + U^y \begin{pmatrix} 0 \\ 1 \\ h_y \end{pmatrix} + \frac{U_n}{\sqrt{a}} \begin{pmatrix} -h_x \\ -h_y \\ 1 \end{pmatrix}, \tag{3.12}$$

and we can calculate that

$$U^x = \frac{h_xh_t}{a}, \tag{3.13}$$

$$U^y = \frac{h_yh_t}{a}, \tag{3.14}$$

$$U_n = \frac{h_t}{\sqrt{a}}. \tag{3.15}$$

3.1.2 Full System of Equations

Using the derivations laid out in section B.1, we are able to express the full two phase fluid system from Chapter 2 using the Monge parametrization. In what follows, we use f_s, f_g, and f_H to indicate partial derivatives with respect to θ_s, θ_g, and H, respectively. The two continuity equations are given by

$$\begin{aligned} &\frac{\partial \theta_s}{\partial t} + \frac{\partial}{\partial x}\left(\theta_s v^x\right) + \frac{\partial}{\partial y}\left(\theta_s v^y\right) \\ &+\frac{\theta_s}{a}\left[h_x\left(v^xh_{xx}+v^yh_{xy}+h_{xt}\right)+h_y\left(v^xh_{xy}+v^yh_{yy}+h_{yt}\right)\right]=0 \end{aligned} \tag{3.16}$$

and

$$\begin{aligned} &\frac{\partial \theta_g}{\partial t} + \frac{\partial}{\partial x}\left(\theta_g w^x\right) + \frac{\partial}{\partial y}\left(\theta_g w^y\right) \\ &+\frac{\theta_g}{a}\left[h_x\left(w^xh_{xx}+w^yh_{xy}+h_{xt}\right)+h_y\left(w^xh_{xy}+w^yh_{yy}+h_{yt}\right)\right]=0. \end{aligned} \tag{3.17}$$

The coincompressibility condition is given by

$$\begin{aligned}&\frac{\partial}{\partial x}\left(\theta_s v^x+\theta_g w^x\right)+\frac{\partial}{\partial y}\left(\theta_s v^y+\theta_g w^y\right)\\&+\frac{1}{a}\left[h_x\left(w^x h_{xx}+w^y h_{xy}+h_{xt}\right)+h_y\left(w^x h_{xy}+w^y h_{yy}+h_{yt}\right)\right]=0.\end{aligned}\tag{3.18}$$

The two tangential force balance equations for the sphingolipid phase are given by

$$\begin{aligned}&\frac{1}{a}\frac{\partial}{\partial x}\left({}_s\tilde{T}^{xx}\theta_s\right)+\frac{1}{a}\frac{\partial}{\partial y}\left({}_s\tilde{T}^{xy}\theta_s\right)\\&-\frac{\theta_s}{a^2}\left({}_s\tilde{T}^{xx}h_y h_{xy}-{}_s\tilde{T}^{xy}(h_x h_{xy}-h_y h_{yy})-{}_s\tilde{T}^{yy}h_x h_{yy}\right)-\theta_s\theta_g\xi(v^x-w^x)\\&-\frac{(1+h_y^2)\theta_s}{a}\frac{\partial}{\partial x}\left\{f_s-\frac{\alpha_s^2}{a}\left[(1+h_y^2)\frac{\partial^2\theta_s}{\partial x^2}-2h_x h_y\frac{\partial^2\theta_s}{\partial x\partial y}+(1+h_x^2)\frac{\partial^2\theta_s}{\partial y^2}\right.\right.\\&\left.\left.+\left(h_x\frac{\partial\theta_s}{\partial x}+h_y\frac{\partial\theta_s}{\partial y}\right)\left[(1+h_y^2)h_{xx}-2h_x h_y h_{xy}+(1+h_x^2)h_{yy}\right]\right]+\sigma\right\}\\&+\frac{h_x h_y\theta_s}{a}\frac{\partial}{\partial y}\left\{f_s-\frac{\alpha_s^2}{a}\left[(1+h_y^2)\frac{\partial^2\theta_s}{\partial x^2}-2h_x h_y\frac{\partial^2\theta_s}{\partial x\partial y}+(1+h_x^2)\frac{\partial^2\theta_s}{\partial y^2}\right.\right.\\&\left.\left.+\left(h_x\frac{\partial\theta_s}{\partial x}+h_y\frac{\partial\theta_s}{\partial y}\right)\left[(1+h_y^2)h_{xx}-2h_x h_y h_{xy}+(1+h_x^2)h_{yy}\right]\right]+\sigma\right\}=0\end{aligned}\tag{3.19}$$

and

$$\begin{aligned}&\frac{1}{a}\frac{\partial}{\partial x}\left({}_s\tilde{T}^{xy}\theta_s\right)+\frac{1}{a}\frac{\partial}{\partial y}\left({}_s\tilde{T}^{yy}\theta_s\right)\\&+\frac{\theta_s}{a^2}\left({}_s\tilde{T}^{xx}h_y h_{xx}-{}_s\tilde{T}^{xy}(h_x h_{xx}-h_y h_{xy})-{}_s\tilde{T}^{yy}h_x h_{xy}\right)-\theta_s\theta_g\xi(v^y-w^y)\\&+\frac{h_x h_y\theta_s}{a}\frac{\partial}{\partial x}\left\{f_s-\frac{\alpha_s^2}{a}\left[(1+h_y^2)\frac{\partial^2\theta_s}{\partial x^2}-2h_x h_y\frac{\partial^2\theta_s}{\partial x\partial y}+(1+h_x^2)\frac{\partial^2\theta_s}{\partial y^2}\right.\right.\\&\left.\left.+\left(h_x\frac{\partial\theta_s}{\partial x}+h_y\frac{\partial\theta_s}{\partial y}\right)\left[(1+h_y^2)h_{xx}-2h_x h_y h_{xy}+(1+h_x^2)h_{yy}\right]\right]+\sigma\right\}\\&-\frac{(1+h_x^2)\theta_s}{a}\frac{\partial}{\partial y}\left\{f_s-\frac{\alpha_s^2}{a}\left[(1+h_y^2)\frac{\partial^2\theta_s}{\partial x^2}-2h_x h_y\frac{\partial^2\theta_s}{\partial x\partial y}+(1+h_x^2)\frac{\partial^2\theta_s}{\partial y^2}\right.\right.\\&\left.\left.+\left(h_x\frac{\partial\theta_s}{\partial x}+h_y\frac{\partial\theta_s}{\partial y}\right)\left[(1+h_y^2)h_{xx}-2h_x h_y h_{xy}+(1+h_x^2)h_{yy}\right]\right]+\sigma\right\}=0,\end{aligned}\tag{3.20}$$

where

$$\begin{aligned}{}_s\tilde{T}^{xx}&=(\eta_s+\epsilon_s)(1+h_y^2)d_v\\&\quad-2\epsilon_s\left(h_x h_y\frac{\partial v^x}{\partial y}+(1+h_y^2)\frac{\partial v^y}{\partial y}+h_y h_{xy}v^x+h_y h_{yy}v^y+h_y h_{yt}\right),\end{aligned}\tag{3.21}$$

$$\begin{aligned}{}_s\tilde{T}^{xy}&=-(\eta_s+\epsilon_s)h_x h_y d_v+\epsilon_s\left[h_x h_y\left(\frac{\partial v^x}{\partial x}+\frac{\partial v^y}{\partial y}\right)+(1+h_x^2)\frac{\partial v^x}{\partial y}+(1+h_y^2)\frac{\partial v^y}{\partial x}\right.\\&\quad\left.+(h_y h_{xx}+h_x h_{xy})v^x+(h_x h_{yy}+h_y h_{xy})v^y+h_y h_{xt}+h_x h_{yt}\right],\end{aligned}\tag{3.22}$$

$$\begin{aligned}{}_s\tilde{T}^{yy}&=(\eta_s+\epsilon_s)(1+h_x^2)d_v\\&\quad-2\epsilon_s\left(h_x h_y\frac{\partial v^y}{\partial x}+(1+h_x^2)\frac{\partial v^x}{\partial x}+h_x h_{xx}v^x+h_x h_{xy}v^y+h_x h_{xt}\right),\end{aligned}\tag{3.23}$$

and the expression d_v is given by

$$
\begin{aligned}
d_v &= a^{\alpha\beta} S_{\alpha\beta} = \nabla_\alpha v^\alpha + \nabla_\alpha U^\alpha - 2HU_n \\
&= \frac{\partial v^x}{\partial x} + \frac{h_x}{a}(v^x h_{xx} + v^y h_{xy} + h_{xt}) + \frac{\partial v^y}{\partial y} + \frac{h_y}{a}(v^x h_{xy} + v^y h_{yy} + h_{yt}).
\end{aligned} \tag{3.24}
$$

The two tangential force balance equations for the glycerolipid phase are given similarly by

$$
\begin{aligned}
&\frac{1}{a}\frac{\partial}{\partial x}\left({}_g\tilde{T}^{xx}\theta_g\right) + \frac{1}{a}\frac{\partial}{\partial y}\left({}_g\tilde{T}^{xy}\theta_g\right) \\
&-\frac{\theta_g}{a^2}\left({}_g\tilde{T}^{xx}h_y h_{xy} - {}_g\tilde{T}^{xy}(h_x h_{xy} - h_y h_{yy}) - {}_g\tilde{T}^{yy}h_x h_{yy}\right) - \theta_s\theta_g\xi(w^x - v^x) \\
&-\frac{(1+h_y^2)\theta_g}{a}\frac{\partial}{\partial x}\left\{f_g - \frac{\alpha_g^2}{a}\left[(1+h_y^2)\frac{\partial^2\theta_g}{\partial x^2} - 2h_x h_y\frac{\partial^2\theta_g}{\partial x\partial y} + (1+h_x^2)\frac{\partial^2\theta_g}{\partial y^2}\right.\right. \\
&\quad\left.\left. + \left(h_x\frac{\partial\theta_g}{\partial x} + h_y\frac{\partial\theta_g}{\partial y}\right)\left[(1+h_y^2)h_{xx} - 2h_x h_y h_{xy} + (1+h_x^2)h_{yy}\right]\right] + \sigma\right\} \\
&\quad+\frac{h_x h_y\theta_g}{a}\frac{\partial}{\partial y}\left\{f_g - \frac{\alpha_g^2}{a}\left[(1+h_y^2)\frac{\partial^2\theta_g}{\partial x^2} - 2h_x h_y\frac{\partial^2\theta_g}{\partial x\partial y} + (1+h_x^2)\frac{\partial^2\theta_g}{\partial y^2}\right.\right. \\
&\quad\left.\left. + \left(h_x\frac{\partial\theta_g}{\partial x} + h_y\frac{\partial\theta_g}{\partial y}\right)\left[(1+h_y^2)h_{xx} - 2h_x h_y h_{xy} + (1+h_x^2)h_{yy}\right]\right] + \sigma\right\} = 0
\end{aligned} \tag{3.25}
$$

and

$$
\begin{aligned}
&\frac{1}{a}\frac{\partial}{\partial x}\left({}_g\tilde{T}^{xy}\theta_g\right) + \frac{1}{a}\frac{\partial}{\partial y}\left({}_g\tilde{T}^{yy}\theta_g\right) \\
&+\frac{\theta_g}{a^2}\left({}_g\tilde{T}^{xx}h_y h_{xx} - {}_g\tilde{T}^{xy}(h_x h_{xx} - h_y h_{xy}) - {}_g\tilde{T}^{yy}h_x h_{xy}\right) - \theta_s\theta_g\xi(w^y - v^y) \\
&\quad+\frac{h_x h_y\theta_g}{a}\frac{\partial}{\partial x}\left\{f_g - \frac{\alpha_g^2}{a}\left[(1+h_y^2)\frac{\partial^2\theta_g}{\partial x^2} - 2h_x h_y\frac{\partial^2\theta_g}{\partial x\partial y} + (1+h_x^2)\frac{\partial^2\theta_g}{\partial y^2}\right.\right. \\
&\quad\left.\left. + \left(h_x\frac{\partial\theta_g}{\partial x} + h_y\frac{\partial\theta_g}{\partial y}\right)\left[(1+h_y^2)h_{xx} - 2h_x h_y h_{xy} + (1+h_x^2)h_{yy}\right]\right] + \sigma\right\} \\
&-\frac{(1+h_x^2)\theta_g}{a}\frac{\partial}{\partial y}\left\{f_g - \frac{\alpha_g^2}{a}\left[(1+h_y^2)\frac{\partial^2\theta_g}{\partial x^2} - 2h_x h_y\frac{\partial^2\theta_g}{\partial x\partial y} + (1+h_x^2)\frac{\partial^2\theta_g}{\partial y^2}\right.\right. \\
&\quad\left.\left. + \left(h_x\frac{\partial\theta_g}{\partial x} + h_y\frac{\partial\theta_g}{\partial y}\right)\left[(1+h_y^2)h_{xx} - 2h_x h_y h_{xy} + (1+h_x^2)h_{yy}\right]\right] + \sigma\right\} = 0.
\end{aligned} \tag{3.26}
$$

Where the expressions ${}_g\tilde{T}^{\alpha\beta}$ are analogous to equations 3.21–3.23. The normal force balance equation is quite complicated, and is given by

$$
\begin{aligned}
&(\eta_s+\epsilon_s)(2H)d_v\theta_s+(\eta_g+\epsilon_g)(2H)d_w\theta_g\\
&+\frac{2\epsilon_s\theta_s}{a^{3/2}}\left\{\left[h_{xy}(1+h_y^2)-h_xh_yh_{yy}\right]\left[\frac{\partial v^y}{\partial x}+\frac{h_y}{a}\left(v^xh_{xx}+v^yh_{xy}+h_{xt}\right)\right]\right.\\
&\qquad\left.+\left[h_{xy}(1+h_x^2)-h_xh_yh_{xx}\right]\left[\frac{\partial v^x}{\partial y}+\frac{h_x}{a}\left(v^xh_{xy}+v^yh_{yy}+h_{yt}\right)\right]\right\}\\
&+\frac{2\epsilon_g\theta_g}{a^{3/2}}\left\{\left[h_{xy}(1+h_y^2)-h_xh_yh_{yy}\right]\left[\frac{\partial w^y}{\partial x}+\frac{h_y}{a}\left(w^xh_{xx}+w^yh_{xy}+h_{xt}\right)\right]\right.\\
&\qquad\left.+\left[h_{xy}(1+h_x^2)-h_xh_yh_{xx}\right]\left[\frac{\partial w^x}{\partial y}+\frac{h_x}{a}\left(w^xh_{xy}+w^yh_{yy}+h_{yt}\right)\right]\right\}\\
&-(2H^2-K)f_H-\frac{1}{2a}\left[(1+h_y^2)\frac{\partial^2 f_H}{\partial x^2}-2h_xh_y\frac{\partial^2 f_H}{\partial x\partial y}+(1+h_x^2)\frac{\partial^2 f_H}{\partial y^2}\right.\\
&\qquad\left.+\left(h_x\frac{\partial f_H}{\partial x}+h_y\frac{\partial f_H}{\partial y}\right)\left[(1+h_y^2)h_{xx}-2h_xh_yh_{xy}+(1+h_x^2)h_{yy}\right]\right]\\
&\qquad-2\left\{\theta_s\left(f_s-\frac{\alpha_s^2}{a}\left[(1+h_y^2)\frac{\partial^2\theta_s}{\partial x^2}-2h_xh_y\frac{\partial^2\theta_s}{\partial x\partial y}+(1+h_x^2)\frac{\partial^2\theta_s}{\partial y^2}\right.\right.\right.\\
&\qquad\left.\left.\left.+\left(h_x\frac{\partial\theta_s}{\partial x}+h_y\frac{\partial\theta_s}{\partial y}\right)\left[(1+h_y^2)h_{xx}-2h_xh_yh_{xy}+(1+h_x^2)h_{yy}\right]\right]\right)\right.\\
&\qquad\left.+\theta_g\left(f_g-\frac{\alpha_g^2}{a}\left[(1+h_y^2)\frac{\partial^2\theta_g}{\partial x^2}-2h_xh_y\frac{\partial^2\theta_g}{\partial x\partial y}+(1+h_x^2)\frac{\partial^2\theta_g}{\partial y^2}\right.\right.\right.\\
&\qquad\left.\left.\left.+\left(h_x\frac{\partial\theta_g}{\partial x}+h_y\frac{\partial\theta_g}{\partial y}\right)\left[(1+h_y^2)h_{xx}-2h_xh_yh_{xy}+(1+h_x^2)h_{yy}\right]\right]\right)\right.\\
&\qquad-\left(f+\frac{\alpha_s^2}{2a}\left[\left(1+h_y^2\right)\left(\frac{\partial\theta_s}{\partial x}\right)^2-2h_xh_y\frac{\partial\theta_s}{\partial x}\frac{\partial\theta_s}{\partial y}+\left(1+h_x^2\right)\left(\frac{\partial\theta_s}{\partial y}\right)^2\right]\right.\\
&\left.\left.+\frac{\alpha_g^2}{2a}\left[\left(1+h_y^2\right)\left(\frac{\partial\theta_g}{\partial x}\right)^2-2h_xh_y\frac{\partial\theta_g}{\partial x}\frac{\partial\theta_g}{\partial y}+\left(1+h_x^2\right)\left(\frac{\partial\theta_g}{\partial y}\right)^2\right]\right)+\sigma\right\}H=0.
\end{aligned}
\tag{3.27}
$$

The above system, when paired with appropriate initial conditions, serves to determine the unknowns $\theta_s, \theta_g, v^x, v^y, w^x, w^y, h$, and σ. Note that if desired, we can omit the coincompressibility equation and instead use the fact that $\theta_s+\theta_g=1$.

3.1.3 Stability Analysis

3.1.3.1 Steady State

One steady state of the system presented is given by $\theta_s=\theta_0=$ constant, $\theta_g=1-\theta_0$, $v^x=v^y=w^x=w^y=h=0$, and $\sigma=\sigma_0=$ constant. Note that the constant σ_0 is not specified due to the fact that $H=0$ when $h=0$. Similarly to section 4.3.2, we suppose

$$\theta_s=\theta_0+\lambda\theta_1, \tag{3.28}$$

$$\theta_g=1-\theta_0-\lambda\theta_1, \tag{3.29}$$

$$v^x=\lambda v_1^x, \tag{3.30}$$

$$v^y = \lambda v_1^y, \tag{3.31}$$

$$w^x = \lambda w_1^x, \tag{3.32}$$

$$w^y = \lambda w_1^y, \tag{3.33}$$

$$h = \lambda h_1, \tag{3.34}$$

$$\sigma = \sigma_0 + \lambda \sigma_1. \tag{3.35}$$

Note that we have used $\theta_g = 1 - \theta_s$ to eliminate one unknown. We substitute into the full system of equations (omitting the coincompressiblity equation), and only keep terms which are first order in λ. The resulting system is

$$\frac{\partial \theta_1}{\partial t} + \theta_0 \left(\frac{\partial v_1^x}{\partial x} + \frac{\partial v_1^y}{\partial y} \right) = 0, \tag{3.36}$$

$$-\frac{\partial \theta_1}{\partial t} + (1-\theta_0) \left(\frac{\partial w_1^x}{\partial x} + \frac{\partial w_1^y}{\partial y} \right) = 0, \tag{3.37}$$

$$\begin{aligned} &\eta_s \left(\frac{\partial^2 v_1^x}{\partial x^2} + \frac{\partial^2 v_1^y}{\partial x \partial y} \right) + \epsilon_s \left(\frac{\partial^2 v_1^x}{\partial x^2} + \frac{\partial^2 v_1^x}{\partial y^2} \right) - (1-\theta_1)\xi \left(v_1^x - w_1^x \right) \\ &-(f_{ss_0} - f_{sg_0}) \frac{\partial \theta_1}{\partial x} - \frac{f_{sH}}{2} \left(\frac{\partial^3 h_1}{\partial x^3} + \frac{\partial^3 h_1}{\partial x \partial y^2} \right) + \alpha_s^2 \left(\frac{\partial^3 \theta_1}{\partial x^3} + \frac{\partial^3 \theta_1}{\partial x \partial y^2} \right) - \frac{\partial \sigma_1}{\partial x} = 0, \end{aligned} \tag{3.38}$$

$$\begin{aligned} &\eta_s \left(\frac{\partial^2 v_1^x}{\partial x \partial y} + \frac{\partial^2 v_1^y}{\partial y^2} \right) + \epsilon_s \left(\frac{\partial^2 v_1^y}{\partial x^2} + \frac{\partial^2 v_1^y}{\partial y^2} \right) - (1-\theta_1)\xi \left(v_1^y - w_1^y \right) \\ &-(f_{ss_0} - f_{sg_0}) \frac{\partial \theta_1}{\partial y} - \frac{f_{sH}}{2} \left(\frac{\partial^3 h_1}{\partial x^2 \partial y} + \frac{\partial^3 h_1}{\partial y^3} \right) + \alpha_s^2 \left(\frac{\partial^3 \theta_1}{\partial x^2 \partial y} + \frac{\partial^3 \theta_1}{\partial y^3} \right) - \frac{\partial \sigma_1}{\partial y} = 0, \end{aligned} \tag{3.39}$$

$$\begin{aligned} &\eta_g \left(\frac{\partial^2 w_1^x}{\partial x^2} + \frac{\partial^2 w_1^y}{\partial x \partial y} \right) + \epsilon_g \left(\frac{\partial^2 w_1^x}{\partial x^2} + \frac{\partial^2 w_1^x}{\partial y^2} \right) - \theta_0 \xi \left(w_1^x - v_1^x \right) \\ &-(f_{sg_0} - f_{gg_0}) \frac{\partial \theta_1}{\partial x} - \frac{f_{sg}}{2} \left(\frac{\partial^3 h_1}{\partial x^3} + \frac{\partial^3 h_1}{\partial x \partial y^2} \right) - \alpha_g^2 \left(\frac{\partial^3 \theta_1}{\partial x^3} + \frac{\partial^3 \theta_1}{\partial x \partial y^2} \right) - \frac{\partial \sigma_1}{\partial x} = 0, \end{aligned} \tag{3.40}$$

$$\begin{aligned} &\eta_g \left(\frac{\partial^2 w_1^x}{\partial x \partial y} + \frac{\partial^2 w_1^y}{\partial y^2} \right) + \epsilon_g \left(\frac{\partial^2 w_1^y}{\partial x^2} + \frac{\partial^2 w_1^y}{\partial y^2} \right) - \theta_0 \xi \left(w_1^y - v_1^y \right) \\ &-(f_{sg_0} - f_{gg_0}) \frac{\partial \theta_1}{\partial y} - \frac{f_{gH_0}}{2} \left(\frac{\partial^3 h_1}{\partial x^2 \partial y} + \frac{\partial^3 h_1}{\partial y^3} \right) - \alpha_g^2 \left(\frac{\partial^3 \theta_1}{\partial x^2 \partial y} + \frac{\partial^3 \theta_1}{\partial y^3} \right) - \frac{\partial \sigma_1}{\partial y} = 0, \end{aligned} \tag{3.41}$$

$$\begin{aligned} &\frac{1}{2} \left[(f_{sH_0} - f_{gH_0}) \left(\frac{\partial^2 \theta_1}{\partial x^2} + \frac{\partial^2 \theta_1}{\partial y^2} \right) + \frac{f_{HH_0}}{2} \left(\frac{\partial^4 h_1}{\partial x^4} + 2 \frac{\partial^4 h_1}{\partial^2 x \partial^2 y} + \frac{\partial^4 h_1}{\partial y_4} \right) \right] \\ &+ (\theta_0 f_{s_0} + (1-\theta_0) f_{g_0} - f_0 + \sigma_0) \left(\frac{\partial^2 h_1}{\partial x^2} + \frac{\partial^2 h_1}{\partial y^2} \right) = 0. \end{aligned} \tag{3.42}$$

We express each perturbation as a linear combination of $e^{\omega_{k,l} t} e^{ikx} e^{ily}$ so that we have

$$\theta_1 = \sum_{k,l} \hat{\theta}_1 e^{\omega_{k,l} t} e^{ikx} e^{ily},$$

$$v_1^x = \sum_{k,l} \hat{v}_1^x e^{\omega_{k,l} t} e^{ikx} e^{ily},$$

$$
\begin{aligned}
v_1^y &= \sum_{k,l} \hat{v}_1^y e^{\omega_{k,l} t} e^{ikx} e^{ily}, \\
w_1^x &= \sum_{k,l} \hat{w}_1^x e^{\omega_{k,l} t} e^{ikx} e^{ily}, \\
&\vdots
\end{aligned}
$$

where the coefficients with hats are constant. Upon substitution into the system 3.36–3.42, we have the following for a given k and l,

$$\omega_{k,l} + \theta_0 \left(ik\hat{v}_1^x + il\hat{v}_1^y\right) = 0, \tag{3.43}$$

$$-\omega_{k,l} + (1-\theta_0) \left(ik\hat{w}_1^x + il\hat{w}_1^y\right) = 0, \tag{3.44}$$

$$\begin{aligned}
&\eta_s(k^2\hat{v}_1^x + kl\hat{v}_1^y) + \epsilon_s(k^2+l^2)\hat{v}_1^x + (1-\theta_0)\xi(\hat{v}_1^x - \hat{w}_1^x) \\
&+ik\left[\left(f_{ss_0} - f_{sg_0} + \alpha_s^2(k^2+l^2)\right)\hat{\theta}_1 - \frac{f_{sH_0}}{2}(k^2+l^2)\hat{h}_1 + \hat{\sigma}_1\right] = 0,
\end{aligned} \tag{3.45}$$

$$\begin{aligned}
&\eta_s(kl\hat{v}_1^x + l^2\hat{v}_1^y) + \epsilon_s(k^2+l^2)\hat{v}_1^y + (1-\theta_0)\xi(\hat{v}_1^y - \hat{w}_1^y) \\
&+il\left[\left(f_{ss_0} - f_{sg_0} + \alpha_s^2(k^2+l^2)\right)\hat{\theta}_1 - \frac{f_{sH_0}}{2}(k^2+l^2)\hat{h}_1 + \hat{\sigma}_1\right] = 0,
\end{aligned} \tag{3.46}$$

$$\begin{aligned}
&\eta_g(k^2\hat{w}_1^x + kl\hat{w}_1^y) + \epsilon_g(k^2+l^2)\hat{w}_1^x + \theta_0\xi(\hat{w}_1^x - \hat{v}_1^x) \\
&+ik\left[\left(f_{sg_0} - f_{gg_0} - \alpha_g^2(k^2+l^2)\right)\hat{\theta}_1 - \frac{f_{gH_0}}{2}(k^2+l^2)\hat{h}_1 + \hat{\sigma}_1\right] = 0,
\end{aligned} \tag{3.47}$$

$$\begin{aligned}
&\eta_g(kl\hat{w}_1^x + l^2\hat{w}_1^y) + \epsilon_g(k^2+l^2)\hat{w}_1^y + \theta_0\xi(\hat{w}_1^y - \hat{v}_1^y) \\
&+il\left[\left(f_{sg_0} - f_{gg_0} - \alpha_g^2(k^2+l^2)\right)\hat{\theta}_1 - \frac{f_{gH_0}}{2}(k^2+l^2)\hat{h}_1 + \hat{\sigma}_1\right] = 0,
\end{aligned} \tag{3.48}$$

$$\begin{aligned}
&\frac{1}{2}\left[(f_{sH_0} - f_{gH_0})(k^2+l^2)\hat{\theta}_1 - \frac{f_{HH_0}}{2}(k^2+l^2)^2\hat{h}_1\right] \\
&+(\theta_0 f_{s_0} + (1-\theta_0)f_{g_0} - f_0 + \sigma_0)(k^2+l^2)\hat{h}_1 = 0.
\end{aligned} \tag{3.49}$$

The system 3.43–3.49 can be written as the matrix equation $M\mathbf{x} = 0$ where $\mathbf{x} = (\hat{\theta}_1, \hat{v}_1^x, \hat{v}_1^y, \hat{w}_1^x, \hat{w}_1^y, \hat{\sigma}_1, \hat{h}_1)$. We solve the equation $\det(M) = 0$ for $\omega_{k,l}$ to yield the following dispersion relationship,

$$\begin{aligned}
\omega_{k,l} = &-\frac{B}{A}(f_{ss_0} + f_{gg_0} - 2f_{sg_0}) \\
&+\frac{B}{A}\frac{(k^2+l^2)\left(f_{sH_0} - f_{gH_0}\right)^2}{(k^2+l^2)f_{HH_0} - 4\left[\theta_0 f_{s_0} + (1-\theta_0)f_{g_0} - f_0 + \sigma_0\right]} - 2\frac{B}{A}(k^2+l^2)\alpha^2,
\end{aligned} \tag{3.50}$$

where

$$B = \theta_0(1-\theta_0)(k^2+l^2), \tag{3.51}$$

and

$$A = (\eta+\epsilon)(k^2+l^2) + \xi, \tag{3.52}$$

and we have assumed for simplicity that $\eta_s = \eta_g = \eta, \epsilon_s = \epsilon_g = \epsilon$, and $\alpha_s = \alpha_g = \alpha$.

The equation for ω_k splits into three parts. The first part describes the mixture's intrinsic nature to phase separate. Using the fact that $\theta_s + \theta_g = 1$, the homogenous free energy density can be written as

$$f^h(\theta_s) = \epsilon_{ss}\theta_s + \epsilon_{gg}(1-\theta_s) + \chi\theta_s(1-\theta_s) + \theta_s \ln\theta_s + (1-\theta_s)\ln(1-\theta_s). \tag{3.53}$$

The expression $f_{ss} + f_{gg} - 2f_{sg}$, evaluated at $\theta_s = \theta_0$ and $\theta_g = 1 - \theta_0$, is the same as the expression $\partial^2 f^h / \partial\theta_s^2$, evaluated at $\theta_s = \theta_0$. The function $f^h(\theta_s)$ is plotted for two different values of χ in Figure 3.2. Figure 3.2a is plotted with $\chi = 1.5$, while Figure 3.2b has $\chi = 2.5$. The self interaction parameters ϵ_{ss} and ϵ_{gg} are taken to be the same in these plots. We notice that for $\chi > 2$, the plot of f^h has a region that is concave down. This concave down region corrosponds to the region where $f_{ss} + f_{gg} - 2f_{sg} < 0$, which destabilizes ω_k. This result matches up with classical phase separation results [15], where a double well potential energy leads to phase separation in the mixture.

The second term describes the effect of curvature on stability. This term is only nonzero when f_{sH_0} and f_{gH_0} are different from each other. Recall that the difference in these two quantities comes from the phases having different bending moduli or spontaneous curvatures. Since $f_{HH_0} > 0$ for a Helfrich-like free energy density, we see that the two

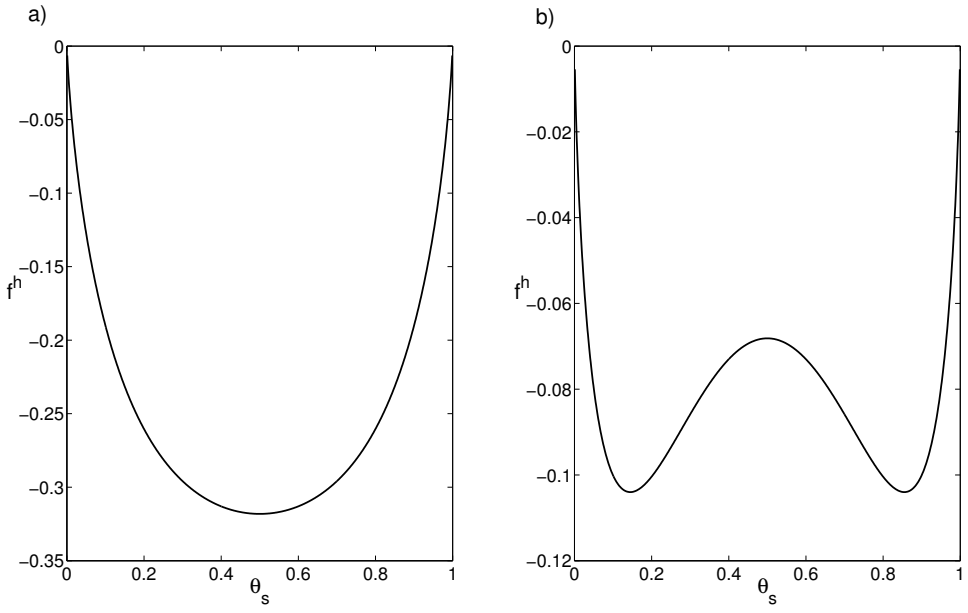

Figure 3.2. Homogeneous free energy density, plotted for different values of χ. a) Homogenous free energy density with $\chi = 1.5$. b) Homogeneous free energy density with $\chi = 2.5$.

phases being different can lead to instability for large wave numbers. Interestingly, low wave numbers can actually be stabilized by curvature if $\theta_0 f_{s_0} + (1-\theta_0) f_{g_0} - f_0 + \sigma_0$ is large and positive. This expression appears as a consequence of the fact that σ_0 is arbitrary for a flat sheet. We will see in the subsequent parametrization that σ_0 must take on a definite value for a nonflat steady state.

The third term in the dispersion relationship describes the effect of the Cahn–Hilliard term, which penalizes sharp gradients in the volume fractions. Because the third term is negative and is higher order in k and l than the first two terms, we see that higher modes are damped out. The damping means that lower order modes may be unstable, while higher order modes are stable. This indicates the existence of a most unstable mode. The most unstable mode will dominate pattern formation in the linear model, an effect that will likely carry over in some degree to the fully nonlinear model. Thus, the conclusion of the Cahn–Hilliard penalty terms in our model leads to pattern formation in a way analogous to the classical Cahn–Hilliard model.

3.2 Axisymmetric Parametrization

3.2.1 Basic Setup and Definitions

We suppose that our surface is axisymmetric and given by

$$\mathbf{r}(u^1, u^2, t) = \mathbf{r}(u, \theta, t) = (x(u,t)\cos(\theta), x(u,t)\sin(\theta), z(u,t))^T, \tag{3.54}$$

where $u \in [0, L]$ parametrizes the generating curve of the axisymmetric shape, and $\theta \in [0, 2\pi]$ is the counterclockwise rotation angle around the z axis. We assume boundary conditions $x(0,t) = x(L,t) = 0$ and $z'(0,t) = z'(L,t) = 0$ where the prime indicates a derivative with respect to u. We further assume that all objects dwelling on the surface (velocities, volume fractions, etc.) are independent of the angle θ so that they too are axisymmetric. Note that this implies that $v^u(0,t) = v^u(L,t) = w^u(0,t) = w^u(L,t) = 0$. These boundary conditions mean that any boundary contributions arising from integrating by parts in the orignal derivation described in Chapter 2 are identically zero. For notational expediency, we suppress the u and t dependence in the following derivation. A schematic picture of our axisymmetric surface is shown in Figure 3.3.

The two tangent vectors are given by

$$\mathbf{t}_u = (x'\cos(\theta), x'\sin(\theta), z')^T \tag{3.55}$$

and

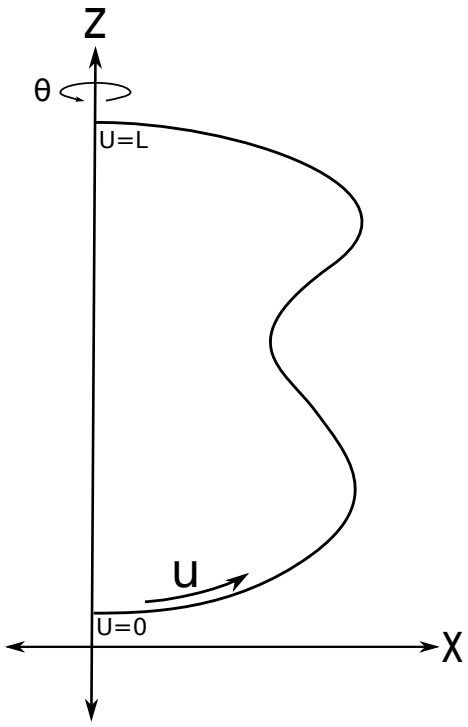

Figure 3.3. An axisymmetric surface.

$$\mathbf{t}_\theta = (-x\sin(\theta), x\cos(\theta), 0)^T. \tag{3.56}$$

This gives a metric tensor of

$$a_{\alpha\beta} = \begin{pmatrix} p^2 & 0 \\ 0 & x^2 \end{pmatrix}, \tag{3.57}$$

where $p^2 = x'^2 + z'^2$ and $\alpha, \beta = u, \theta$. The determinant of the metric tensor is given by

$$a = \det(a_{\alpha\beta}) = p^2 x^2. \tag{3.58}$$

The inverse metric tensor is given by

$$a^{\alpha\beta} = \begin{pmatrix} \frac{1}{p^2} & 0 \\ 0 & \frac{1}{x^2} \end{pmatrix}, \tag{3.59}$$

and inward unit normal vector by

$$\begin{aligned} \mathbf{n} &= \frac{\mathbf{t}_u \times \mathbf{t}_\theta}{\sqrt{a}} \\ &= \frac{1}{p}(-z'\cos(\theta), -z'\sin(\theta), x')^T. \end{aligned} \tag{3.60}$$

Note that we use the inward unit normal so that the mean curvature of a sphere will be a positive constant instead of a negative constant. The coefficients of the second fundamental

form are given by $b_{\alpha\beta} = \frac{\partial^2 \mathbf{r}}{\partial u^\alpha \partial u^\beta} \cdot \mathbf{n}$. This yields

$$b_{\alpha\beta} = \begin{pmatrix} \frac{q}{p} & 0 \\ 0 & \frac{xz'}{p} \end{pmatrix}, \tag{3.61}$$

where $q = -x''z' + x'z''$. To define the mean and Gaussian curvatures, we need

$$b^\alpha_\beta = a^{\alpha\gamma} b_{\gamma\beta} = \begin{pmatrix} \frac{q}{p^3} & 0 \\ 0 & \frac{z'}{px} \end{pmatrix}. \tag{3.62}$$

From that we have the mean curvature

$$H = \frac{1}{2}\mathrm{Tr}(b^\alpha_\beta) = \frac{1}{2}\left(\frac{q}{p^3} + \frac{z'}{px}\right), \tag{3.63}$$

and the Gaussian curvature

$$K = \det\left(b^\alpha_\beta\right) = \frac{qz'}{p^4 x}. \tag{3.64}$$

We will also need

$$b^{\alpha\beta} = a^{\alpha\lambda} a^{\beta\mu} b_{\lambda\mu} = \begin{pmatrix} \frac{q}{p^5} & 0 \\ 0 & \frac{z'}{px^3} \end{pmatrix} \tag{3.65}$$

and

$$b^{\alpha\beta} b_{\alpha\beta} = (4H^2 - 2K) = \left(\frac{q^2}{p^6} + \frac{z'^2}{p^2 x^2}\right). \tag{3.66}$$

The equation

$$\frac{\partial \mathbf{r}}{\partial t} = U_n \mathbf{n} \tag{3.67}$$

implies that

$$\frac{\partial x}{\partial t} = -\frac{z'}{p} U_n \tag{3.68}$$

and

$$\frac{\partial z}{\partial t} = \frac{x'}{p} U_n. \tag{3.69}$$

3.2.2 Full System of Equations

Using the details shown in section B.2, we are able to express the full two phase system derived in Chapter 2 in the axisymmetric parametrization. In what follows, we use f_s, f_g, and f_H to express partial derivatives of the free energy density with respect to θ_s, θ_g, and

H. The full system of equations is given by

$$\frac{\partial \theta_s}{\partial t} + v^u \theta_s' + \theta_s d_v = 0, \quad (3.70)$$

$$\frac{\partial \theta_g}{\partial t} + w^u \theta_g' + \theta_g d_w = 0, \quad (3.71)$$

$$\begin{aligned} &\frac{\eta_s + \epsilon_s}{p^2}\left[\theta_s d_v\right]' + \frac{2\epsilon_s}{p^2}\left[-v^u\left(\frac{p}{x}\right)\left(\frac{x'\theta_s}{p}\right)' + \left(\frac{1}{x}\right)\left(\frac{z'\theta_s U_n}{p}\right)' - \frac{\theta_s q x'}{p^3 x}U_n\right] \\ &-\theta_s\theta_g\xi\left(v^u - w^u\right) - \frac{\theta_s}{p^2}\left[f_s - \frac{\alpha_s^2}{p^2}\left(\theta_s'' - \theta_s'\left(\frac{p'}{p} - \frac{x'}{x}\right)\right) + \sigma\right]' = 0, \end{aligned} \quad (3.72)$$

$$\begin{aligned} &\frac{\eta_g + \epsilon_g}{p^2}\left[\theta_g d_w\right]' + \frac{2\epsilon_g}{p^2}\left[-w^u\left(\frac{p}{x}\right)\left(\frac{x'\theta_g}{p}\right)' + \left(\frac{1}{x}\right)\left(\frac{z'\theta_g U_n}{p}\right)' - \frac{\theta_g q x'}{p^3 x}U_n\right] \\ &-\theta_s\theta_g\xi\left(w^u - v^u\right) - \frac{\theta_g}{p^2}\left[f_g - \frac{\alpha_g^2}{p^2}\left(\theta_g'' - \theta_g'\left(\frac{p'}{p} - \frac{x'}{x}\right)\right) + \sigma\right]' = 0, \end{aligned} \quad (3.73)$$

$$\begin{aligned} &\left(\eta_s + \epsilon_s\right)(2H)\,\theta_s d_v - \frac{2\epsilon_s\theta_s}{p^2}\left[v^u\left(\frac{qx'}{px}\right) + \left(\frac{z'}{x}\right)(pv^u)' - \frac{2qz'}{p^2 x}U_n\right] \\ &+\left(\eta_g + \epsilon_g\right)(2H)\,\theta_g d_w - \frac{2\epsilon_g\theta_g}{p^2}\left[w^u\left(\frac{qx'}{px}\right) + \left(\frac{z'}{x}\right)(pw^u)' - \frac{2qz'}{p^2 x}U_n\right] \\ &-\left(2H^2 - K\right)f_H - \frac{1}{2p^2}\left[f_H'' - f_H'\left(\frac{p'}{p} - \frac{x'}{x}\right)\right] \\ &-\left[\theta_s f_s - \frac{\theta_s\alpha_s^2}{p^2}\left(\theta_s'' - \theta_s'\left(\frac{p'}{p} - \frac{x'}{x}\right)\right) + \theta_g f_g - \frac{\theta_g\alpha_g^2}{p^2}\left(\theta_g'' - \theta_g'\left(\frac{p'}{p} - \frac{x'}{x}\right)\right)\right. \\ &\left. -f - \frac{\alpha_s^2}{2p^2}(\theta_s')^2 - \frac{\alpha_g^2}{2p^2}(\theta_g')^2 + \sigma\right](2H) = 0, \end{aligned} \quad (3.74)$$

$$v^{u\prime} + v^u\left(\frac{p'}{p} + \frac{x'}{x}\right) - \left(\frac{q}{p^3} - \frac{z'}{px}\right)U_n - d_v = 0, \quad (3.75)$$

$$w^{u\prime} + w^u\left(\frac{p'}{p} + \frac{x'}{x}\right) - \left(\frac{q}{p^3} - \frac{z'}{px}\right)U_n - d_w = 0, \quad (3.76)$$

$$\frac{\partial x}{\partial t} + \frac{z'}{p}U_n = 0, \quad (3.77)$$

$$\frac{\partial z}{\partial t} - \frac{x'}{p}U_n = 0, \quad (3.78)$$

$$\frac{\epsilon_s}{p^2}\left\{\left[\theta_s v^{\theta\prime}\right]' + \theta_s v^{\theta\prime}\left(\frac{3x'}{x} - \frac{p'}{p}\right)\right\} - \theta_s\theta_g\xi\left(v^\theta - w^\theta\right) = 0, \quad (3.79)$$

$$\frac{\epsilon_g}{p^2}\left\{\left[\theta_g w^{\theta\prime}\right]' + \theta_g w^{\theta\prime}\left(\frac{3x'}{x} - \frac{p'}{p}\right)\right\} - \theta_s\theta_g\xi\left(w^\theta - v^\theta\right) = 0. \quad (3.80)$$

Notice in the above system the velocities in the u direction, v^u and w^u, are completely decoupled from the velocities in the θ direction, v^θ and w^θ. Clearly, the final two equations can be solved by choosing $v^\theta = w^\theta = 0$. We make this assumption and eliminate the final two equations from the system.

3.2.3 Stability Analysis

3.2.3.1 Steady State

One steady state of the above system is given by

$$\theta_s = \theta_0 = \text{constant}, \tag{3.81}$$

$$\theta_g = 1 - \theta_0, \tag{3.82}$$

$$v^u = 0, \tag{3.83}$$

$$w^u = 0, \tag{3.84}$$

$$U_n = 0, \tag{3.85}$$

$$d_v = 0, \tag{3.86}$$

$$d_w = 0, \tag{3.87}$$

$$H = H_0 = \text{constant}, \tag{3.88}$$

$$K = K_0 = \text{constant}, \tag{3.89}$$

$$\sigma = \sigma_0 = \text{constant}. \tag{3.90}$$

The only $H = \text{constant}$ shape that meets the appropriate boundary conditions is a sphere. Let

$$x_0' = p_0 \cos\left(\frac{\pi}{L}u\right) \tag{3.91}$$

and

$$z_0' = p_0 \sin\left(\frac{\pi}{L}u\right), \tag{3.92}$$

where $p_0 = \text{constant}$. Then

$$x_0'' = -\frac{p_0\pi}{L}\sin\left(\frac{\pi}{L}u\right) \tag{3.93}$$

and

$$z_0'' = \frac{p_0\pi}{L}\cos\left(\frac{\pi}{L}u\right) \tag{3.94}$$

so that

$$\begin{aligned} q_0 &= -x_0''z_0' + x_0'z_0'' \\ &= \frac{p_0^2\pi}{L}. \end{aligned} \tag{3.95}$$

Then

$$\begin{aligned} H_0 &= \frac{1}{2}\left(\frac{q_0}{p_0^3} + \frac{z_0'}{p_0 x_0}\right) \\ &= \frac{\pi}{L p_0} \end{aligned} \tag{3.96}$$

and

$$\begin{aligned} K_0 &= \frac{q_0 z_0'}{p_0^4 x_0} \\ &= \left(\frac{\pi}{L p_0}\right)^2 \\ &= H_0^2, \end{aligned} \tag{3.97}$$

so

$$2H_0^2 - K_0 = H_0^2. \tag{3.98}$$

That means that for the normal force balance equation to be satisfied at steady state, we need

$$\sigma_0 = f_0 - \theta_0 f_{s_0} - (1-\theta_0) f_{g_0} - \frac{H_0}{2} f_{H_0}. \tag{3.99}$$

This is different than what we saw in section 3.1.3 where the steady state value σ_0 was not specified due to the fact that H_0 was zero.

3.2.3.2 Perturbation of Steady State

To explore the stability of the system, we examine a perturbation of the steady state values,

$$\theta_s = \theta_0 + \lambda\theta_1, \tag{3.100}$$

$$\theta_g = 1 - \theta_0 - \lambda\theta_1, \tag{3.101}$$

$$v^u = \lambda v_1, \tag{3.102}$$

$$w^u = \lambda w_1, \tag{3.103}$$

$$U_n = \lambda U_{n_1}, \tag{3.104}$$

$$d_v = \lambda d_{v_1}, \tag{3.105}$$

$$d_w = \lambda d_{w_1}, \tag{3.106}$$

$$H = H_0 + \lambda H_1, \tag{3.107}$$

$$K = K_0 + \lambda K_1, \tag{3.108}$$

$$\sigma = \sigma_0 + \lambda\sigma_1, \tag{3.109}$$

where H_0, K_0, and σ_0 are the steady state values given above.

Substituting the perturbed steady state into the system, using the identities presented in section B.2.5 and keeping first order terms in λ yields the linear system

$$\dot{\theta}_1 + \theta_0 d_{v_1} = 0, \tag{3.110}$$

$$-\dot{\theta}_1 + (1-\theta_0) d_{w_1} = 0, \tag{3.111}$$

$$\begin{aligned}
&(\eta_s + \epsilon_s) d'_{v_1} + 2\epsilon_s \left[v_1 \left(\frac{\pi}{L}\right)^2 + H_0 U'_{n_1} \right] - (1-\theta_0)\xi p_0^2 (v_1 - w_1) \\
&- \left[(f_{ss_0} - f_{sg_0})\theta'_1 + f_{sH_0} H'_1 - \frac{\alpha_s^2}{p_0^2} \left(\theta''_1 + \frac{\pi}{L} \cot\left(\frac{\pi}{L} u\right) \theta'_1 \right)' + \sigma'_1 \right] = 0,
\end{aligned} \tag{3.112}$$

$$\begin{aligned}
&(\eta_g + \epsilon_g) d'_{w_1} + 2\epsilon_g \left[w_1 \left(\frac{\pi}{L}\right)^2 + H_0 U'_{n_1} \right] - \theta_0 \xi p_0^2 (w_1 - v_1) \\
&- \left[(f_{sg_0} - f_{gg_0})\theta'_1 + f_{gH_0} H'_1 + \frac{\alpha_g^2}{p_0^2} \left(\theta''_1 + \frac{\pi}{L} \cot\left(\frac{\pi}{L} u\right) \theta'_1 \right)' + \sigma'_1 \right] = 0,
\end{aligned} \tag{3.113}$$

$$\begin{aligned}
&(\eta_s + \epsilon_s)\theta_0 d_{v_1} - \epsilon_s \theta_0 \left[p_0 H_0 \cot\left(\frac{\pi}{L} u\right) v_1 + v'_1 - 2H_0 U_{n_1} \right] \\
&+ (\eta_g + \epsilon_g)(1-\theta_0) d_{w_1} - \epsilon_g (1-\theta_0) \left[p_0 H_0 \cot\left(\frac{\pi}{L} u\right) w_1 + w'_1 - 2H_0 U_{n_1} \right] \\
&- \frac{1}{4H_0 p_0^2} \left[(f_{sH_0} - f_{gH_0}) \left(\theta''_1 + \frac{\pi}{L} \cot\left(\frac{\pi}{L} u\right) \theta'_1 \right) \right. \\
&\left. + f_{HH_0} \left(H''_1 + \frac{\pi}{L} \cot\left(\frac{\pi}{L} u\right) H'_1 \right) \right] - \frac{H_0}{2} \left[(f_{sH_0} - f_{gH_0})\theta_1 + f_{HH_0} H_1 \right] \\
&+ \frac{f_{H_0}}{2} H_1 - \left\{ \theta_0 \left[(f_{ss_0} - f_{sg_0})\theta_1 + f_{sH_0} H_1 \right] + (1-\theta_0) \left[(f_{sg_0} - f_{gg_0})\theta_1 \right. \right. \\
&\left. \left. + f_{gH_0} H_1 \right] + \frac{(1-\theta_0)\alpha_g^2 - \theta_0 \alpha_s^2}{p_0^2} \left(\theta''_1 + \frac{\pi}{L} \cot\left(\frac{\pi}{L} u\right) \theta'_1 \right) + \sigma_1 \right\} = 0,
\end{aligned} \tag{3.114}$$

$$v'_1 + \frac{\pi}{L} \cot\left(\frac{\pi}{L} u\right) v_1 - 2H_0 U_{n_1} - d_{v_1} = 0, \tag{3.115}$$

$$w'_1 + \frac{\pi}{L} \cot\left(\frac{\pi}{L} u\right) w_1 - 2H_0 U_{n_1} - d_{w_1} = 0, \tag{3.116}$$

where $\dot{\theta}_1$ indicates a partial derivative with respect to time.

3.2.3.3 Derivation of Final Linear Equation for H

Notice that the above system is underdetermined. There are eight unknowns, but only seven equations. The eighth equation comes from the time derivative of H_1. We have

$$2H = \frac{q}{p^3} + \frac{z'}{px}. \tag{3.117}$$

From this, we find

$$2H_1 = \frac{q_1}{p_0^3} - \frac{4\pi}{L p_0^2} p_1 + \frac{\pi}{L p_0^2} \csc\left(\frac{\pi}{L} u\right) z'_1 - \left(\frac{\pi}{L p_0}\right)^2 \csc\left(\frac{\pi}{L} u\right) x_1. \tag{3.118}$$

We now substitue for q_1 and p_1 so that everything is in terms of x and z. Using the definitions of p and q we have

$$p_1 = \cos\left(\frac{\pi}{L}u\right) x_1' + \sin\left(\frac{\pi}{L}u\right) z_1' \tag{3.119}$$

and

$$q_1 = \frac{p_0\pi}{L}\sin\left(\frac{\pi}{L}u\right) z_1' - p_0 \sin\left(\frac{\pi}{L}u\right) x_1'' + p_0\cos\left(\frac{\pi}{L}u\right) z_1'' + \frac{p_0\pi}{L}\cos\left(\frac{\pi}{L}u\right) x_1'. \tag{3.120}$$

Upon substitution, this yields

$$\begin{aligned} 2H_1 = \frac{1}{p_0}\Bigg[&-\frac{3\pi}{L}\sin\left(\frac{\pi}{L}u\right) z_1' + \cos\left(\frac{\pi}{L}u\right) z_1'' - \frac{3\pi}{L}\cos\left(\frac{\pi}{L}u\right) x_1' - \sin\left(\frac{\pi}{L}u\right) x_1''\Bigg] \\ &+ \frac{\pi}{Lp_0^2}\csc\left(\frac{\pi}{L}u\right) z_1' - \left(\frac{\pi}{Lp_0}\right)^2 \csc\left(\frac{\pi}{L}u\right) x_1. \end{aligned} \tag{3.121}$$

We now take the time derivative of both sides to find $\dot{H}_1$ in terms of $\dot{x}_1, \dot{z}_1$ and their derivatives. Given that

$$\dot{x} = -\frac{z'}{p}U_n, \tag{3.122}$$

we have

$$\dot{x}_1 = -\sin\left(\frac{\pi}{L}u\right) U_{n_1}, \tag{3.123}$$

$$\dot{x}_1' = -\frac{\pi}{L}\cos\left(\frac{\pi}{L}u\right) U_{n_1} - \sin\left(\frac{\pi}{L}u\right) U_{n_1}', \tag{3.124}$$

$$\dot{x}_1'' = \left(\frac{\pi}{L}\right)^2 \sin\left(\frac{\pi}{L}u\right) U_{n_1} - \frac{2\pi}{L}\cos\left(\frac{\pi}{L}u\right) U_{n_1}' - \sin\left(\frac{\pi}{L}u\right) U_{n_1}''. \tag{3.125}$$

And from

$$\dot{z} = \frac{x'}{p}U_n, \tag{3.126}$$

we have

$$\dot{z}_1' = -\frac{\pi}{L}\sin\left(\frac{\pi}{L}u\right) U_{n_1} + \cos\left(\frac{\pi}{L}u\right) U_{n_1}' \tag{3.127}$$

$$\dot{z}_1'' = -\left(\frac{\pi}{L}\right)^2 \cos\left(\frac{\pi}{L}u\right) U_{n_1} - \frac{2\pi}{L}\sin\left(\frac{\pi}{L}u\right) U_{n_1}' + \cos\left(\frac{\pi}{L}u\right) U_{n_1}''. \tag{3.128}$$

Substituting into the equation for $\dot{H}_1$ and simplifying, we have

$$2\dot{H}_1 = \frac{1}{p_0^2}\left[U_{n_1}'' + \frac{\pi}{L}\cot\left(\frac{\pi}{L}u\right) U_{n_1}'\right] + 2H_0^2 U_{n_1}. \tag{3.129}$$

This is the eighth equation necessary to close the system.

3.2.3.4 Eigenfunctions of the system

In section 3.1.3, we expressed each perturbation as a linear combination of the eigenfunctions of the system so we could derive a system of linear equations. In order to more easily find the eigenfunctions of our system, we first make a change of variables. Let

$$s = \cos\left(\frac{\pi}{L}u\right). \tag{3.130}$$

Then

$$\frac{d}{du} = -\frac{\pi}{L}\sqrt{1-s^2}\frac{d}{ds} \tag{3.131}$$

and

$$\frac{d^2}{du^2} = \left(\frac{\pi}{L}\right)^2\left((1-s^2)\frac{d^2}{ds^2} - s\frac{d}{ds}\right). \tag{3.132}$$

This yields the system

$$\dot{\theta}_1 + \theta_0 d_{v_1} = 0, \tag{3.133}$$

$$-\dot{\theta}_1 + (1-\theta_0)d_{w_1} = 0, \tag{3.134}$$

$$\begin{aligned}(\eta_s+\epsilon_s)\left(-\sqrt{1-s^2}\right)d'_{v_1} + 2\epsilon_s\left[p_0H_0v_1 + H_0\left(-\sqrt{1-s^2}\right)U'_{n_1}\right]\\ -(1-\theta_0)\xi\left(\frac{p_0}{H_0}\right)(v_1-w_1)\end{aligned} \tag{3.135}$$

$$-\left(-\sqrt{1-s^2}\right)\left[(f_{ss_0}-f_{sg_0})\theta'_1 + f_{sH_0}H'_1 - \alpha_s^2H_0^2\left((1-s^2)\theta''_1 - 2s\theta'_1\right)' + \sigma'_1\right] = 0,$$

$$\begin{aligned}(\eta_g+\epsilon_g)\left(-\sqrt{1-s^2}\right)d'_{w_1} + 2\epsilon_g\left[p_0H_0w_1 + H_0\left(-\sqrt{1-s^2}\right)U'_{n_1}\right]\\ -\theta_0\xi\left(\frac{p_0}{H_0}\right)(w_1-v_1)\end{aligned} \tag{3.136}$$

$$-\left(-\sqrt{1-s^2}\right)\left[(f_{sg_0}-f_{gg_0})\theta'_1 + f_{gH_0}H'_1 + \alpha_g^2H_0^2\left((1-s^2)\theta''_1 - 2s\theta'_1\right)' + \sigma'_1\right] = 0,$$

$$\begin{aligned}\theta_0\left\{(\eta_s+\epsilon_s)d_{v_1} - \epsilon_sH_0\left[p_0\left(\frac{s}{\sqrt{1-s^2}}v_1 - \sqrt{1-s^2}v'_1\right) - 2U_{n_1}\right]\right\}\\ +(1-\theta_0)\left\{(\eta_g+\epsilon_g)d_{w_1} - \epsilon_gH_0\left[p_0\left(\frac{s}{\sqrt{1-s^2}}w_1 - \sqrt{1-s^2}w'_1\right) - 2U_{n_1}\right]\right\}\\ -\frac{H_0}{4}\left[(f_{sH_0}-f_{gH_0})\left((1-s^2)\theta''_1 - 2s\theta'_1\right) + f_{HH_0}\left((1-s^2)H''_1 - 2sH'_1\right)\right]\\ -\frac{H_0}{2}\left((f_{sH_0}-f_{gH_0})\theta_1 + f_{HH_0}H_1\right) + \frac{f_{H_0}}{2}H_1\\ -\left[\theta_0((f_{ss_0}-f_{sg_0})\theta_1 + f_{sH_0}H_1) + (1-\theta_0)((f_{sg_0}-f_{gg_0})\theta_1 + f_{gH_0}H_1)\right.\\ \left.+((1-\theta_0)\alpha_g^2 - \theta_0\alpha_s^2)H_0^2\left((1-s^2)\theta''_1 - 2s\theta'_1\right) + \sigma_1\right] = 0,\end{aligned} \tag{3.137}$$

$$p_0H_0\left(\frac{s}{\sqrt{1-s^2}}v_1 - \sqrt{1-s^2}v'_1\right) - 2H_0U_{n_1} - d_{v_1} = 0, \tag{3.138}$$

$$p_0H_0\left(\frac{s}{\sqrt{1-s^2}}w_1 - \sqrt{1-s^2}w'_1\right) - 2H_0U_{n_1} - d_{w_1} = 0, \tag{3.139}$$

$$-2\dot{H}_1 + H_0^2\left[(1-s^2)U''_{n_1} - 2sU'_{n_1}\right] + 2H_0^2U_{n_1} = 0, \tag{3.140}$$

where the prime now indicates a partial derivative with respect to s.

We can notice in the above system a combination of Legendre and associated Legendre

functions multiplied by exponentials in time work as eigenfunctions. We assume

$$\theta_1 = \hat{\theta}_1 e^{\omega_n t} P_n(s), \tag{3.141}$$

$$v_1 = \hat{v}_1 e^{\omega_n t} P_n^1(s), \tag{3.142}$$

$$w_1 = \hat{w}_1 e^{\omega_n t} P_n^1(s), \tag{3.143}$$

$$U_{n_1} = \hat{U}_{n_1} e^{\omega_n t} P_n(s), \tag{3.144}$$

$$d_{v_1} = \hat{d}_{v_1} e^{\omega_n t} P_n(s), \tag{3.145}$$

$$d_{w_1} = \hat{d}_{w_1} e^{\omega_n t} P_n(s), \tag{3.146}$$

$$H_1 = \hat{H}_1 e^{\omega_n t} P_n(s), \tag{3.147}$$

$$\sigma_1 = \hat{\sigma}_1 e^{\omega_n t} P_n(s), \tag{3.148}$$

where $P_n(s)$ is the Legendre function of the first kind of order n, and $P_n^1(s)$ is the associated Legendre function of order n defined by

$$P_n^1(s) = -\sqrt{1-s^2}\frac{dP_n(s)}{ds}. \tag{3.149}$$

We note that

$$(1-s^2)\frac{d^2P_n}{ds^2} - 2s\frac{dP_n}{ds} = -n(n+1)P_n \tag{3.150}$$

and

$$\begin{aligned} &\frac{s}{\sqrt{1-s^2}}\left(-\sqrt{1-s^2}\frac{dP_n}{ds}\right) - \sqrt{1-s^2}\frac{d}{ds}\left(-\sqrt{1-s^2}\frac{dP_n}{ds}\right) \\ &= (1-s^2)\frac{d^2P_n}{ds^2} - 2s\frac{dP_n}{ds} \\ &= -n(n+1)P_n. \end{aligned} \tag{3.151}$$

After substitution into the system, we end up with the linear system

$$\omega\hat{\theta}_1 + \theta_0\hat{d}_{v_1} = 0, \tag{3.152}$$

$$-\omega\hat{\theta}_1 + (1-\theta_0)\hat{d}_{w_1} = 0, \tag{3.153}$$

$$\begin{aligned} (\eta_s + \epsilon_s)\hat{d}_{v_1} + 2\epsilon_s\left[p_0 H_0 \hat{v}_1 + H_0\hat{U}_{n_1}\right] - (1-\theta_0)\xi\left(\frac{p_0}{H_0}\right)(\hat{v}_1 - \hat{w}_1) \\ - \left[(f_{ss_0} - f_{sg_0} + n(n+1)H_0^2\alpha_s^2)\hat{\theta}_1 + f_{sH_0}\hat{H}_1 + \hat{\sigma}_1\right] = 0, \end{aligned} \tag{3.154}$$

$$\begin{aligned} (\eta_g + \epsilon_g)\hat{d}_{w_1} + 2\epsilon_g\left[p_0 H_0 w_1 + H_0\hat{U}_{n_1}\right] - \theta_0\xi\left(\frac{p_0}{H_0}\right)(\hat{w}_1 - \hat{v}_1) \\ - \left[(f_{gs_0} - f_{gg_0} - n(n+1)H_0^2\alpha_g^2)\hat{\theta}_1 + f_{gH_0}\hat{H}_1 + \hat{\sigma}_1\right] = 0, \end{aligned} \tag{3.155}$$

$$\begin{aligned}
&\theta_0\left\{(\eta_s+\epsilon_s)\hat{d}_{v_1}+\epsilon_s\left[p_0H_0n(n+1)\hat{v}_1+2H_0\hat{U}_{n_1}\right]\right\}\\
&+(1-\theta_0)\left\{(\eta_g+\epsilon_g)\hat{d}_{w_1}+\epsilon_g\left[p_0H_0n(n+1)\hat{w}_1+2H_0\hat{U}_{n_1}\right]\right\}\\
&+\left(\frac{H_0}{4}n(n+1)-\frac{H_0}{2}\right)\left[(f_{sH_0}-f_{gH_0})\hat{\theta}_1+f_{HH_0}\hat{H}_1\right]+\frac{f_{H_0}}{2}\hat{H}_1 \qquad (3.156)\\
&-\Big[\theta_0((f_{ss_0}-f_{sg_0}+n(n+1)H_0^2\alpha_s^2)\hat{\theta}_1+f_{sH_0}\hat{H}_1)\\
&+(1-\theta_0)((f_{sg_0}-f_{gg_0}-n(n+1)H_0^2\alpha_g^2)\hat{\theta}_1+f_{gH_0}\hat{H}_1)+\hat{\sigma}_1\Big]=0,\\
&-p_0H_0n(n+1)\hat{v}_1-2H_0\hat{U}_{n_1}-\hat{d}_{v_1}=0, \qquad (3.157)\\
&-p_0H_0n(n+1)\hat{w}_1-2H_0\hat{U}_{n_1}-\hat{d}_{w_1}=0, \qquad (3.158)\\
&-2\omega\hat{H}_1-H_0^2n(n+1)\hat{U}_{n_1}+2H_0^2\hat{U}_{n_1}=0. \qquad (3.159)
\end{aligned}$$

3.2.3.5 Dispersion Relationship

This linear system 3.152–3.159 can be written as the matrix equation $M\mathbf{x}=0$ where

$$\mathbf{x}=(\hat{\theta}_1,\hat{d}_{v_1},\hat{d}_{w_1},\hat{v}_1,\hat{w}_1,\hat{U}_{n_1},\hat{H}_1,\hat{\sigma}_1)^T, \qquad (3.160)$$

and M is a matrix of the coefficients given in the above system. For $\mathbf{x}\neq\mathbf{0}$, the system is only satisfied if $\det(M)=0$. Under the assumptions $\epsilon_s=\epsilon_g=\epsilon,\eta_s=\eta_g=\eta$ and $\alpha_s=\alpha_g=\alpha$, the expression $\det(M)$ is the following quadratic polynomial in ω_n,

$$\begin{aligned}
&A\epsilon\omega_n^2\\
&+n(n+1)\left\{\frac{A}{16}\left[2H_0f_{H_0}+(n-1)(n+2)H_0^2f_{HH_0}\right]\right.\\
&\quad\left.+B\epsilon\left[(f_{ss_0}+f_{gg_0}-2f_{sg_0})+2n(n+1)H_0^2\alpha^2\right]\right\}\omega_n\\
&+\frac{n^2(n+1)^2B}{16}\left\{-(n-1)(n+2)H_0^2\left(f_{sH_0}-f_{gH_0}\right)^2\right.\\
&\left.+\left[2H_0f_{H_0}+(n-1)(n+2)H_0^2f_{HH_0}\right]\left[(f_{ss_0}+f_{gg_0}-2f_{sg_0})+2n(n+1)H_0^2\alpha^2\right]\right\}=0,
\end{aligned} \qquad (3.161)$$

where

$$A=H_0^2(\eta+\epsilon)n(n+1)-2H_0^2\epsilon+\xi \qquad (3.162)$$

$$B=H_0^2\theta_0(1-\theta_0). \qquad (3.163)$$

For $n=0$, the above polynomial becomes $A\epsilon\omega_n^2=0$. Thus, the $n=0$ mode is time independent. This mode corresponds to the Legendre polynomial $P_0(\cos(\pi u/L))=1$. To understand the meaning of this mode, we look at the resulting shape when the mode is perturbed. Recall that the shape evolution is given by

$$\dot{x}=-\frac{z'}{p}U_n, \qquad (3.164)$$

$$\dot{z} = \frac{x'}{p} U_n. \tag{3.165}$$

That means that the first order perturbations of x and z for $n = 0$ are given by

$$\dot{x}_1 = -\sin\left(\frac{\pi}{L}u\right) U_{n_1}, \tag{3.166}$$

$$\dot{z}_1 = \cos\left(\frac{\pi}{L}u\right) U_{n_1}. \tag{3.167}$$

Since U_{n_1} is a linear combination of exponentials in time multipled by Legendre polynomials, we see that for $n = 0$, x_1 is $-\sin(\pi u/L)\hat{U}_{n_1} t$ and z_1 is $\cos(\pi u/L)\hat{U}_{n_1} t$. Since the original sphere is given by $x_0 = p_0 L/\pi \sin(\pi u/L), z_0 = -p_0 L/\pi \cos(\pi u/L)$, it follows that the $n = 0$ mode is simply a contraction or expansion of the sphere. Since the total area is fixed, it is clear that this mode has no effect on shape.

In the derivation of the polynomial, we divided by $n-1$. Thus, the equation $\det(M) = 0$ is true for $n = 1$ regardless of the ω_n value chosen. The $n = 1$ mode corresponds to the Legendre polynomial $P_1(\cos(\pi u/L)) = \cos(\pi u/L)$. For this mode, the shape is given by

$$x = \frac{p_0 L}{\pi} \sin\left(\frac{\pi}{L}u\right) - \lambda \frac{\hat{U}_{n_1}}{\omega_1} e^{\omega_1 t} \sin\left(\frac{\pi}{L}u\right) \cos\left(\frac{\pi}{L}u\right) + \mathcal{O}(\lambda^2) \tag{3.168}$$

$$z = -\frac{p_0 L}{\pi} \cos\left(\frac{\pi}{L}u\right) + \lambda \frac{\hat{U}_{n_1}}{\omega_1} e^{\omega_1 t} \cos^2\left(\frac{\pi}{L}u\right) + \mathcal{O}(\lambda^2). \tag{3.169}$$

Consider a small perturbation to the parametrization given by $U = u + \lambda\phi(u)$, where ϕ is some unknown function. Expanding in λ yields

$$x = \frac{p_0 L}{\pi} \sin\left(\frac{\pi}{L}u\right) + \lambda \cos\left(\frac{\pi}{L}u\right) \left[p_0 \phi(u) - \frac{\hat{U}_{n_1}}{\omega_1} e^{\omega_1 t} \sin\left(\frac{\pi}{L}u\right)\right] + \mathcal{O}(\lambda^2) \tag{3.170}$$

$$z = -\frac{p_0 L}{\pi} \cos\left(\frac{\pi}{L}u\right) + \lambda \left[p_0 \sin\left(\frac{\pi}{L}u\right) \phi(u) + \frac{\hat{U}_{n_1}}{\omega_1} e^{\omega_1 t} \cos^2\left(\frac{\pi}{L}u\right)\right] + \mathcal{O}(\lambda^2). \tag{3.171}$$

Choose

$$\phi(u) = \frac{\hat{U}_{n_1}}{\omega_1 p_0} e^{\omega_1 t} \sin\left(\frac{\pi}{L}u\right). \tag{3.172}$$

Then we have

$$x = \frac{p_0 L}{\pi} \sin\left(\frac{\pi}{L}u\right) + \mathcal{O}(\lambda^2) \tag{3.173}$$

$$z = -\frac{p_0 L}{\pi} \cos\left(\frac{\pi}{L}u\right) + \lambda \left(\frac{\hat{U}_{n_1}}{\omega_1} e^{\omega_1 t}\right) + \mathcal{O}(\lambda^2). \tag{3.174}$$

We see via the reparametrization that to first order in λ, the $n = 1$ mode corresponds to a vertical translation, but not a change in shape. In the following section, we explore the dispersion relationship for $n > 1$.

3.2.3.6 Analysis of the Dispersion Relationship

To analyze the behavior of the dispersion relationship 3.161, recall the behavior of the roots of the quadratic equation

$$\alpha\omega^2 + \beta\omega + \gamma = 0, \tag{3.175}$$

for $\alpha > 0$ as shown in Figure 3.4. If either β or γ is negative, at least one of the roots has positive real part. For our situation, we can calculate that $\beta^2 - 4\alpha\gamma > 0$, so the roots of the dispersion relationship are always real.

By examining the dispersion relationship, we notice that there are essentially three important expressions that highlight three different paths to instability. These three expressions are

$$(f_{ss_0} + f_{gg_0} - 2f_{sg_0}) + 2n(n+1)H_0^2\alpha^2, \tag{3.176}$$

$$2H_0 f_{H_0} + (n-1)(n+2)H_0^2 f_{HH_0}, \tag{3.177}$$

and

$$(n-1)(n+2)H_0^2\left(f_{sH_0} - f_{gH_0}\right)^2. \tag{3.178}$$

The first two expressions appear added together in the β coefficient and multiplied in the γ coefficient. The third appears subtracted in the γ coefficient.

Expression 3.176 describes the tendency for phase separation to occur when the interaction parameter χ is large enough. For $\chi > 2$, $f_{ss_0} + f_{gg_0} - 2f_{sg_0} < 0$. This effect is similar to the effect seen in the dispersion relationship for the Monge parametrization seen earlier in this chapter. The second part of the expression shows the stabilizing effect of the Cahn–Hilliard penalty terms. As expected, this stabilizing effect dominates all other effects

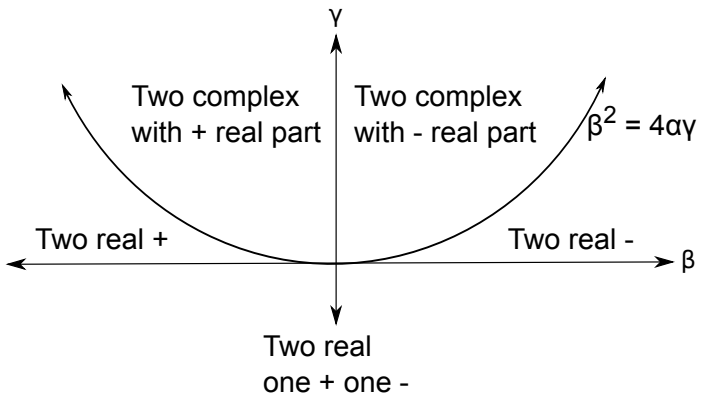

Figure 3.4. Behavior of quadratic roots.

in the dispersion relationship for large enough n so that high wave numbers are always stable. We note that the stabilization is more important for smaller spherical steady states (large H_0).

Expression 3.177 describes instability caused by the steady state curvature being smaller than the preferred curvature. This is an effect that was not seen in the Monge parametrization. If both phases have a nonzero and positive spontaneous curvature, then $f_{H_0} < 0$ for H_0 small enough. This effect is only important for small n due to the fact that $f_{HH_0} > 0$.

Expression 3.178 describes instability caused by the two phases responding differently to curvature. This same effect was seen in the analyses of both the one dimensonal model and the Monge parametrization. We notice that the two phases being different is always destabilizing and that this effect is more pronounced for smaller spherical steady states.

Since full dispersion relationship for the axisymmetric parametrization is quite complicated, we seek to understand it more fully by examining three cases. First, we assume that the free energy density is independent of curvature. In this case, the two solutions of the dispersion relationship are given by

$$\omega_n = 0 \tag{3.179}$$

$$\omega_n = -\frac{n(n+1)B}{A}(f_{ss_0} + f_{gg_0} - 2f_{sg_0}) - \frac{2n^2(n+1)^2B}{A}H_0^2\alpha^2. \tag{3.180}$$

As expected, stability depends on the value of χ, but not on shape. We note that though instability exists, this instability affects the tangential flow of the lipids, but does not affect the shape of the membrane. We can see this by examining the matrix M. For f independent of H, the matrix M can be modified using elementary row operations, which do not change the value of the determinant to have the block diagonal form

$$M = \begin{pmatrix} M_{11} & 0 \\ 0 & M_{22} \end{pmatrix}, \tag{3.181}$$

where

$$M_{11} = \begin{pmatrix} \omega_n & \theta & 0 & 0 & 0 \\ 0 & \theta & 1-\theta & 0 & 0 \\ 0 & 0 & 1 & 0 & p_0H_0n(n+1) \\ 0 & 0 & 0 & p_0H_0n(n+1) & \frac{(1-\theta_0)p_0H_0n(n+1)}{\theta_0} \\ 0 & 0 & 0 & 0 & -\frac{p_0}{\omega_nH_0\theta}\{Bn(n+1)[(f_{ss_0}+f_{gg_0}-2f_{sg_0}) \\ & & & & +2n(n+1)H_0^2\alpha^2] + A\omega_n\} \end{pmatrix}, \tag{3.182}$$

and

$$M_{22} = \begin{pmatrix} \frac{2H_0(n-1)(n+2)\epsilon}{n(n+1)} & 0 & 0 \\ \frac{H_0^2}{2}(n-1)(n+2) & \omega_n & 0 \\ 0 & 0 & -1 \end{pmatrix}. \tag{3.183}$$

We see that equation 3.179 corresponds to $\det M_{22} = 0$, while equation 3.180 corresponds to $\det M_{11} = 0$. This means that for nonzero ω_n given by equation 3.180, the expansion coefficients $\hat{U}_{n_n}, \hat{H}_n$, and $\hat{\sigma}_n$ must be zero. Thus the instability affects the distributions and velocities of the volume fractions but does not correspond to a change in membrane shape.

We see the instability graphically in Figure 3.5. Figure 3.5a shows a plot of the positive root of the dispersion relationship when $\chi = 2.5, H = 0.05$, and $\alpha = 0$. Figure 3.5b shows the same plot for $\chi = 2.5, H = 0.05$, and $\alpha = 1$. Notice how nonzero α damps out higher wave numbers so that there exists a most unstable mode. Unless otherwise specified, the parameters in this and all subsequent figures are $\eta = \epsilon = \xi = K_bT = \nu = 1$.

For our second case, we suppose $\kappa_s = \kappa_g$ and $C_s = C_g$ so that the two phases respond similarly to curvature. This implies that $f_{sH_0} = f_{gH_0}$. Under these conditions, the dispersion relationship can be factored to reveal the two roots

$$\omega_n^b = -\frac{n(n+1)}{16\epsilon}\left(2H_0 f_{H_0} + (n-1)(n+2)H_0^2 f_{HH_0}\right), \tag{3.184}$$

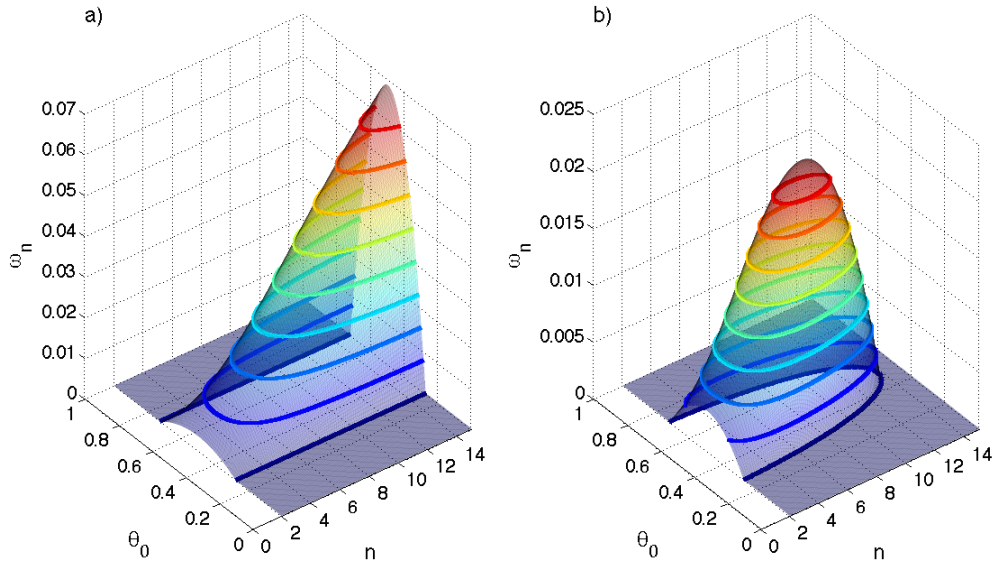

Figure 3.5. Stability for free energy independent of curvature. a) The positive root of the dispersion relationship plotted as a function of θ_0 and n for $\chi = 2.5$ and $\alpha = 0$. b) The positive root of the dispersion relationship plotted as a function of θ_0 and n for $\chi = 2.5$ and $\alpha = 1$. The contour lines in both figures are merely present for ease of visualization.

$$\omega_n^s = -\frac{n(n+1)B}{A}(f_{ss_0} + f_{gg_0} - 2f_{sg_0}) - \frac{2n^2(n+1)^2B}{A}H_0^2\alpha^2. \tag{3.185}$$

The superscript b indicates that the root depends on the resistance to bending, while the superscript s indicates dependence on the homogenous free energy density without bending. Notice that the root 3.185 is the same as the root 3.180 that we found when the free energy density was independent of curvature.

We can see from equations 3.184–3.185 that instability can arise in two different ways. It can arise either because H_0 is smaller than the spontaneous curvature of the two phases, or because χ is sufficiently large. We can see these two types of behavior in Figure 3.6. We have plotted the largest positive root of the dispersion relationship as a function of θ_0 and n for $\kappa_s = \kappa_g = C_s = C_g = 1, \chi = 2.5, H_0 = 0.05$, and $\alpha = 1$. Notice how there are two distinct bulges. The first corresponds to ω_n^b, while the second corresponds to ω_n^s. The heavy red curve shows ω_n^b, while the heavy black curve shows ω_n^s, each plotted for $\theta_0 = 0.5$. We can see that the two curves cross, giving rise to the two different bulges in the surface. We note that both bulges disappear for large enough H_0. The first because of the $H_0^2 f_{HH_0}$ term in ω_n^b and the second because of the $H_0^2\alpha^2$ term in ω_n^s.

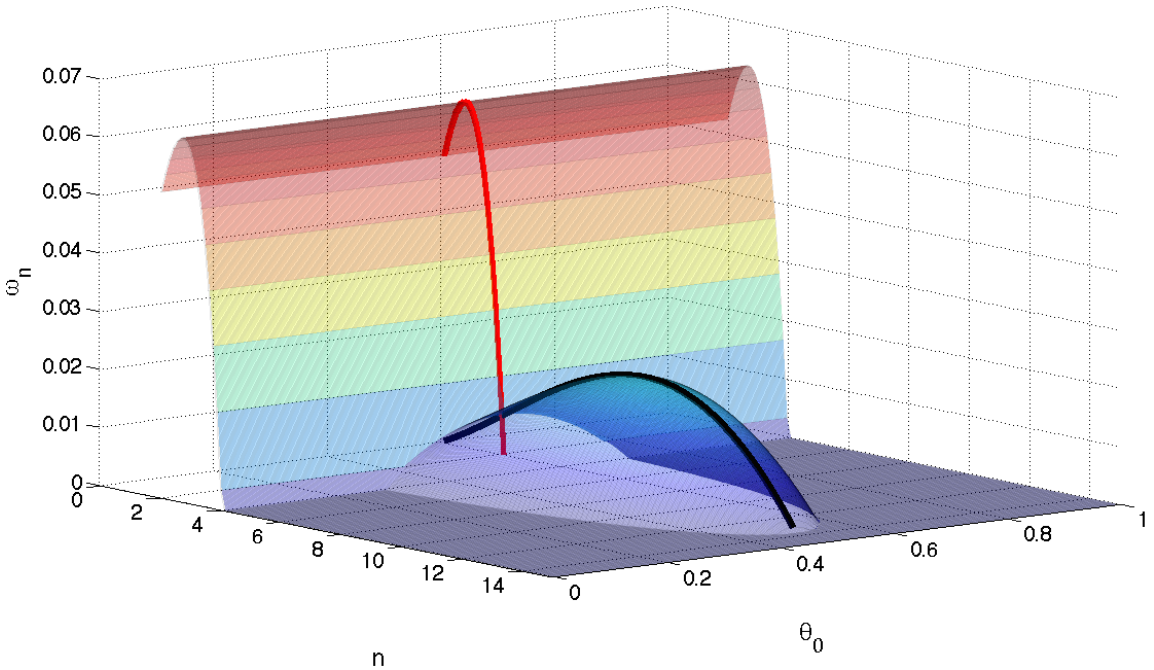

Figure 3.6. Stability for phases with the same constants. Parameter values are $\kappa_s = \kappa_g = C_s = C_g = 1, \chi = 2.5, H = 0.05$, and $\alpha = 1$. The heavy red curve is a plot of ω_n^b for $\theta_0 = 0.5$. The heavy black curve is a plot of ω_n^s for $\theta_0 = 0.5$.

It is somewhat surprising that there is curvature induced instability in the case where $\kappa_s = \kappa_g$ and $C_s = C_g$. In this case, the curvature dependent terms in the free energy density are given by

$$\frac{\kappa_s\theta_s}{2}(2H - C_s)^2 + \frac{\kappa_s\theta_g}{2}(2H - C_s)^2 = \frac{\kappa_s}{2}(2H - C_s)^2 \tag{3.186}$$

so that curvature and volume fraction are decoupled. Given this fact, we would not expect phase separation and shape changes to affect each other. We will see that this intuition is valid.

For $f_{sH_0} = f_{gH_0}$, we are again able to perform elementary row operations on the matrix M to write it in the block diagonal form

$$M = \begin{pmatrix} M_{11} & 0 \\ 0 & M_{22} \end{pmatrix}. \tag{3.187}$$

The matrix M_{11} is the same as 3.182 corresponding to ω_n^s, but M_{22} is now given by

$$M_{22} = \begin{pmatrix} \frac{H_0(n-1)(n+2)}{8n(n+1)\omega_n}\left[n(n+1)(2H_0 f_{H_0}\right. & 0 & 0 \\ \left.+(n-1)(n+2)H_0^2 f_{HH_0}) + 16\epsilon\omega_n\right] & & \\ \frac{H_0^2}{2}(n-1)(n+2) & \omega_n & 0 \\ 0 & \frac{1}{4}\left[2f_{H_0} + (n-1)(n+2)f_{HH_0}\right] & -1 \\ & -f_{gH_0} & \end{pmatrix}, \tag{3.188}$$

corresponding to ω_n^b. Thus when $\omega = \omega_n^s$, we have that $\theta_1, d_{v_1}, d_{w_1}, v_1$, and w_1 are nonzero, but U_{n_1}, H_1, and σ_1 are identically zero. Similarly, when $\omega = \omega_n^b$, we have that $\theta_1, d_{v_1}, d_{w_1}$, v_1, and w_1 are identically zero, but U_{n_1}, H_1, and σ_1 are nonzero. It follows that shape changes and tangential lipid flow are decoupled when $f_{sH_0} = f_{gH_0}$.

For our third case, we suppose that the two phases respond differently to curvature. In this most general situation, shape and tangential lipid flow are no longer decoupled. In this case, we can truly have curvature induced lipid flow. All three expressions 3.176–3.178 affect the stability of the steady state with 3.176 and 3.177 having a larger effect for smaller H_0 values and 3.178 having a larger effect for larger H_0 values. We can see the effect of changing H_0 in Figure 3.7 where we have plotted the zero isosurface of ω_n. Parameter values are $\kappa_s = 6, \kappa_g = 1, C_s = 2, C_g = 1$, and $\alpha = 1$. We have also used $\chi = 0$, so we only see instability caused by curvature. Spherical steady states with mean curvature smaller than the preferred curvatures of the two phases correspond to regions below the lower surface and are unstable due to the effect of expression 3.177. This is similar to the second case where the phases responded similarly to curvature. In this third case, we have a new source of instability. Spherical steady states with mean curvature much larger than the preferred

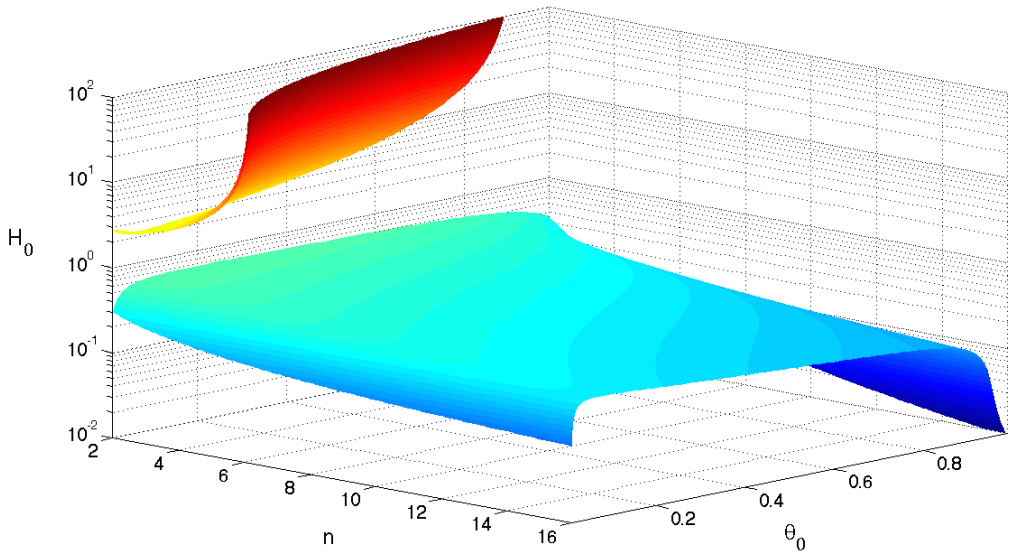

Figure 3.7. Zero Isosurface of ω_n. Parameter values are $\kappa_s = 6$, $\kappa_g = 1$, $C_s = 2$, $C_g = 1, \chi = 0$, and $\alpha = 1$. Regions below the lower surface and above the upper surface are unstable.

curvatures of the two lipids correspond to regions above the upper surface and are unstable due to the effect of expression 3.178.

While Figure 3.7 provides information about stability as a function of θ_0, n, and H_0, it does not provide information about the most unstable modes or the resulting shape. It is possible to extract this information from the linear stability analysis results. We first choose a mean curvature H_0. This allows us to plot the largest possible root of ω_n as a function of θ_0 and n as shown in Figure 3.8a. We have chosen $H_0 = 0.3$ and all other parameter values the same as Figure 3.7. We see that the surface has a maximum at approximately $\theta_0 = 0.4$ and $n = 4$. Thus for $H_0 = 0.3$ and $\theta_0 = 0.4$, the pattern formation will be dominated by P_4 and P_4^1. We have plotted the Legendre polynomial $P_4(\cos(u))$ for $u \in [0, \pi]$ in Figure 3.8b. Since we have a specific value of ω_n for our given values of H_0, θ_0 and n, we can substitute that value into the matrix M. This value of ω_n makes M singular so that it has a nontrivial null space. The null vector of M describes the relationship between the expansion coefficients of the perturbations from the steady state values. We have used this relationship in Figures 3.8c and d. In Figure 3.8c, we plot the perturbed generating curve using $\theta_0 = 0.4, n = 4$, and the small expansion parameter $\lambda = 0.1$. The arrows correspond to U_{n_1} and show the motion of the surface. In Figure 3.8d, we plot the perturbed shape with overlaid perturbed θ_s distribution. In this figure, $H_0 = 0.3$ is smaller than the two preferred curvatures $C_s = 2$ and $C_g = 1$. Because θ_s has a larger bending modulus than

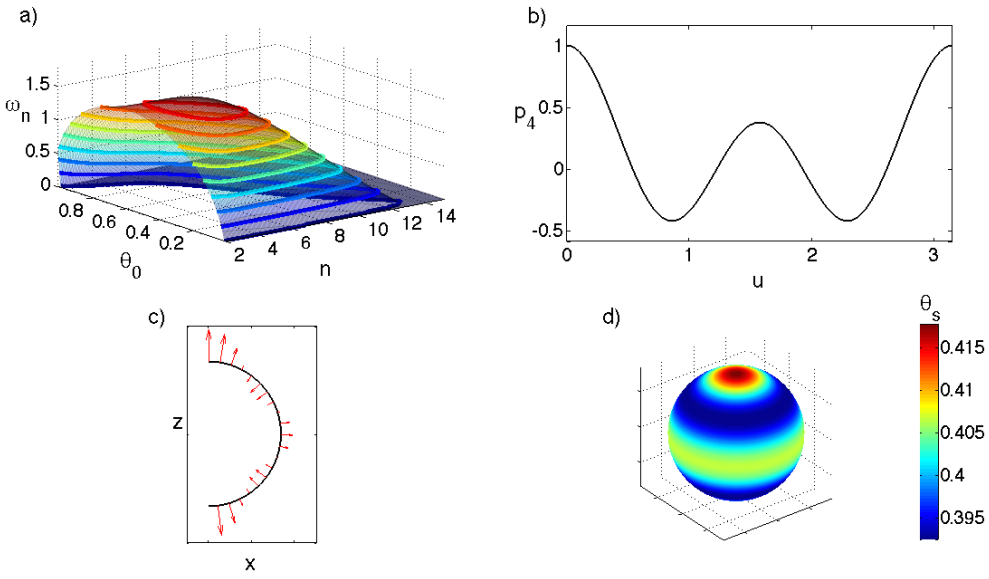

Figure 3.8. Shape associated with the most unstable mode. Parameter values are the same as Figure 3.7 except that $H_0 = 0.3$ in all plots, and $\theta_0 = 0.4$ and $\lambda = 0.1$ in b, c, and d. a) The largest positive root of ω_n. b) A plot of $p_4(\cos u)$. c) The perturbed generating curve with normals overlaid. d) The perturbed surface with θ_s values overlaid.

θ_g ($\kappa_s = 6$ and $\kappa_g = 1$), we see that regions with higher θ_s tend to bulge out to increase curvature toward C_s, while regions with lower θ_s tend to bulge inward.

While a full numerical simulation is necessary to explore the dynamics of the model far from steady state, this analysis provides information about the initial pattern formation in the system. For any set of parameters that exhibits a most unstable mode, we are able perform similar analysis and glean information about the patterns and shapes that will likely be observed in the full system.

3.3 Conclusion

In this chapter, we explored two specific parametrizations of the general model derived in Chapter 2. The first parametrization explored was the Monge parametrization. The Monge parametrization describes the surface by giving the height above the x-y plane. Because motion is described via changes in height rather than changes in the normal direction, it was necessary to use the general coordinate version of the two phase equations. While the Monge parametrization is quite intuitive to understand, the resulting equations are complicated due to the fact that the resulting metric and curvature tensors are not diagonal tensors.

After deriving the full system, we explored the system by examining the stability of a flat sheet. We found that stability depends on three factors. The first factor determining

stability is the value of the interaction parameter χ. For large χ, the system tends to phase separate. The second factor is the value of $f_{sH_0} - f_{gH_0}$, which reflects the differences between the two phases. We found that when phases are sufficiently different, it is possible to have curvature induced phase separation. The third factor affecting stability is the Cahn–Hilliard penalty term. This term uniformly stabilizes and has larger effect for higher wave numbers. Thus high wave numbers are always stabilized. Further, this stabilization leads to the existance of a most unstable mode and affects pattern formation in the system.

The second parametrization explored was an axisymmetric parametrization. In this parametrization, it is valid to use the surface fixed form of the general two phase system. We derived the axisymmetric form of the full system, finding it to be less complicated than in the Monge parametrization due to the fact that certain tensors are diagonal, and partial derivatives with respect to the angular direction are identically zero.

We explored the system by examining perturbations of a spherical steady state. We discovered that the eigenfunctions of the system are given by Legendre functions. We found that in addition to the factors affecting stability in the Monge parametrization, the axisymmetric system can go unstable if the curvature of the sphere is smaller than the spontaneous curvatures of the two phases. We explored specific forms of the free energy density and found that shape changes and phase separation are decoupled if the two phases respond indentically to curvature. Finally, we used information from the null vectors of the matrix M to explore the shape and behavior of the perturbations of the sphere.

CHAPTER 4

CURVATURE-INDUCED PHASE SEPARATION IN ONE DIMENSION

The Golgi apparatus is an important membraneous organelle. Located in the secretory pathway between the endoplasmic reticulum and the plasma membrane, it is a central location for lipid synthesis and lipid and protein modification and sorting [7]. This protein sorting is not fully understood, though some authors have hypothesized that it may be accomplished via phase separation [63]. Various authors have examined the effects of curvature on phase separation, both in the context of the Golgi apparatus [12] and otherwise [26, 61]. In the following sections, we describe a one-dimensional simplification of the equations presented in Chapter 2 and use the simplification to explore curvature-induced phase separation in a single Golgi cisterna.

We first describe the simplifications and assumptions that lead to the one-dimensional model. We then analyze the model equations to show analytically that they exhibit phase separation under certain regimes and that the phase separation is enhanced by the influence of curvature. We further show that curvature effects can induce phase separation when the system is in close proximity to a critical point as has been demonstrated experimentally [61]. Finally, we present numerical simulations of the model equations and explore different model behaviors.

4.1 One-Dimensional Simplification

We model a single Golgi cisterna as a simple closed curve in $\mathbb{R}^2$ of length L. We define $\phi(x)$, where x is the arc length, to be the angle between the tangent to the curve and the horizontal as shown in Figure 4.1.

Many of the components of the two-dimensional system such as the metric and curvature tensors do not have one-dimensional equivalents. We choose to proceed as follows: Since there is no stretching in an arc length parametrization, we treat all of the metric tensors

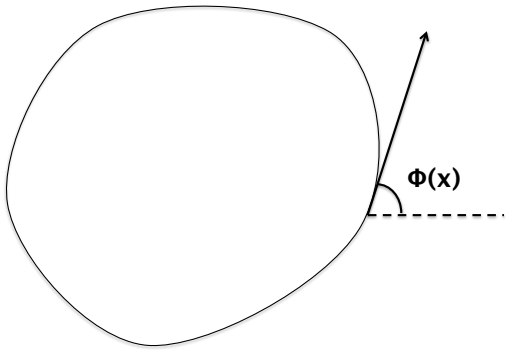

Figure 4.1. Representative Golgi cisterna. $\phi(x)$ is defined to be the angle between the tangent vector and the horizontal.

as the single number one. As a result, all quantities that arose from the time derivative of the metric tensor in the two-dimensional derivation (namely the HU_n terms) are zero. We define the curvature via

$$H = \frac{d\phi}{dx}. \tag{4.1}$$

We treat all covariant derivatives as partial derivatives with respect to the arc length variable x. We further assume that at any time t, the current shape of the cisterna corresponds to the shape that minimizes the free energy of the system. The equation resulting from this assumption (derived in Section 4.1.1) takes the place of the force balance equation in the normal direction.

The one-dimensional form of the rate of strain tensor for the sphingolipid phase is

$$S_s = \frac{\partial v}{\partial x} \tag{4.2}$$

so that the stress tensor has the simple form

$$T_s = \eta_s \frac{\partial v}{\partial x}, \tag{4.3}$$

where the dilational and shear viscosity parameters have been combined into a single parameter η_s. The rate of strain and stress tensors for the glycerolipid phase have an identical form, but with w instead of v.

4.1.1 Free Energy Density and Shape Equation

The free energy density is assumed to be the same as in Chapter 2, but we neglect the Cahn–Hilliard penalty terms for simplicity. Thus the free energy density is given by

$$f(\theta_s, \theta_g, \phi_x) = f^h(\theta_s, \theta_g) + f^b(\theta_s, \theta_g, \phi_x), \tag{4.4}$$

where ϕ_x indicates the partial derivative of ϕ with respect to x, the homogenous free energy density is given by

$$f^h(\theta_s, \theta_g) = \epsilon_{ss}\theta_s + \epsilon_{gg}\theta_g + \frac{K_b T}{\nu}\left(\chi\theta_s\theta_g + \theta_s \ln\theta_s + \theta_g \ln\theta_g\right), \tag{4.5}$$

and the bending free energy density is given by

$$f^b(\theta_s, \theta_g, \phi_x) = \frac{\kappa_s\theta_s}{2}\left(2\phi_x - C_s\right)^2 + \frac{\kappa_g\theta_g}{2}\left(2\phi_x - C_g\right)^2. \tag{4.6}$$

To find the shape of the cisterna, we minimize f over all functions $\phi(x)$ that meet certain criteria. First, we only want closed curves that have a single loop. This means we must have $\phi(0) = \phi(L) - 2\pi$. Second, we want smooth curves. Thus we want ϕ to be smooth and further need $\phi_x(0) = \phi_x(L)$. Finally, we only want closed curves. This can by accomplished by guaranteeing that

$$\int_0^L \sin(\phi(x))dx = \int_0^L \cos(\phi(x))dx = 0. \tag{4.7}$$

Using the Lagrange multipliers λ and μ to guarantee conditions 4.7, we seek to minimize

$$F = \int_0^L f(\theta_s, \theta_g, \phi_x)dx - \lambda\int_0^L \sin(\phi(x))dx - \mu\int_0^L \cos(\phi(x))dx \tag{4.8}$$

over all ϕ that meet our desired boundary conditions. We find the first variation (see section A.4), set it equal to zero, and recover the following Euler–Lagrange equation:

$$\frac{\partial}{\partial x}f_H + \lambda\cos(\phi) - \mu\sin(\phi) = 0, \tag{4.9}$$

where f_H indicates $\partial f/\partial\phi_x$, the partial derivative with respect to curvature. Note that we do not pick up any boundary contributions when integrating by parts because the condition $\phi(0) = \phi(L) - 2\pi$ guarantees that $\delta\phi$ is L periodic. Since we are on a closed curve, we assume the f_H is also L periodic.

4.2 The Full One-Dimensional System

Taking into account the simplifications described in Section 4.1, the full system of equations is given by

$$\frac{\partial\theta_s}{\partial t} + \frac{\partial}{\partial x}(\theta_s v) = 0, \tag{4.10}$$

$$\frac{\partial\theta_g}{\partial t} + \frac{\partial}{\partial x}(\theta_g w) = 0, \tag{4.11}$$

$$\eta_s\frac{\partial}{\partial x}\left(\theta_s\frac{\partial v}{\partial x}\right) - \theta_s\theta_g\xi(v - w) - \theta_s\frac{\partial}{\partial x}\left(\frac{\partial f}{\partial\theta_s} + \sigma\right) = 0, \tag{4.12}$$

$$\eta_g\frac{\partial}{\partial x}\left(\theta_g\frac{\partial w}{\partial x}\right) - \theta_s\theta_g\xi(w - v) - \theta_g\frac{\partial}{\partial x}\left(\frac{\partial f}{\partial\theta_g} + \sigma\right) = 0, \tag{4.13}$$

$$\frac{\partial}{\partial x} f_H + \lambda \cos(\phi) - \mu \sin(\phi) = 0, \tag{4.14}$$

$$\frac{\partial}{\partial x} (\theta_s v + \theta_g w) = 0, \tag{4.15}$$

for $x \in [0, L]$. We assume that θ_s, θ_g, v, and w are periodic, $\phi(0) = \phi(L) - 2\pi$, and $\phi_x(0) = \phi_x(L)$. Along with the system 4.10–4.15, we have the two constraints

$$\int_0^L \sin(\phi(x))dx = 0, \tag{4.16}$$

$$\int_0^L \cos(\phi(x))dx = 0. \tag{4.17}$$

4.2.1 Further Assumptions and Simplifications

We first assume a small amount of diffusion in the continuity equations 4.10–4.11,

$$\frac{\partial \theta_s}{\partial t} + \frac{\partial}{\partial x}(\theta_s v) = \epsilon \frac{\partial^2 \theta_s}{\partial x^2}, \tag{4.18}$$

$$\frac{\partial \theta_g}{\partial t} + \frac{\partial}{\partial x}(\theta_g w) = \epsilon \frac{\partial^2 \theta_g}{\partial x^2}, \tag{4.19}$$

where ϵ is a small diffusion coefficient. As described in [71], this small amount of diffusion does not change the qualitative features of the model, but ensures that solutions remain continuous and smooth even in the event of phase separation. Note further that this assumption does not affect the coincompressiblity condition.

Our second assumption deals with the coincompressibility condition 4.15, which states that $\theta_s v + \theta_g w$ is equal to a constant. We suppose that the constant is zero so that

$$\theta_s v + \theta_g w = 0. \tag{4.20}$$

This assumption allows us to eliminate pressure from the system. Multiply equation 4.12 by θ_g and equation 4.13 by θ_s and subtract. Define $V = v - w$. Using equation 4.20 and the fact that $\theta_s + \theta_g = 1$, we have

$$v = \theta_g V, \tag{4.21}$$

$$w = -\theta_s V \tag{4.22}$$

so that the entire system the entire system can be written as the following four equations:

$$\theta_s + \theta_g = 1, \tag{4.23}$$

$$\frac{\partial \theta_s}{\partial t} + \frac{\partial}{\partial x}(\theta_s \theta_g V) - \epsilon \frac{\partial^2 \theta_s}{\partial x^2} = 0, \tag{4.24}$$

$$\eta_s \theta_g \frac{\partial}{\partial x}\left(\theta_s \frac{\partial}{\partial x}(\theta_g V)\right) + \eta_g \theta_s \frac{\partial}{\partial x}\left(\theta_g \frac{\partial}{\partial x}(\theta_s V)\right) - \xi \theta_s \theta_g V - \theta_s \theta_g \frac{\partial}{\partial x}(f_s - f_g) = 0, \tag{4.25}$$

$$\frac{\partial}{\partial x} f_H + \lambda \cos(\phi) - \mu \sin(\phi) = 0, \quad (4.26)$$

with the appropriate boundary conditions and constraints. The notation f_s and f_g in equation 4.25 indicates partial derivatives with respect to θ_s and θ_g.

4.3 Model Analysis

4.3.1 Nondimensionalization

We introduce the nondimensional quantities

$$\begin{aligned} \hat{x} &= \frac{x}{L}, & \hat{\epsilon}_{ii} &= \frac{\epsilon_{ii}}{K_b T}, \\ \hat{V} &= \frac{V}{V^0}, & \hat{\kappa}_i &= \frac{\kappa_i}{K_b T}, \\ \hat{t} &= \left(\frac{v^0}{L}\right) t, & \hat{C}_i &= L C_i, \end{aligned}$$

where $i = s, g$. This gives the homogeneous free energy density

$$\begin{aligned} f^h(\theta_s, \theta_g) &= \frac{K_b T}{\nu} \left(\hat{\epsilon}_{ss}\theta_s + \hat{\epsilon}_{gg}\theta_g + \chi\theta_s\theta_g + \theta_s \ln\theta_s + \theta_g \ln\theta_g\right) \\ &= \frac{K_b T}{\nu} \hat{f}^h(\theta_s, \theta_g), \end{aligned} \quad (4.27)$$

and the bending free energy density

$$\begin{aligned} f^b\left(\theta_s, \theta_g, \phi_x\right) &= \frac{K_b T}{\nu} \frac{\nu}{L^2} \left(\frac{\hat{\kappa}_s \theta_s}{2} \left(2\phi_{\hat{x}} - \hat{C}_s\right)^2 + \frac{\hat{\kappa}_g \theta_g}{2} \left(2\phi_{\hat{x}} - \hat{C}_g\right)^2\right) \\ &= \frac{K_b T}{\nu} \upsilon \hat{f}^b(\theta_s, \theta_g, \phi_{\hat{x}}), \end{aligned} \quad (4.28)$$

where $\upsilon = \nu / L^2$. We define the total free energy density to be

$$f\left(\theta_s, \theta_g, \phi_x\right) = \frac{K_b T}{\nu} \hat{f}\left(\theta_s, \theta_g, \phi_{\hat{x}}\right), \quad (4.29)$$

where

$$\hat{f}\left(\theta_s, \theta_g, \phi_{\hat{x}}\right) = \hat{f}^h(\theta_s, \theta_g) + \upsilon \hat{f}^b\left(\theta_s, \theta_g, \phi_{\hat{x}}\right). \quad (4.30)$$

Suppressing the hats, the entire system can be written in nondimensional form

$$\theta_s + \theta_g = 1, \quad (4.31)$$

$$\frac{\partial \theta_s}{\partial t} + \frac{\partial}{\partial x}(\theta_s \theta_g V) - \epsilon \frac{\partial^2 \theta_s}{\partial x^2} = 0, \quad (4.32)$$

$$\eta\theta_g \frac{\partial}{\partial x}\left(\theta_s \frac{\partial}{\partial x}(\theta_g V)\right) + \theta_s \frac{\partial}{\partial x}\left(\theta_g \frac{\partial}{\partial x}(\theta_s V)\right) - \alpha\theta_s\theta_g V - \beta\theta_s\theta_g \frac{\partial}{\partial x}(f_s - f_g) = 0, \quad (4.33)$$

$$\frac{\partial}{\partial x} f_H + \lambda \cos(\phi) - \mu \sin(\phi) = 0, \quad (4.34)$$

for $x \in [0,1]$ with constraints

$$\int_0^1 \sin(\phi)dx = \int_0^1 \cos(\phi)dx = 0, \tag{4.35}$$

$$\phi(0) - \phi(1) = 2\pi, \tag{4.36}$$

and θ_s, θ_g, and V periodic on $[0,1]$. The nondimensional parameters in equation 4.33 are given by $\eta = \eta_s/\eta_g, \alpha = \xi L^2/\eta_g$, and $\beta = K_b TL/(\eta_g v^0 \nu)$. A fourth nondimensional parameter, $\upsilon = \nu/L^2$, appears inside the free energy density.

4.3.2 Linear Stability Analysis

One steady state of the system 4.31–4.36 is given by $\theta_s = \theta_0 =$ constant, $\theta_g = 1 - \theta_0$, $V = 0, \phi = 2\pi x, \lambda = 0$, and $\mu = 0$. We wish to explore the stability of this steady state. We suppose

$$\theta_s = \theta_0 + \gamma\theta_1(x,t), \tag{4.37}$$

$$\theta_g = 1 - \theta_0 - \gamma\theta_1(x,t), \tag{4.38}$$

$$V = \gamma V_1(x,t), \tag{4.39}$$

$$\phi = 2\pi x + \gamma\phi_1(x,t), \tag{4.40}$$

$$\lambda = \gamma\lambda_1, \tag{4.41}$$

$$\mu = \gamma\mu_1, \tag{4.42}$$

where γ is a small paramter. We substitute into the system 4.31–4.36, and keep terms that are linear in γ. This yields

$$\frac{\partial\theta_1}{\partial t} + \theta_0(1-\theta_0)\frac{\partial V_1}{\partial x} - \epsilon\frac{\partial^2\theta_1}{\partial x^2} = 0, \tag{4.43}$$

$$\begin{aligned}[\eta(1-\theta_0) + \theta_0]\frac{\partial^2 V_1}{\partial x^2} - \alpha V_1 \\ -\beta\left[(f_{ss_0} + f_{gg_0} - 2f_{sg_0})\frac{\partial\theta_1}{\partial x} + (f_{sH_0} - f_{gH_0})\frac{\partial^2\phi_1}{\partial x^2}\right] = 0,\end{aligned} \tag{4.44}$$

$$f_{HH_0}\frac{\partial^2\phi_1}{\partial x^2} + (f_{sH_0} - f_{gH_0})\frac{\partial\theta_1}{\partial x} + \frac{\lambda_1 + i\mu_1}{2}e^{2\pi ix} + \frac{\lambda_1 - i\mu_1}{2}e^{-2\pi ix} = 0, \tag{4.45}$$

$$\int_0^1 \phi_1\left(e^{2\pi ix} + e^{-2\pi ix}\right)dx = 0, \tag{4.46}$$

$$\int_0^1 \phi_1\left(e^{2\pi ix} - e^{-2\pi ix}\right)dx = 0, \tag{4.47}$$

$$\phi_1(1) - \phi_1(0) = 0, \tag{4.48}$$

where the sine and cosine terms have been replaced with complex exponentials and the notation f_{sH_0} indicates a mixed partial derivative with respect to θ_s and with respect to

the curvature ϕ_x and evaluated at the steady state values.

We now express all functions as series using complex exponentials:

$$\theta_1(x,t) = \sum_k \hat{\theta}_k e^{\omega_k t} e^{2\pi i k x}, \tag{4.49}$$

$$V_1(x,t) = \sum_k \hat{V}_k e^{\omega_k t} e^{2\pi i k x}, \tag{4.50}$$

$$\phi_1(x,t) = \sum_k \hat{\phi}_k e^{\omega_k t} e^{2\pi i k x}, \tag{4.51}$$

where the terms with hats are the constant expansion coefficients. Note that the Lagrange multipliers mey take on different values for each wavenumber k.

Consider the result of substituting the k^{th} term into the linearize system. The constraint equations 4.46–4.47 are satisfied by orthogonality for all $k \neq 1$. Since the Lagrange multipliers are introduced to guarantee that the constraint equations are satisfed, we can choose $\lambda_k = \mu_k = 0$ for $k \neq 1$.

For $k = 1$, the only way the constraints are satisfied is if $\hat{\phi}_1 = 0$. In this case, we choose $\lambda_1 = i\mu_1$ with $\lambda_1 = (2\pi i k)\left(f_{sH_0} - f_{gH_0}\right)\hat{\theta}_k e^{\omega_k t}$ to satisfy the shape equation. We now have a system of two equations in two unknows. Since we are interested in the interplay between shape and phase separation, we consider modes $k > 1$ where shape and phase separation are coupled. We have the system of three equations in three unknowns for each k:

$$\left(\omega_k + (2\pi k)^2\epsilon\right)\hat{\theta}_k + (2\pi i k)\theta_0(1-\theta_0)\hat{V}_k = 0, \tag{4.52}$$

$$\begin{aligned} -(2\pi i k)\beta(f_{ss_0} + f_{gg_0} - 2f_{sg_0})\hat{\theta}_k \\ -\left[(2\pi k)^2(\eta(1-\theta_0)+\theta_0) + \alpha\right]\hat{V}_k + (2\pi k)^2\beta(f_{sH_0} - f_{gH_0})\hat{\phi}_k = 0, \end{aligned} \tag{4.53}$$

$$(2\pi i k)\left(f_{sH_0} - f_{gH_0}\right)\hat{\theta}_k - (2\pi k)^2 f_{HH_0}\hat{\phi}_k = 0. \tag{4.54}$$

This system can be expressed as the matrix equation $M\mathbf{x} = 0$, where $\mathbf{x} = (\hat{\theta}_k, \hat{V}_k, \hat{\phi}_k)^T$. The matrix equation is only true for nonzero $\mathbf{x}$ when the determinant of M is zero. We solve $\det(M) = 0$ for ω_k and find the following dispersion relationship:

$$\omega_k = -\frac{B}{A}\left(f_{ss_0} + f_{gg_0} - 2f_{sg_0}\right) + \frac{B}{A}\frac{\left(f_{sH_0} - f_{gH_0}\right)^2}{f_{HH_0}} - (2\pi k)^2\epsilon, \tag{4.55}$$

where

$$B = (2\pi k)^2\beta\theta_0(1-\theta_0), \tag{4.56}$$

and

$$A = (2\pi k)^2(\eta(1-\theta_0)+\theta_0) + \alpha. \tag{4.57}$$

The dispersion relationship 4.55 is very similar to the dispersion relationship for the Monge parametrization, equation 3.50. The first term describes the inherent tendency to phase separate when the interactions parameter χ is greater than 2.

The second term describes curvature-induced phase separation. Since the Helfrich bending energy is a quadratic function of curvature, $f_{HH_0} > 0$, and this second term is always nonnegative. It destabilizes the steady state when f_{sH_0} and f_{gH_0} are different. This occurs when the two phases have different bending moduli or spontaneous curvatures. Since sphingolipids and glycerolipids have different biophysical properties, we expect that curvature in a golgi cisterna would serve to destabilize the steady state. Specifically, curvature can destabilize the steady state under situations where phase separation would not normally occur. For example, if χ is slightly less than two, curvature can cause the system to go unstable, as has been observed experimentally in [61].

The third term in the equation 4.55 describes the effect of diffusion. Notice that this term looks very similar to the term arising from the Cahn–Hilliard penalty terms in the Monge parametrization. It is always negative and increases in magnitude as the wavenumber increases. Thus, diffusion serves to stabilize high wavenumber perturbations. Further, this damping of high wave numbers implies the existence of a most unstable mode. This most unstable mode, corresponding to the largest value of ω_k, is the fastest growing mode upon random perturbation of the steady state and describes the patterns formed, at least initially when the full system is well described by the linearized system.

4.3.3 Integration to See Phase Separated Solutions

While the linear stability analysis performed in Section 4.3.2 allows us to see when the evenly mixed circular steady state will go unstable, it does not provide us with information about whether the loss of stability corresponds to phase separation. In this section, we show that the inclusion of diffusion in the continuity equation 4.32, in addition to ensuring that solutions stay smooth, also allows us to see that phase separation actually occurs.

Written in conservation form, equation 4.32 is

$$\frac{\partial \theta_s}{\partial t} + \frac{\partial}{\partial x}\left(\theta_s \theta_g V - \epsilon \frac{\partial \theta_s}{\partial x}\right) = 0.$$

While $\partial\theta_s/\partial t$ is clearly zero when $V = 0$ and $\theta_s = \theta_0$, it is also zero when the flux, given by $\theta_s\theta_g V - \epsilon\partial\theta_s/\partial x$, is zero. Assuming that the flux is zero, we have

$$V = \epsilon \frac{\partial \theta_s/\partial x}{\theta_s \theta_g}. \tag{4.58}$$

Substituting this value into equation 4.33 and making use of equation 4.31 yields

$$\epsilon\left[(1-\theta_s)\frac{\partial}{\partial x}\left(\theta_s\frac{\partial}{\partial x}\left(\frac{\partial\theta_s/\partial x}{\theta_s}\right)\right)+\theta_s\frac{\partial}{\partial x}\left((1-\theta_s)\frac{\partial}{\partial x}\left(\frac{\partial\theta_s/\partial x}{1-\theta_s}\right)\right)-\alpha\frac{\partial\theta_s}{\partial x}\right]$$
$$-\theta_s(1-\theta_s)\frac{\partial}{\partial x}(f'(\theta_s))=0. \qquad (4.59)$$

Note that we have replaced $f_s - f_g$ with $f'(\theta_s)$ where the prime indicates a derivative with respect to θ_s, and $f(\theta_s)$ is the result of replacing θ_g with $1-\theta_s$ in $f(\theta_s,\theta_g)$. We can integrate twice (with the second integration coming after multiplying each term by $\partial\theta_s/\partial x$) to yield

$$\frac{\partial\theta_s}{\partial x}=$$
$$\pm\left(\frac{2}{\epsilon}\frac{\theta_s(1-\theta_s)}{\eta(1-\theta_s)+\theta_s}\left[\epsilon\alpha(\theta_s\ln\theta_s+(1-\theta_s)\ln(1-\theta_s))+\beta f(\theta_s)+k_1\theta_s+k_2\right]\right)^{\frac{1}{2}}, \qquad (4.60)$$

where k_1 and k_2 are integration constants. Notice that for $\epsilon << 1$, the right hand side of equation 4.60 is very large except where $\epsilon\alpha(\theta_s\ln\theta_s+(1-\theta_s)\ln(1-\theta_s))+\beta f(\theta_s)+k_1\theta_s+k_2=0$. Thus where θ_s is not almost constant, it is either increasing or decreasing rapidly. This behavior indicates a phase separated steady state solution where the discontinuities between the two phases have been smoothed out by the diffusion.

4.4 Results

4.4.1 Numerical Implementation

To further explore the interplay between curvature and phase separation, we seek to numerically simulate the system 4.31–4.36. All simulations are performed using the software Matlab. We discretize the system using a finite volume method on a staggered grid as described in [71]. We calculate θ_s and θ_g at cell centers, and V and ϕ at cell edges. We calculate all spatial derivatives using centered differences. We implement the following algorithm at each time point.

1. Solve the shape equation to find ϕ.
2. Solve the force balance equation to find V.
3. Step forward in time to find θ_s at the next time point.
4. Update $\theta_g = 1-\theta_s$.

We describe the details of steps one, two, and three of the algorithm in the following paragraphs.

We solve shape equation 4.34 along with constraints 4.35 using a Newton method. We discretize the shape equation and constraints using centered differences for the derivatives and Riemann sums for the integrals. Without loss of generality, we assume that $\phi(0)=0$. Note that the shape equation 4.34 only has unique solutions up to a constant because any

shift in ϕ can be absorbed into the Lagrange multipliers λ and μ. Thus $\phi(0)$ is known and $\phi(1)$ is chosen via equation 4.36, so the unknowns in the system are interior values of $\phi, \phi_x(0), \lambda$, and μ. We iterate the discretized system until the error is sufficiently small and then calculate ϕ_x from ϕ. This Newton iteration must occur at each time step, so we save $\phi, \phi_x(0), \lambda$, and μ at each time step to be used as starting guesses in the subsequent step.

In addition to providing ϕ_x for the free energy density used in the force balance equation, the function $\phi(x)$ resulting from the Newton iteration also allows us to visualize the shape corresponding to the minimum free energy. We define

$$p(x) = \int_0^x \sin(\phi(x'))dx', \tag{4.61}$$

$$q(x) = \int_0^x \cos(\phi(x'))dx'. \tag{4.62}$$

Plotting $p(x)$ vs $q(x)$ gives the shape corresponding to the minimum free energy for given θ_s and θ_g.

Once the shape has been calculated, we can solve the force balance equation 4.33. In discretizing the variable coefficient Laplacian, the centered differences require θ_s and θ_g at cell edges. We calculate these values using linear interpolation of the two adjacent cell-center values. Discretization of the force balance equation 4.33 results in a largely tridiagonal system where the only off-diagonal terms are those resulting from periodicity. We use the Matlab function mldivide (the backslash operator) to solve this matrix system.

The continuity equation 4.32 requires simulating an advection-diffusion equation. We implement the advection term using first order upwinding and the diffusion term using either Crank–Nicolson or backward Euler [38]. We choose the time step adaptively following the method implemented in [71]. We repeat the algorithm until a steady state is reached.

4.4.2 Numerical Results

We saw analytical evidence in Section 4.3.2 that the the system can phase separate both in the presence and absence of curvature. In Figure 4.2, we show phase separation of the system in the situation where $\kappa_s = \kappa_g = 0$. The phase separation in this case is driven completely by the homogeneous free energy density. Further, since $f_H = 0$, the shape equation is identically zero, so the phase separation does not affect the shape of the cisterna. Figure 4.2a shows snapshots in time of an initial θ_s distribution taken to be a small cosine perturbation of $\theta_s = 0.5$. The parameters are chosen to be $\eta = \alpha = \beta = 1, \epsilon = 10^{-7}$, and $\chi = 2.5$ so that $f(\theta_s)$ is a double well potential as is shown in Figure 4.2b.

The more interesting cases arise when curvature is included. There, local membrane

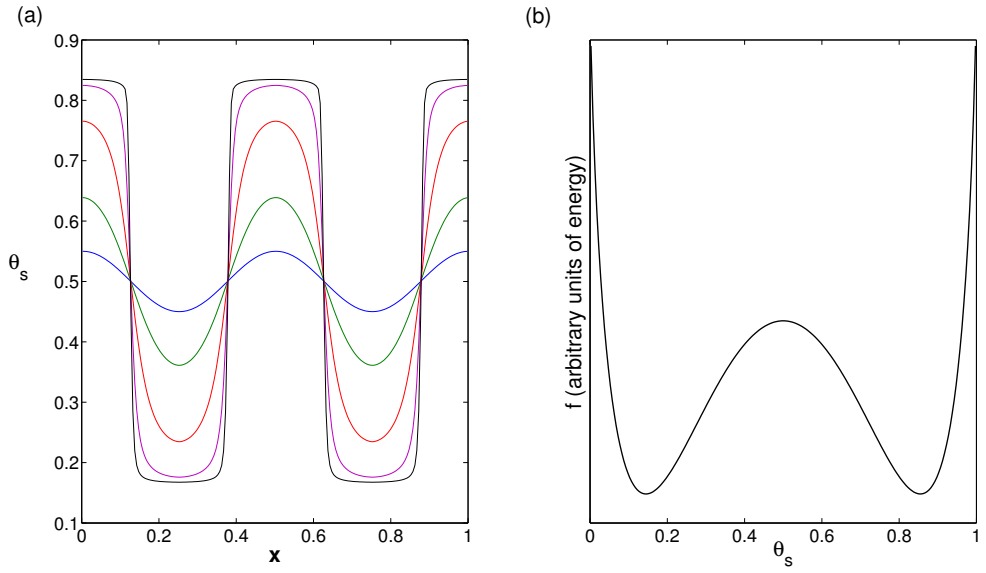

Figure 4.2. Phase separation in the absence of curvature. Parameters values are $\eta = \alpha = \beta = 1, \epsilon = 10^{-7}$, and $\chi = 2.5$. a) Snapshots in time of an initial θ_s distribution of $0.5(1 + 0.1\cos(4\pi x))$. b) The double well free energy density responsible for the phase separation.

shape influences the dynamic behavior of the lipids. With the inclusion of curvature, it is possible to induce phase separation under situations where it would not happen otherwise. This can happen because the different phases have different bending moduli, different spontaneous curvature, or both. In Figure 4.3 we show phase separation caused by one of the phases being stiffer than the other. Here, we have used parameter values $\eta = \alpha = \beta = 1, \upsilon = 10^{-3}, \epsilon = 10^{-5}, \chi = 1.9, \kappa_s = 5, \kappa_g = 1$, and $C_s = C_g = 0$. Sphingolipids preferentially associate with cholesterol and form thicker bilayers than glycerolopids [28]. For this reason, we assume that sphingolipids are more resistant to curvature. Figure 4.3a shows snapshots in time of the same initial θ_s distribution as Figure 4.2. Note that $\chi < 2$, so we see that the phase separation is indeed caused by curvature effects. Notice further that phase separation does not occur symmetrically under these conditions. Rather, long regions of relatively large θ_s develop, separated by short regions of very low θ_s. In Figure 4.3b, we have plotted the final shape of the cisterna with an overlaid heat map indicating regions of high and low sphingolipid volume fraction. We see that the regions of high θ_s correspond to areas of low curvature, while the regions of low θ_s correspond to areas of high curvature.

Curvature induced phase separation can also be caused by the different phases having different spontaneous curvature. In Figure 4.4a we have used $\kappa_s = \kappa_g = 1, C_s = -15$, and $C_g = 15$ and all other parameters the same as Figure 4.3. Figure 4.4b has $\kappa_s = 2$,

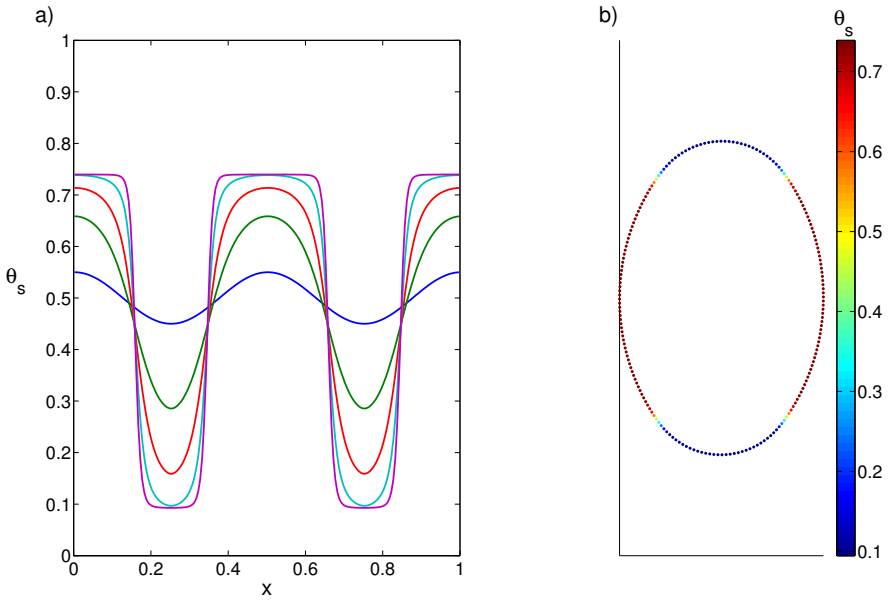

Figure 4.3. Phase separation caused by different bending moduli. Parameter values are $\eta = \alpha = \beta = 1, \upsilon = 10^{-3}, \epsilon = 10^{-5}, \chi = 1.9, \kappa_s = 5, \kappa_g = 1$, and $C_s = C_g = 0$. a) Snapshots in time of an initial θ_s distribution of $0.5(1 + 0.1\cos(4\pi x))$. b) The resulting shape of the cisterna with a heat map overlaid to indicate areas of high θ_s.

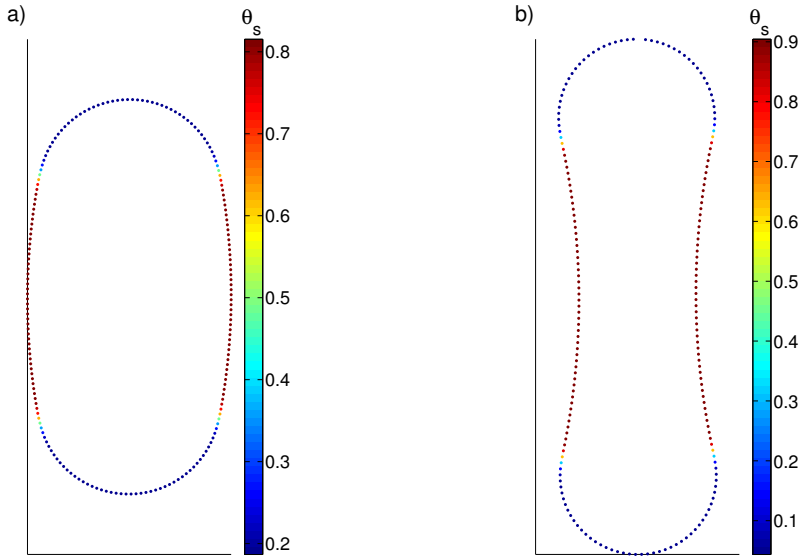

Figure 4.4. Phase separation caused by different spontaneous curvatures. Both shapes result from an initial θ_s distribution of $0.5(1 + 0.1\cos(4\pi x))$. All unspecified parameter values are the same as in Figure 4.3. a) Cisternal shape when $\kappa_s = \kappa_g = 1, C_s = -15$, and $C_g = 15$. b) Cisternal shape when $\kappa_s = 2, \kappa_g = 1, C_s = -15$, and $C_g = 15$.

$\kappa_g = 1, C_s = -15$, and $C_g = 15$. Notice how the combination of different bending moduli and spontaneous curvatatures can result in interesting shapes.

We should note that elongated elliptical shapes as shown in Figure 4.4 are not the only possible shapes produced by the model. Rather, the final pattern resulting from phase separation may depend on the initial perturbation. We see this in Figure 4.5. Each shape in the figure corresponds to a different wavenumber cosine perturbation of $\theta_s = 0.5$.

A more relevent consideration than what happens to a specific wavenumber perturbation is whether a dominant pattern emerges from a random initial perturbation in the volume fraction. Recall from Section 4.3.2 that the diffusion term in the dispersion relationship given in equation 4.55 damps out high wave numbers, so there exists a most unstable mode. We expect that this mode will dominate the pattern formation in the linear system and will likely also have a dominant effect on the patterns formed in the full nonlinear system. This phenomenon is explored in Figure 4.6. We choose the parameter values $\chi = 1.5$, $\kappa_s = 5$, $\kappa_g = 1, C_s = -5, C_g = 1, \epsilon = 10^{-3.5}, \upsilon = 0.001$, and $\eta = \alpha = \beta = 1$ so that the $k = 2, 3$, and 4 modes are unstable, while all higher modes are stable as shown in Figure 4.6a. The initial θ_s distribition is taken to be

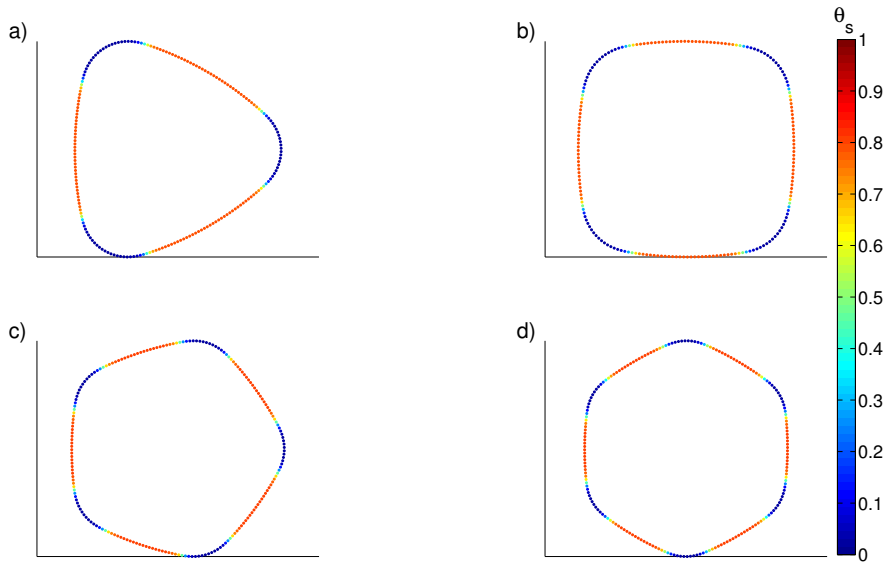

Figure 4.5. Various shapes depending on the initial θ_s distribution. In this figure, $\kappa_s = 5, \kappa_g = 1, C_s = -4, C_g = 0, \chi = 1.9$, and all the other paramaters are the same as Figure 4.3. Each shape corresponds to a different initial condition: a) $\theta_s = 0.5(1+0.1\cos(6\pi x))$. b) $\theta_s = 0.5(1+0.1\cos(8\pi x))$. c) $\theta_s = 0.5(1+0.1\cos(10\pi x))$. d) $\theta_s = 0.5(1+0.1\cos(12\pi x))$.

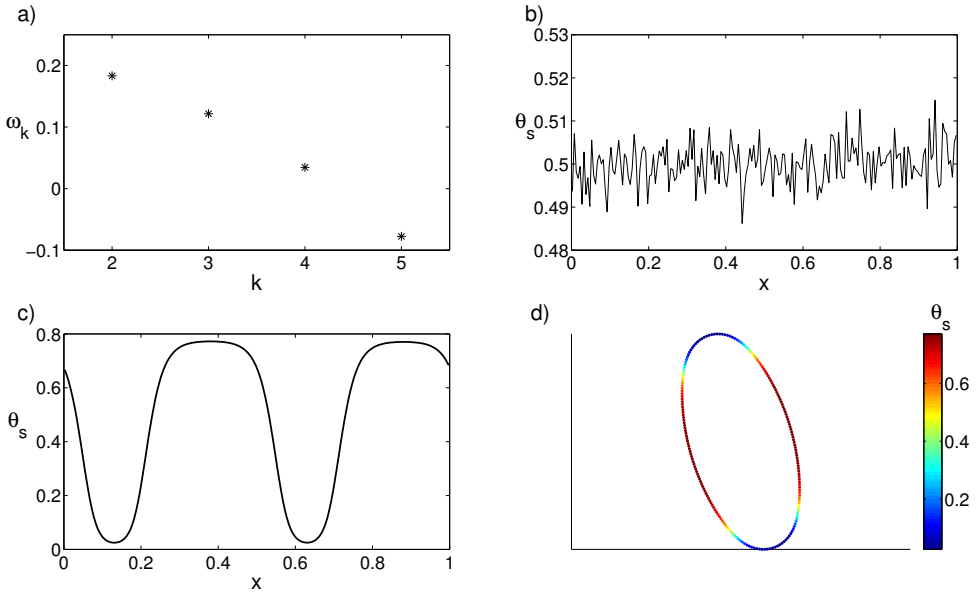

Figure 4.6. Phase separation of a random perturbation. Parameter values are $\chi = 1.5, \kappa_s = 5, \kappa_g = 1, C_s = -5, C_g = 1$, and $\epsilon = 10^{-3.5}$. All other parameter values are the same as Figure 4.3. a) The dispersion relationship plotted as a function of k. b) The initial θ_s perturbation. c) The final θ_s distribution after phase separation. d) The final shape of the cisterna with overlaid θ_s values.

$$\theta_s = 0.5 + \sum_{k=1}^{100} 0.01r\left(\cos(2\pi kx) + \sin(2\pi kx)\right), \tag{4.63}$$

where r is a random number drawn from a normal distribution that has been truncated between -10 and 10. One such random distribution is shown in Figure 4.6b. Since the $k = 2, 3$, and 4 modes are the only unstable modes, we expect them to dominate the pattern formation, with the $k = 2$ mode dominating most often because it is the largest. This intuition is born out in simulations. Figure 4.6c shows the final θ_s distribution, and Figure 4.6d the final shape corresponding to the initially random distribution given in Figure 4.6b. Notice how the final distribution looks like a $k = 2$ mode, and the final shape given in Figure 4.6d has the ellipsoidal shape we have seen in other figures.

In the previous paragraphs, we have been exploring the interplay between curvature and phase separation. In reality, while the shape of a cisterna may be influenced by the lipids in the membrane, it is likely determined at least in part by interactions with the cytoskeleton [67]. That leads to the question of whether an imposed membrane shape can induce phase separation in the model. This behavior is demonstrated in Figure 4.7. Here, $\phi(x)$ is imposed to be $6.28 - 6.279\tanh(1/.1\sin(4\pi(x - 1/8)))$ at each time step. This strange functional

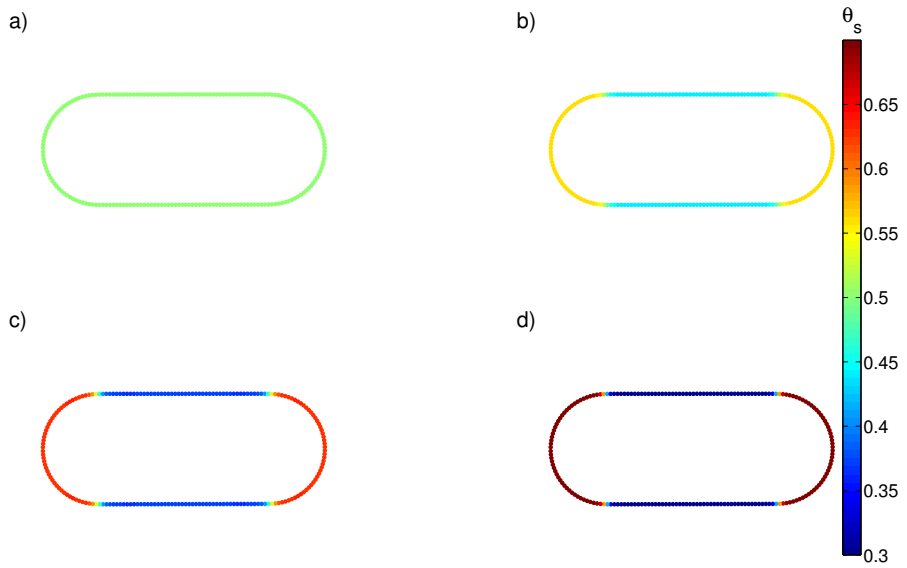

Figure 4.7. Phase separation under imposed curvature. Parameters values are $\kappa_s = \kappa_g = 1, C_s = 10, C_g = 0, \chi = 1.8, \epsilon = 10^{-7}$, and all others the same as Figure 4.3. a) The initial distribution $\theta_s = 0.5$. b) A snapshot early in the simulation of phase separation beginning to occur. c) A snapshot later in the simulation. d) The final phase separated state.

form corresponds to the elongated pill shape shown in the figure. The simulation is started with a constant initial condition, $\theta_s = 0.5$, and snapshots are taken in time. We see as time progressed from a) to d) that the imposed curvature is able to induce phase separation in an initially homogeneous membrane. While phase separation here is caused by the two phases having different spontaneous curvature, it can also be caused by the two phases having different bending moduli (not shown). This situation of imposed curvature causing phase separation is similar to the experimental results discussed in [26], where the introduction of a membrane tubule induces phase separation. We note that this phenomenon has been modeled in [31]. Unlike the current model, the model in [31] is purely a steady state model with no dynamics.

CHAPTER 5

LIPID ASYMMETRY AND FLIP-FLOP

It has long been known that the lipids in biological membranes are distributed asymmetrically between different leaflets of the lipid bilayer [64]. Classical experiments showed that lipid motion is rapid within a bilayer leaflet, but that flip-flop between leaflets is slow and occurs with a half time on the order of hours [45]. Given this paradigm, it has been assumed that lipid flip-flop and the maintenance of transbilayer asymmetry is a protein-mediated process [35]. However, experiments done in the Conboy lab at the University of Utah have cast doubt on this reigning paradigm, finding that flip-flop can occur on a much faster time scale under physiological conditions [40]. The older experiments were done by modifying the head group of a lipid in order to visualize asymmetry, a process that could clearly affect the dynamics of lipid flip-flop. The newer experiments were done using a method called sum frequency vibrational spectroscopy (SFVS) on planar supported lipid bilayers (PSLBs) [41]. Briefly, the method involves making a bilayer with asymmetric leaflets by using deuterated lipids to create one of the leaflets and regular lipids to create the other leaflet. The two leaflets are combined to create an asymmetric PSLB. (See [1] for a description of the method). The method of SFVS is used to visualize the loss of asymmetry and thereby characterize the rate of lipid flip-flop. Briefy, two lasers of different wavelength are focused on the PSLB. The wavelength of one of the lasers is varied so that the magnitude of the measured signal strength changes depending on the vibrational frequencies of different molecular configurations. The method is useful because destructive interference causes symmetric bilayers to yield no signal while asymmetric bilayers yield a signal. Thus the experimenter can use the decay of signal intensity to characterize the loss of asymmetry caused by lipid flip-flop. (See [41] for a description of the method.) Not only have experiments shown faster flip-flop, the experimenters have used the method with modified lipid head groups to reproduce the slow rates of flip-flop seen previously [41].

5.1 Lipid Flip-Flop as an Inducer of Curvature

5.1.1 Model Motivation and Description

Building on the idea that lipids may be able to transition quickly between leaflets of the bilayer, we seek to explore the interplay between lipid flip-flop and membrane curvature. The motivation comes from considering vesicle formation in the multivesicular body (MVB). The MVB is an organelle in the endocytic pathway where proteins are tagged and sorted either towards degradation in the lysosome or towards transport and reuse in other parts of the cell [30]. This process of sorting proteins into intralumenal vesicals (ILVs) is largely controlled by endosomal sorting complexes required for transport (ESCRT proteins), but there remain questions as to the exact mechanisms of vesicle formation [4]. Though ESCRTs seem to be important in most situations, there are certain situations where ILVs form in the absence of ESCRT proteins [44, 62], leading to the hypothesis that vesicle budding in the MVB may be largely controlled by lipid dynamics [4]. We develop a simple stochastic model to explore this hypothesis.

We suppose we have a lipid bilayer with two leaflets, each with the thickness given by d so that the bilayer has a thickness of $2d$. We suppose further that the section of the bilayer we are considering has a total of N lipids, n of which are part of the inner leaflet and $N-n$ of which are part of the outer leaflet. We view the system as a discrete Markov process on n as shown in Figure 5.1. Let $p_n(t)$ be the probability that there are n lipids in the inner leaflet at time t. Let α_i be the transition rate from $n=i$ to $n=i+1$ and β_i be the transition rate from $n=i$ to $n=i-1$. This yields the master equation

$$\frac{dp_i}{dt} = \alpha_{i-1}p_{i-1} + \beta_{i+1}p_{i+1} - (\alpha_i + \beta_i)p_i, \tag{5.1}$$

for $i = 1, 2, \cdots, N-1$, and

$$\frac{dp_0}{dt} = -\alpha_0 p_0 + \beta_1 p_1, \tag{5.2}$$

$$\frac{dp_N}{dt} = \alpha_{N-1}p_{N-1} - \beta_N p_N. \tag{5.3}$$

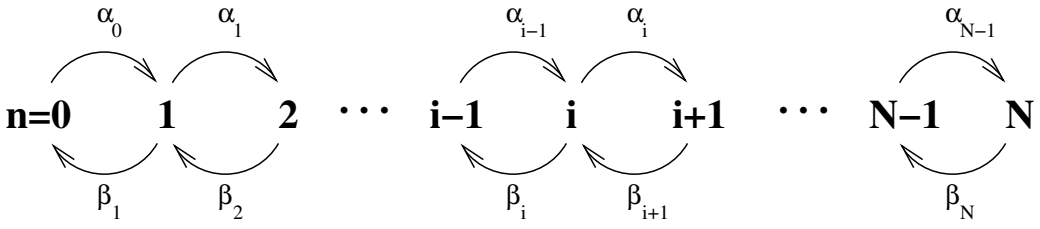

Figure 5.1. Markov chain describing flip-flop.

Using the fact that probabilities add to 1, the master equation is solved at steady state to yield

$$p_0 = \frac{1}{1 + \sum_{n=1}^{N} \Pi_{i=1}^{n} \frac{\alpha_{i-1}}{\beta_i}}, \tag{5.4}$$

$$p_n = p_0 \Pi_{i=1}^{n} \frac{\alpha_{i-1}}{\beta_i}, \text{ for } n = 1, 2, \cdots, N. \tag{5.5}$$

Suppose there is an energy E_n associated with state n and that there is an energy barrier between states as shown in Figure 5.2. Let A_n be the energy barrier for transitions from state n to state $n+1$ and A_{-n} be the energy barrier for transitions from state $n+1$ to state n. Define $\Delta E_n = E_{n+1} - E_n$. We assume that transitions follow Arrhenius-type behavior and take the transition rates to be

$$\alpha_n = \gamma \exp\left(\frac{-A_n}{k_b T}\right), \tag{5.6}$$

$$\beta_n = \gamma \exp\left(\frac{-A_{-n}}{k_b T}\right), \tag{5.7}$$

where k_b is Boltzmannn's constant, T is absolute temperature, and γ is a constant. Using these transition rates, the steady state probabilities become

$$p_n = \frac{\exp\left(\frac{-E_n}{k_b T}\right)}{\sum_{n=0}^{N} \exp\left(\frac{-E_n}{k_b T}\right)} \tag{5.8}$$

for $n = 0, 1, 2, \cdots, N$. This is exactly the Boltzmannn distribution.

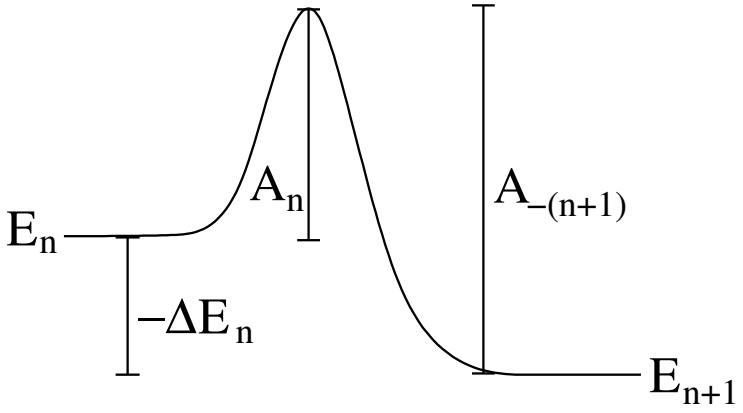

Figure 5.2. Schematic drawing of an energy landscape. E_n is the energy of state n, A_n is the activation energy for transitions from state n to state $n+1$, A_{-n} is the activation energy for transitions from state n to state $n-1$, and $\Delta E_n = E_{n+1} - E_n$.

5.1.2 Energy from Curvature

To investigate the interaction between lipid flip-flop and membrane curvature, we desire a form of E_n that depends on curvature. We derive this form using a spherical cap approximation as shown in Figure 5.3. Assume that the two opposite faces of the bilayer are maintained at a constant separation $2d$. Thus, area differences between the two leaflets in the bilayer impose a curvature on the membrane. Using the spherical cap approximation, it is relatively easy to derive a formula for the curvature of the sperical cap. We denote the curvature $c = 1/r$ where r is the radius of the midline of the membrane. We find that

$$c = \frac{1}{d}\frac{\sqrt{A_{out}} - \sqrt{A_{in}}}{\sqrt{A_{out}} + \sqrt{A_{in}}} \tag{5.9}$$

where A_{out} is the area of the outer leaflet, A_{in} is the area of the inner leaflet, and d is the thickness of each leaflet. The area of the midline is given by

$$A_{mid} = \left(\frac{\sqrt{A_{out}} + \sqrt{A_{in}}}{2}\right)^2. \tag{5.10}$$

To express the energy in terms of our stochastic variable n, we suppose that each lipid head group has cross-sectional area a. Then the area of the inner and outer leaflets are given by $A_{in} = na$ and $A_{out} = (N - n)a$. For the energy, we follow the Helfrich model [27]. Recall that the Helfrich model gives the bending energy per unit area

$$E_b = \frac{\kappa_b}{2}(2H - c_0)^2 + \kappa_g K, \tag{5.11}$$

where H is the mean curvature, K is the Gaussian curvature, κ_b is the bending modulus, κ_g is the Gaussian bending modulus, and c_0 is the spontaneous curvature. For a spherical cap, $H = 1/r$. The Gauss–Bonnet theorem states that the integral of the Guassian curvature

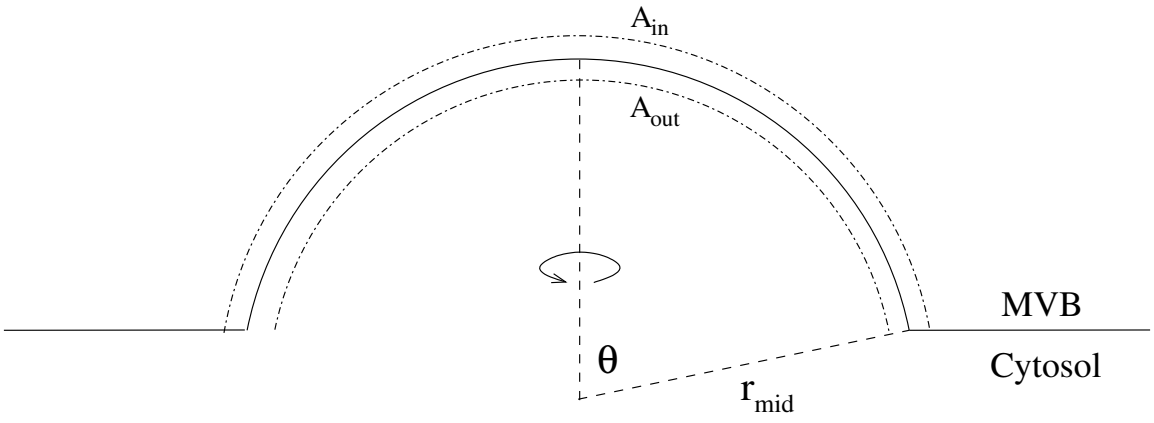

Figure 5.3. Schematic drawing of a spherical cap budding into the MVB.

over a surface stays constant if the surface does not change topology, so the Gaussian curvature enters into the energy as an additive constant, and we can neglect it. We further assume that $c_0 = 0$, meaning that the preferred state of the membrane is flat. This yields the bending energy for state n

$$\begin{aligned} E_b &= \frac{2\kappa_b}{d^2}\left(A_{mid}\right)\left(\frac{\sqrt{N-n}-\sqrt{n}}{\sqrt{N-n}+\sqrt{n}}\right)^2 \\ &= \frac{\kappa_b a}{2d^2}(\sqrt{N-n}-\sqrt{n})^2. \end{aligned} \tag{5.12}$$

We use a lattice model as described in section 2.6.2 to calculate the energetic contribution from entropy to be

$$E_{ent} = k_b T\left[n\ln\left(\frac{n}{N}\right) + (N-n)\ln\left(\frac{N-n}{N}\right)\right]. \tag{5.13}$$

This yields a free energy for state n,

$$E_n = \frac{\kappa_b a}{2d^2}(\sqrt{N-n}-\sqrt{n})^2 + k_b T\left[n\ln\left(\frac{n}{N}\right) + (N-n)\ln\left(\frac{N-n}{N}\right)\right]. \tag{5.14}$$

For given parameter values, we can use equation 5.8 to visualize the probability distribution for n where E_n comes from equation 5.14. Since each n corresponds to a given curvature, we can also visualize the probability distribution for c. We use $\kappa_b = 20k_bT$, $d = 2$ nm, and $a = 40\mathring{A}^2$, numbers that are fairly standard based on the literature [43, 1, 74]. A weakness in this model formulation comes in choosing a reasonable value for N. The value chosen essentially reflects the ratio between bending resistence in the bilayer and compression resistance in the lipids making the bilayer. If bending resistance is much larger than compression resistance, a flip of one lipid will cause a very small change in curvature, and N should be taken to be large. On the other hand, if the bending resistance is much smaller than the compression resistance, a flip of one lipid will cause a large change in curvature, and N should be taken to be small. For visualization purposes, we use the fact that a typical ILV has a diameter of 25–50 nm [30]. This yields a value of approximately 2500 lipids per leaflet, so we choose N to be 5000. The resulting probability distribution is shown in Figure 5.4. Note that a spherical vesicle of radius 25 nm has curvature $4\times10^7 m^{-1}$. We can see from Figure 5.4 that the probability of spontaneously forming a vesicle of this radius through flip-flop is virtually zero. For larger and smaller values of N, the probability distribution is more or less sharply peaked around $c = 0$ as we would expect.

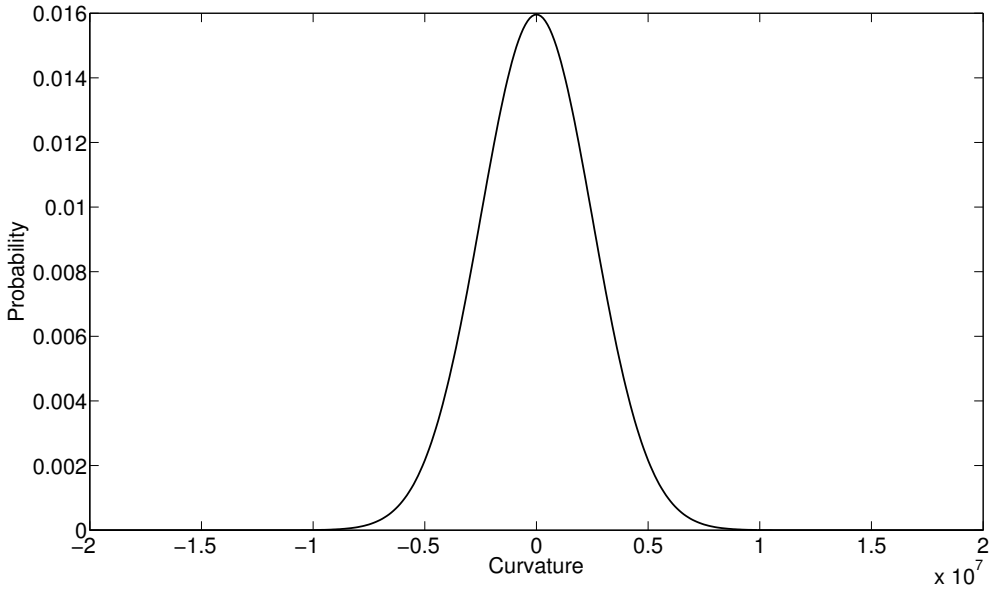

Figure 5.4. Probability density function for curvature. Parameter values are $\kappa_b = 10k_bT, d = 2$ nm, $a = 50\mathring{A}^2$, and $N = 5000$.

5.1.3 Mean First Passage Time

Though a complete vesicle is unlikely to form simply from membrane fluctuations caused by lipid flip-flop, it is interesting to ask how long on average one must wait before a specific curvature is realized. It has been hypothesized that ESCRT III, the protein largely responsible for vesicle fission, may be able to detect and stabilize negative membrane curvature [4]. This could help explain ESCRT III's involvement in ILV budding in certain protazoa that lack the earlier ESCRT machinery and its involvement in HIV budding. We would like to calculate the average time it takes for an initially flat membrane to achieve a given curvature.

Because our system is a temporally homogeneous Markov process (the transition rates do not depend explicitly on time), we can follow the method presented in [22] to find an analytic expression for the mean first passage time. The average time it takes for a system starting at $n = n_0$ to first arrive at $n = n_1$ is given by

$$T_1(n_0 \to n_1) = \sum_{m=n_0}^{n_1-1} e^{\phi(m)} \sum_{n=0}^{m} \frac{e^{-\phi(n)}}{\alpha_n}, \tag{5.15}$$

where

$$\phi(n) = \begin{cases} 0 & \text{for } n = 0 \\ \sum_{j=1}^{n} \ln\left(\frac{\beta_j}{\alpha_j}\right) & \text{for } n \geq 1. \end{cases} \tag{5.16}$$

In order to use equations 5.15–5.16, we need explicit formulas for α_n and β_n. In general, α_n and β_n are given by equations 5.6–5.7. We suppose that $A_n = A^* + (1/2)\Delta E_n$ and $A_{-(n+1)} = A^* - (1/2)\Delta E_n$. Then $A_n - A_{-(n+1)} = -\Delta E_n$ as shown in Figure 5.2, and we still recover the correct Boltzmannn behavior at steady state. This gives

$$\alpha_n = \gamma \exp\left(\frac{-A^*}{k_b T}\right) \exp\left(\frac{-\Delta E_n}{2k_b T}\right), \tag{5.17}$$

$$\beta_n = \gamma \exp\left(\frac{-A^*}{k_b T}\right) \exp\left(\frac{\Delta E_{n-1}}{2k_b T}\right). \tag{5.18}$$

The energy independent flip rate has been measured experimentally by the Conboy lab [41], allowing us to take $\gamma \exp(-A^*/(k_b T))$ as a known quantity. We assume that the bilayer is initially flat with $n_0 = N/2$ and calculate the mean first passage time to n_1. We assume the n is the number of lipids on the MVB lumenal leaflet of the membrane and choose $n_1 > N/2$ so that the bud is forming into the lumen of the MVB. We choose values of n_1 and calculate the mean first passage time to that value. The results are shown in Table 5.1 where we used the literature value $\gamma \exp(A^*/k_b T) = 200 \times 10^{-5} s^{-1}$ and other parameters as described in Figure 5.4. As we can see from the table, it takes hours on average for one lipid to flip from the outer to the inner leaflet. It takes over a day on average for 10 lipids to flip from the outer to the inner leaflet. This allows us to conclude that even for the faster flip rate measured by the Conboy lab, lipid flip-flop is not expected to be a significant inducer of curvature and spontaneous vesicle formation in the MVB. The researchers do mention that the experiments were conducted with lipids 5 °C below their melting temperature and that lipids in biological membranes are usually in the liquid phase [41], so it is quite possible that the native flip-flop rate used here is slower than the physiological rate. In order for the process described above to take place on physiologically relevant time scales, though, the flip rate would have to be orders of magnitude faster than the one described here. It remains to be seen whether the physiological flip rate meets this criterion. It is also not known what curvature ESCRT III prefers to bind and stabilize. Having better data on these biological questions will allow us to say more definitively whether flip-flop might be significant in the MVB.

5.2 Electrostatic Induction of Lipid Asymmetry

5.2.1 Model Motivation and Description

In addition to showing the lipid flip-flop may be faster than previously assumed, researchers in the Conboy lab showed that electrostatic interactions can maintain bilayer asymmetry [8]. Other research on vesicle budding in the multivesicular body showed that

Table 5.1. Mean first passage time starting from $n_0 = N/2$.

n_1	N	curvature	time (hours)
n_0+1	1000	5×10^5	2.02
	5000	1×10^5	4.42
	10000	5×10^4	6.22
n_0+10	1000	5×10^6	30.4
	5000	1×10^6	51.8
	10000	5×10^5	69.4

vesicles can form in the absence of proteins, but only in the presence of a specific negatively charged lipid and a strong pH gradient [44]. We wondered whether the significance of the pH gradient lay in some ability to maintain an asymmetric distribution of charged lipids across the membrane. The following model uses the Poisson–Boltzmann equation to address this question.

We assume that we have an infinite flat lipid bilayer of thickness $2d$ in an electrolyte bath. Instead of assuming the all lipids are the same as we did in the previous model, we assume the lipids are either neutral or negatively charged. The negative charges are located at spatial locations $x = \pm d$ and have charge density (charged particles/area) C_L at $x = -d$ and C_R at $x = d$. We assume that there are no charges for $|x| < d$ and that there is an infinite electrolyte bath for $|x| > d$. In the bath, there are positively charged sodium ions with concentration n, positively charged hydrogen ions with concentration h, and negatively charged chloride ions with concentration c. We assume that $h \to H_L, n \to Na_L$, and $c \to Cl_L$ as $x \to -\infty$ and $h \to H_R, n \to Na_R$, and $c \to Cl_R$ as $x \to \infty$. We further assume that the electrostatic potential $\phi \to 0$ as $x \to \pm\infty$. Finally, we assume electroneutrality far from the membrane so that $Na_L + H_L = Cl_L$ and $Na_R + H_R = Cl_R$. A schematic description of the model setup is shown in Figure 5.5.

5.2.1.1 Bath Equations

In the electrolyte bath, we use the steady state Nernst–Planck equation to describe the concentration of each electrolyte [34]. The Nernst–Planck equation states that ion flux is caused by concentration gradients and gradients in the chemical potential. We assume zero flux, yielding

$$\frac{dh}{dx} + \frac{F}{RT} h \frac{d\phi}{dx} = 0, \tag{5.19}$$

$$\frac{dn}{dx} + \frac{F}{RT} n \frac{d\phi}{dx} = 0, \tag{5.20}$$

$$\frac{dc}{dx} - \frac{F}{RT} c \frac{d\phi}{dx} = 0, \tag{5.21}$$

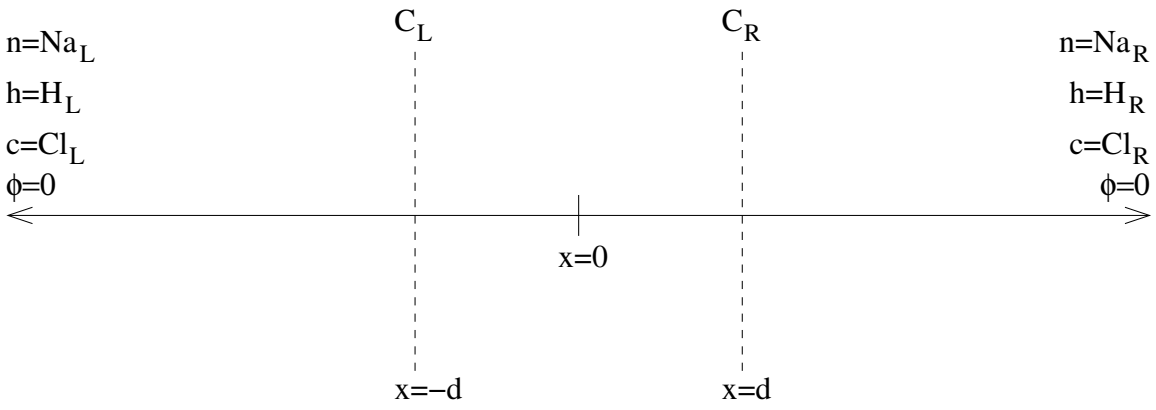

Figure 5.5. Schematic drawing of an infinite bilayer containing charged lipids. The bilayer is sitting in an electrolyte bath. C_L and C_R are the charge densities of negatively charged lipid head groups one the surfaces of the left and right leaflets, respectively. n is sodium concentration, h is hydrogen concentration, and c is chloride concentration. All concentrations approach the given limiting values as $|x| \to \infty$. ϕ is the electrostatic potential caused by the charged particles.

where F is Faraday's constant, R is the universal gas constant, and T is the absolute temperature. Note that the charge on hydrogen and sodium is $+1$ and the charge on chlorine is -1. Using the boundary conditions at $x = \pm\infty$, we find that

$$h = H_{R,L} \exp\left(\frac{-F}{RT}\phi\right), \tag{5.22}$$

$$n = Na_{R,L} \exp\left(\frac{-F}{RT}\phi\right), \tag{5.23}$$

$$c = Cl_{R,L} \exp\left(\frac{F}{RT}\phi\right), \tag{5.24}$$

where the R subscript is taken for $x > d$ and the L subscript is taken for $x < -d$.

To get an equation for the electrostatic potential ϕ, we use Guass' law, which states that the electric flux through the boundary of a region is equal to the sum of the charges inside the region. In the bath, this gives Poisson's equation

$$\frac{d^2\phi}{dx^2} = \frac{qN_a}{\epsilon_0 D_w}(c - h - n), \tag{5.25}$$

where q is the charge on an electron, ϵ_0 is the permittivity of a vacuum, and D_w is the dialectric constant of water. Using equations 5.22–5.24 and the fact that $Na_{R,L} + H_{R,L} = Cl_{R,L}$, we have the Poisson Boltzmannn equation

$$\frac{d^2\phi}{dx^2} = \frac{2qN_aCl_L}{\epsilon_0 D_w} \sinh\left(\frac{F}{RT}\phi\right), \tag{5.26}$$

for $x < -d$ and

$$\frac{d^2\phi}{dx^2} = \frac{2qN_aCl_R}{\epsilon_0 D_w}\sinh\left(\frac{F}{RT}\phi\right), \tag{5.27}$$

for $x > d$.

Under conditions that $\frac{F}{RT}\phi \ll 1$, $\sinh\left(\frac{F}{RT}\phi\right) \approx \frac{F}{RT}\phi$. Define

$$\kappa_L^2 = 2qN_aFCl_L/(\epsilon_0 D_w RT), \tag{5.28}$$

$$\kappa_R^2 = 2qN_aFCl_R/(\epsilon_0 D_w RT). \tag{5.29}$$

The expression $1/\kappa_i$ for $i = L, R$ has units of length and is called the Debye length. Solving the linearized forms of 5.26–5.27 and making use of boundary conditions as $x \to \pm\infty$ yields

$$\phi(x) = \phi(-d)\exp(\kappa_L(x+d)), \tag{5.30}$$

for $x < -d$, and

$$\phi(x) = \phi(d)\exp(\kappa_R(d-x)), \tag{5.31}$$

for $x > d$, where $\phi(-d)$ and $\phi(d)$ are the (so far) unknown values of ϕ at the two faces of the membrane.

5.2.1.2 Lipid Equations

Inside the lipid bilayer (for $|x| < d$), we assume that $h = n = c = 0$. To find equations for ϕ, we use the integral form of Gauss' law, which for an infinite sheet is given by

$$A\int_{x_0}^{x_f}\frac{d}{dx}\left(D(x)\frac{d\phi}{dx}\right)dx = -A\int_{x_0}^{x_f}\frac{zq}{\epsilon_0}\rho(x)dx, \tag{5.32}$$

where A is some arbitrary cross-sectional area, $D(x)$ is the space dependent dialectric constant of the medium, z is the valence of the charged particle, and $\rho(x)$ is the charge density. We use equation 5.32 and integrate across the left leaflet from $x = -d^-$ to $x = -d^+$. The right hand side of 5.32 is the enclosed charge and is given by AqC_L/ϵ_0. At $x = -d^-$, we are in the bath with dialectric constant D_w, and at $x = -d^+$, we are in the lipid with dialectric constant D_l. Thus, using 5.32 across the left leaflet yields

$$D_l\phi_x(-d^+) - D_w\phi_x(-d^-) = \frac{qC_L}{\epsilon_0}, \tag{5.33}$$

where ϕ_x indicates a first derivative with respect to x. Similarly, using equation 5.32 across the right leaflet yields

$$D_w\phi_x(d^+) - D_l\phi_x(d^-) = \frac{qC_R}{\epsilon_0}. \tag{5.34}$$

Since the electric field E is defined via $E = -\nabla\phi$, and we expect E to remain finite as

long as charge density remains finite, it follows that $\phi(x)$ is continuous everywhere. Thus $\phi(-d^-) = \phi(-d^+) = \phi(-d)$ and $\phi(d^-) = \phi(d^+) = \phi(d)$. Further, since there are no charges inside the membrane and $D(x) = D_l$ is constant, we have $d^2\phi/dx^2 = 0$ for $|x| < d$. This yields the relationship

$$\phi_x(-d^+) = \phi_x(d^-) = \frac{\phi(d) - \phi(-d)}{2d}. \tag{5.35}$$

Finally, using equations 5.30–5.31, we have

$$\phi_x(-d^-) = \kappa_L \phi(-d) \tag{5.36}$$

and

$$\phi_x(d^+) = -\kappa_R \phi(d). \tag{5.37}$$

The system of equations 5.33–5.37 can be solved to yield

$$\phi(-d) = \frac{-qdC_0}{\epsilon_0 D_w}\left[\frac{D_l(\hat{C}_L + \hat{C}_R) + 2dD_w\kappa_R\hat{C}_L}{dD_l(\kappa_L + \kappa_R) + 2d^2 D_w\kappa_L\kappa_R}\right], \tag{5.38}$$

$$\phi(d) = \frac{-qdC_0}{\epsilon_0 D_w}\left[\frac{D_l(\hat{C}_L + \hat{C}_R) + 2dD_w\kappa_L\hat{C}_R}{dD_l(\kappa_L + \kappa_R) + 2d^2 D_w\kappa_L\kappa_R}\right]. \tag{5.39}$$

where $\hat{C}_L = C_L/C_0$ and $\hat{C}_R = C_R/C_0$ are nondimensional charge densities, making the terms in brackets nondimensional. Using equations 5.22–5.24, 5.30–5.31, and 5.38–5.39, the system is fully determined for given input parameters $H_{L,R}, Na_{L,R}, \hat{C}_{L,R}$ and C_0.

5.2.2 Electrostatic Free Energy and Lipid Asymmetry

Given a volume V with charge density ρ and electrostatic potiential ϕ, the electrostatic free energy is given by [14]

$$G_{el} = \frac{1}{2}\int_V \rho\phi dV. \tag{5.40}$$

In our situation, ρ is given by $qN_a(h+n-c)$, which is $-2qN_aCl_{L,R}\sinh(F\phi/(RT))$ depending on whether $x < -d$ or $x > d$. Using the same linear approximation for the hyperbolic sine that we used earlier, we have

$$\begin{aligned} G_{el} = \frac{A}{2}\Bigg[\int_{-\infty}^{-d} -\epsilon_0 D_w\kappa_L^2(\phi(x))^2 dx + \int_d^{\infty} -\epsilon_0 D_w\kappa_R^2(\phi(x))^2 dx \\ -qC_0(\hat{C}_L\phi(-d) + \hat{C}_R\phi(d))\Bigg], \end{aligned} \tag{5.41}$$

where A is the area of one leaflet of the membrane. We solve equation 5.41 to yield

$$G_{el} = \frac{-Aq^2dC_0^2}{4\epsilon_0 D_w}\left[d\kappa_L(\hat{\phi}(-d))^2 + d\kappa_R(\hat{\phi}(d))^2 - 2(\hat{C}_L\hat{\phi}(-d) + \hat{C}_R\hat{\phi}(d))\right], \tag{5.42}$$

where $\hat{\phi}(-d)$ and $\hat{\phi}(d)$ are the nondimensional potentials (bracketed terms) from equations 5.38–5.39. Thus the bracketed term above is a nondimensional free energy.

To explore whether pH gradients can maintain an asymmetric distribution of charged lipids, we suppose that $H_{L,R}$ and $Na_{L,R}$ are given. We assume that $C_L + C_R = C_0$, where C_0 is some given maximal charge distribution. Then $\hat{C}_L + \hat{C}_R = 1$. We take C_0 to be $0.1/a_0$, where a_0 is the area of one lipid head group, meaning that 10% of the lipids making up the membrane are negatively charged. Under the assumption that lipids can flip between leaflets of the bilayer, we numerically minimize the electrostatic free energy given in equation 5.42 to find the steady state distribution of charged lipids. The results are shown in Table 5.2 for $Na_L = Na_R = 0.1M$ and various pH gradients. Other parameters are $d = 2nM$ and $a_0 = 40\mathring{A}^2$. We use $D_w = 80.4$ as the dialectric constant of water, and $D_l = 2$, the dialectric constant of oil, as the dialectric constant of the lipids. We can see that with this bath electrolyte concentration, pH gradients have very little effect on lipid asymmetry. The reason for this lack of pH dependence is clear. For these high bath electrolyte concentrations, even large changes in pH correspond to relatively small changes in the overall electrostatics of the system. Unfortunately, the linear assumption used to simplify equations 5.26–5.27 is not valid for low bath electrolyte concentrations.

5.2.3 Nonlinear Poisson Boltzmann Formulation

For $Na_{L,R}$ and $Cl_{L,R}$ small, it is not true that $F\phi/(RT) \ll 1$. We must work with equations 5.26–5.27 in their nonlinear form. By multiplying each side by $d\phi/dx$ and using the conditions that ϕ and $d\phi/dx \to 0$ and $x \to \pm\infty$, we can integrate once and find that

$$\frac{d\phi}{dx} = \pm\kappa_L \left(\frac{RT}{F}\right) \sqrt{2\left(\cosh\left(\frac{F}{RT}\phi\right) - 1\right)}, \tag{5.43}$$

for $x < -d$, and

$$\frac{d\phi}{dx} = \pm\kappa_R \left(\frac{RT}{F}\right) \sqrt{2\left(\cosh\left(\frac{F}{RT}\phi\right) - 1\right)}, \tag{5.44}$$

Table 5.2. Leaflet asymmetry imposed by various pH gradients. The sodium concentration is taken to be $0.1M$.

H_L	H_R	C_L
10^{-7}	$10^{-7.4}$	0.5000
10^{-4}	$10^{-7.4}$	0.5001
10^{-3}	$10^{-7.4}$	0.5012
10^{-2}	$10^{-7.4}$	0.5119

for $x > d$. Because the membrane charges are negative, we expect ϕ to be negative at $x = \pm d$. Thus, we choose the negative branch in equation 5.43 and the positive branch in equation 5.44. We perform further algebra inside the square root to yield

$$\frac{d\phi}{dx} = -2\kappa_L \left(\frac{RT}{F}\right) \left|\sinh\left(\frac{F}{2RT}\phi\right)\right|, \tag{5.45}$$

for $x < -d$, and

$$\frac{d\phi}{dx} = 2\kappa_R \left(\frac{RT}{F}\right) \left|\sinh\left(\frac{F}{2RT}\phi\right)\right|, \tag{5.46}$$

for $x > d$. Because the lipid equations described in section 5.2.1.2 are not affected by the nonlinear assumption, we can follow the same logic but use equations 5.45–5.46 instead of 5.36–5.37 to find the following pair of nonlinear equations for $\phi(-d)$ and $\phi(d)$:

$$\frac{D_l(\phi(d) - \phi(-d))}{2d} + D_w\kappa_L \left(\frac{2RT}{F}\right) \left|\sinh\left(\frac{F}{2RT}\phi(d)\right)\right| = \frac{qC_0\hat{C}_L}{\epsilon_0}, \tag{5.47}$$

$$-\frac{D_l(\phi(d) - \phi(-d))}{2d} + D_w\kappa_R \left(\frac{2RT}{F}\right) \left|\sinh\left(\frac{F}{2RT}\phi(-d)\right)\right| = \frac{qC_0\hat{C}_R}{\epsilon_0}. \tag{5.48}$$

We solve the system 5.47–5.48 numerically and use the resulting values for $\phi(-d)$ and $\phi(d)$ as boundary conditions to numerically integrate equations 5.45–5.46. We use the resulting profiles for ϕ to calculate the electrostatic free energy

$$\Delta G_{el} = \frac{A}{2}\left[\int_{-\infty}^{-d} -2qN_aCl_L \sinh\left(\frac{F}{RT}\phi(x)\right)\phi(x)dx \right.$$
$$\left. + \int_{d}^{\infty} -2qN_aCl_R \sinh\left(\frac{F}{RT}\phi(x)\right)\phi(x)dx - qC_0(\hat{C}_L\phi(-d) + \hat{C}_R\phi(d))\right],$$

where the integrations are done numerically using the trapezoidal rule.

As expected, when bath electrolyte concentrations are high, the results from the nonlinear theory are very similar to the results from the linear theory. Even large pH gradients cause very little asymmetry in the bilayer. As bath concentrations are lowered, however, pH gradents have a more significant effect.

Figure 5.6 shows the electrostatic free energy plotted as a function of $\hat{C}_L$, the proportion of negatively charged lipids in the left leaflet. The pH is 3 in the left bath and 7.4 in the right bath. Notice that for large bath electrolyte concentrations, charged lipids are almost evenly split between the two leaflets of the bilayer. As bath electrolyte concentrations decrease, the minimum moves to the right. For salt bath concentrations of 0.1 mM, the minimum energy corresponds to approximately 66.5% of the charged lipids in the left leaflet.

For a more realistic pH gradient of 5 on one side of the membrane and 7.4 on the other, similar to the physiological pH gradient in the MVB [44], less than 51% of the charged lipids

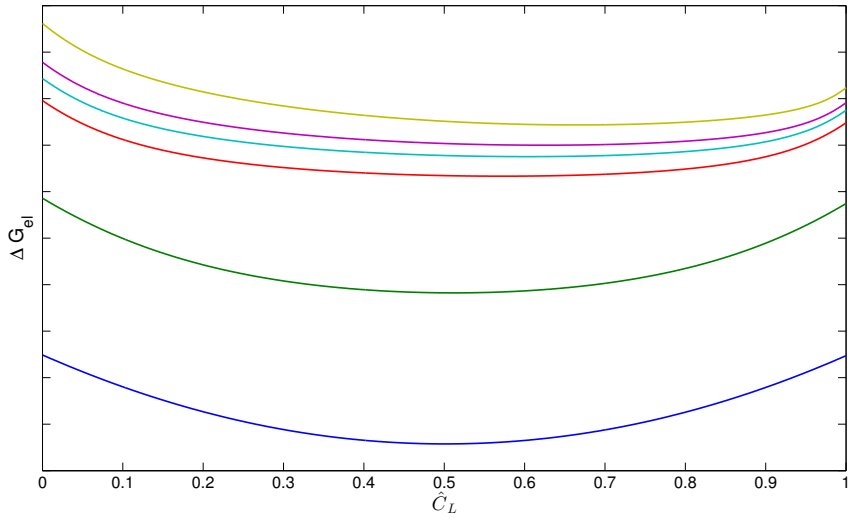

Figure 5.6. Energy ΔG_{el} plotted as a function of scaled $\hat{C}_L$. The blue, green, red, cyan, magenta, and yellow curves correspond to $Na_{L,R} = 100mM, 10mM, 1mM, 0.5mM, 0.3mM$, and $0.1mM$, respectively. The pH in the left bath is 3, and the pH in the right bath is 7.4. All other parameters are the same as described previously.

are in the left leaflet, even at a bath electrolyte concentrations of 0.1mM, indicating that pH gradients are not significant inducers of bilayer asymmetry under the conditions modeled. It is likely that actual electrolyte concentrations in the MVB are higher than 0.1mM [52], further emphasizing the idea that pH gradients are not major inducers of lipid asymmetry, at least as described by the current model. The fact remains, however, that pH gradients seem to be important in the formation of vesicles in the MVB body. The significance of those gradients remains an interesting question in cellular physiology.

5.3 Conclusion

We developed and explored two models based on the idea that lipids may flip rapidly between the two leaflets of the bilayer in a protein independent way. In the first model, we found that though the model predicted a range of steady state curvatures, the waiting times to transition from a flat membrane to a curved membrane corresponding to the initiation of a vesicle are too long to be physiologically relevant, at least under the parameters used from the literature. In the second model, we found that unless salt concentrations are very low, pH gradients are not likely to be significant inducers of bilayer asymmetry.

CHAPTER 6

CONCLUSION

Biological membranes are important structural units in the cell. More than just serving as barriers between different compartments inside the cell, membranes themselves behave in interesting and dynamic ways that can affect cellular function. In this dissertation, we have focused on two specific behaviors of membranes, the tangential flows of the lipids that form the bilayer, and the flip-flop of lipids between leaflets in the bilayer.

In the majority of this dissertation, we worked to develop and analyze a two phase fluid model of a membrane. Our main goal was to explore the interplay between membrane shape and phase separation. While there have been experimental findings indicating the existence of curvature-induced phase separation, there has been limited mathematical treatment of the phenomenon. Through our model, we were able to explore situations, both in one dimension and in two dimensions, under which curvature can cause phase separation. We hypothesized that one specific situtation where curvature induced phase separation may be important is in the proper functioning of the Golgi apparatus.

In the latter part of this dissertation, we briefly explored some of the implications of facile lipid flip-flop between the two leaflets of the bilayer. We were specifically interested in understanding some of the processes that may contribute to vesicle budding in the multivesicular body. Though our explorations did not yield substantial information about the processes of vesicle formation, we still find the experiments indicating more rapid flip-flop to be compelling. The conventional belief is that flip-flop is a very slow process in the absence of specific proteins, and it remains to be seen what implications rapid flip-flop may have on the understanding of cellular processes.

6.1 Future Work

We believe the work presented in this dissertation to be substantial and original work that serves to enhance our understanding of biological membranes. Even so, there always remains more work that can be done. We conclude with several brief descriptions of ideas for future work.

In our derivation of the two phase fluid equations presented in Chapter 2, we included viscosity of the membrane lipids, but neglected to take into account the fluid in which the membrane is embedded. Many papers that model the flow of a single phase on a membrane take into account the viscous nature of the ambient fluid [3, 10, 29, 46, 49, 53, 72]. Some even neglect the membrane viscosity and only model the viscosity of the embedding fluid[46, 56]. In general, authors have modeled the ambient fluid as an incompressible Newtonian fluid. They assume a no slip boundary between the ambient fluid and the surface fluid. Though no slip does not make sense in the context of our two phase model, it may be reasonable to include a drag term between the surface phases and the ambient fluid similar to the drag term between the two phases. This inclusion of the ambient fluid is one relatively obvious and interesting extension to the current model, which may serve to make it more physiologically relevant.

Related to the issue of the ambient fluid is the issue of volume conservation. Our model preserves the area of the membrane, but does not conserve the volume inside closed surfaces. In other words, our membrane is permeable. Many of the interesting shapes resulting from the study of the shape equation arise via the combination of conserved area and conserved volume [57]. While we have chosen not to conserve volume in our formulation, it can likely be done by means of a Lagrange multiplier. This would allow us to explore the effects of volume conservation even without including the ambient fluid.

Another interesting extension of the two phase model is to include lipids with charged head groups. Electrostatic repulsion could be included as another term in the free energy density. This would enable electrostatic effects to enter naturally as new forcing terms in the force balance equations. If desired, a second Lagrange multiplier could be used to ensure charge neutrality, though this would likey require the inclusion of the ambient fluid since there exist negatively charged, but no positively charged lipids. The work presented in Chapter 5 regarding electrostatics could serve as a nice starting point in this exploration of the effects of charged lipids. A biologically relevant question is whether phase separation of charged lipids can serve as an initiator of vesicle bud formation or tubule formation.

A further use of the work presented in Chapter 5 could be to combine flip-flop with the two phase model derived in Chapter 2 to serve as a basis for a fluid model describing the bilayer nature of a membrane. This has been investiged to some extent in [50] and [46], but only in the context of one lipid species. Our model describes the membrane as a single surface, but the membrane is in fact made up of two surfaces maintained at an approximately fixed distance apart. If lipids can truly undergo rapid flip-flop, the two

surfaces actually exchange area with each other. This could have important impacts on the shape of a bilayer.

An additional idea for future investigation involves the one-dimensional form of the full model presented in Chapter 4. In that derivation we made the assumption that our closed surface is actually a closed curve in the plane. While this assumption allowed us to greatly simplify the system, it introduced a certain amount of ambiguity due to the fact that many two-dimensional elements used to describe a surface do not have one-dimensional analogues. We made the further assumption that shape equilibrates instantaneously so that the shape is given by minimizing the free energy instead of balancing forces in the normal direction. An alternative one-dimensional derivation is to assume that the two-dimensional surface is cylindrically shaped, but uniform in one direction as shown in Figure 6.1. If we assume the surface is uniform and infinite in the y direction, the shape is given by a simple closed curve in the x–z plane. In this case, the two-dimensional elements such as the metric tensor and curvature tensor are well defined even though the problem is essentially one-dimensional. It would be interesting to see if the system resulting from this alternate derivation behaves differently in any fundamental ways than the system explored in the current chapter.

A final extension of the current work involves the numerical simulation of the full two-dimensional system. We were able to perform linear stability analysis of the equations, but that analysis does not provide much information about the system at later times. A functioning numerical simulation would allow us to explore the nonlinear dynamics of the system as it phase separates and changes shape. We would be able to describe more fully the behaviors of the two-dimensional system and the biological relevance of those behaviors.

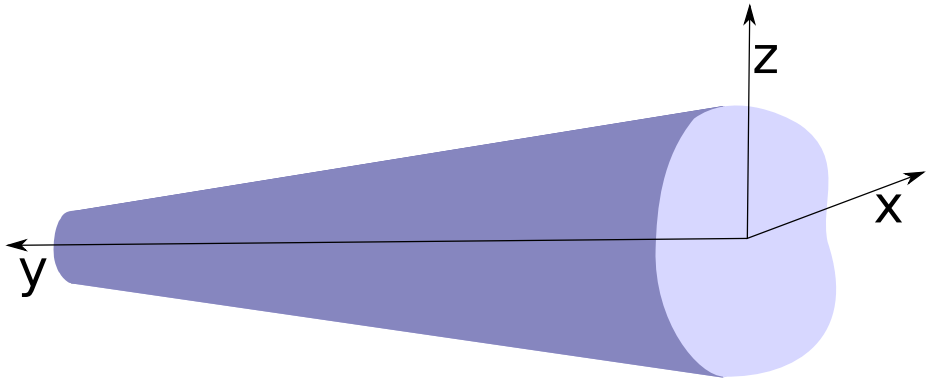

Figure 6.1. Two-dimensional surface, uniform in one dimension.

APPENDIX A

CALCULATIONS TO SUPPLEMENT CHAPTER 2

A.1 Time Derivatives of Geometric Quantities

We wish to calculate the time derivatives of various geometric quantities. Most of these quantities are only needed in the surface fixed coordinates, though a few of them are needed in both the surface fixed and general coordinates.

A.1.1 Surface-Fixed Coordinates

For the time derivative of the tangent vector, we have

$$\begin{aligned}\frac{\partial}{\partial t}\mathbf{t}_\alpha &= \frac{\partial}{\partial t}\frac{\partial}{\partial \xi^\alpha}\mathbf{r} \\ &= \frac{\partial}{\partial \xi^\alpha}\frac{\partial \mathbf{r}}{\partial t} \\ &= \frac{\partial}{\partial \xi^\alpha}(U_n\mathbf{n}) \\ &= \frac{\partial U_n}{\partial \xi^\alpha}\mathbf{n} - U_n b_\alpha^\gamma \mathbf{t}_\gamma,\end{aligned} \tag{A.1}$$

where we have used the fact that $\frac{\partial \mathbf{r}}{\partial t} = U_n\mathbf{n}$ in surface-fixed coordinates. From there, it follows that

$$\begin{aligned}\frac{\partial}{\partial t}a_{\alpha\beta} &= \frac{\partial}{\partial t}\mathbf{t}_\alpha \cdot \mathbf{t}_\beta + \mathbf{t}_\alpha \cdot \frac{\partial}{\partial t}\mathbf{t}_\beta \\ &= (-U_n b_\alpha^\gamma \mathbf{t}_\gamma)\cdot \mathbf{t}_\beta - \mathbf{t}_\alpha \cdot U_n b_\beta^\gamma \mathbf{t}_\gamma \\ &= -U_n b_\alpha^\gamma a_{\gamma\beta} - U_n b_\beta^\gamma a_{\alpha\gamma} \\ &= -2U_n b_{\alpha\beta},\end{aligned} \tag{A.2}$$

where we have used the fact that $\mathbf{t}_\alpha$ and $\mathbf{n}$ are orthogonal and $b_{\alpha\beta}$ is symmetric.

To calculate the derivative of the square root of the metric, we use equation A.23. Thus

$$\begin{aligned}\frac{\partial a}{\partial t} &= a a^{\alpha\beta}\frac{\partial}{\partial t}a_{\alpha\beta} \\ &= a a^{\alpha\beta}(-2U_n b_{\alpha\beta}) \\ &= -4aHU_n.\end{aligned} \tag{A.3}$$

To calculate the time derivative of the inverse metric tensor, we use the fact that $a^{\alpha\lambda}a_{\lambda\mu} = \delta^{\alpha}_{\mu}$. It follows that

$$\begin{aligned}
\frac{\partial}{\partial t}(a^{\alpha\lambda})a_{\lambda_\mu} &= -a^{\alpha\lambda}\frac{\partial}{\partial t}(a_{\lambda\mu}) \\
\Rightarrow \frac{\partial}{\partial t}(a^{\alpha\lambda})a_{\lambda_\mu}a^{\mu\beta} &= -a^{\mu\beta}a^{\alpha\lambda}\frac{\partial}{\partial t}(a_{\lambda\mu}) \\
\Rightarrow \frac{\partial}{\partial t}(a^{\alpha\lambda})\delta^{\beta}_{\lambda} &= -a^{\alpha\lambda}a^{\beta\mu}\frac{\partial}{\partial t}(a_{\lambda\mu}) \\
\Rightarrow \frac{\partial}{\partial t}(a^{\alpha\beta}) &= -a^{\alpha\lambda}a^{\beta\mu}\frac{\partial}{\partial t}(a_{\lambda\mu}) \\
\Rightarrow \frac{\partial}{\partial t}(a^{\alpha\beta}) &= 2U_n b^{\alpha\beta}.
\end{aligned} \tag{A.4}$$

Using $\mathbf{n}\cdot\mathbf{t}_\alpha = 0$, we calculate the time derivative of the unit normal,

$$\begin{aligned}
\frac{\partial \mathbf{n}}{\partial t}\cdot\mathbf{t}_\alpha &= -\mathbf{n}\cdot\frac{\partial}{\partial t}\mathbf{t}_\alpha \\
\Rightarrow \frac{\partial \mathbf{n}}{\partial t}\cdot\mathbf{t}_\alpha &= -\frac{\partial U_n}{\partial u_\alpha} \\
\Rightarrow \frac{\partial \mathbf{n}}{\partial t} &= -a^{\lambda\mu}\frac{\partial U_n}{\partial \xi^\mu}\mathbf{t}_\lambda.
\end{aligned} \tag{A.5}$$

To calculate $\frac{\partial}{\partial t}b_{\alpha\beta}$, we use equation 2.8, which states $\frac{\partial \mathbf{n}}{\partial \xi^\beta} = -b_{\alpha\beta}a^{\alpha\lambda}\mathbf{t}_\lambda$. We initially focus on the derivatives of the left and right hand sides of the equation individually.

$$\begin{aligned}
\frac{\partial}{\partial t}\frac{\partial \mathbf{n}}{\partial \xi^\beta} &= \frac{\partial}{\partial \xi^\beta}\frac{\partial \mathbf{n}}{\partial t} \\
&= -\frac{\partial}{\partial \xi^\beta}(a^{\lambda\mu}\frac{\partial U_n}{\partial \xi^\mu}\mathbf{t}_\lambda) \\
&= (a^{\lambda\gamma}\Gamma^{\mu}_{\gamma\beta} + a^{\gamma\mu}\Gamma^{\lambda}_{\gamma\beta})\frac{\partial U_n}{\partial \xi^\mu}\mathbf{t}_\lambda - a^{\lambda\mu}\frac{\partial}{\partial \xi^\beta}\frac{\partial U_n}{\partial \xi^\mu}\mathbf{t}_\lambda - a^{\lambda\mu}\frac{\partial U_n}{\partial \xi^\mu}(\Gamma^{\gamma}_{\beta\lambda}\mathbf{t}_\gamma + b_{\lambda\beta}\mathbf{n}) \\
&= a^{\lambda\gamma}\Gamma^{\mu}_{\gamma\beta}\frac{\partial U_n}{\partial \xi^\mu}\mathbf{t}_\lambda - a^{\lambda\mu}\frac{\partial}{\partial \xi^\beta}\frac{\partial U_n}{\partial \xi^\mu}\mathbf{t}_\lambda - a^{\lambda\mu}\frac{\partial U_n}{\partial \xi^\mu}b_{\lambda\beta}\mathbf{n} \\
&= -a^{\lambda\mu}\left(\frac{\partial}{\partial \xi^\beta}\frac{\partial U_n}{\partial \xi^\mu} - \frac{\partial U_n}{\partial \xi^\gamma}\Gamma^{\gamma}_{\mu\beta}\right)\mathbf{t}_\lambda - a^{\lambda\mu}\frac{\partial U_n}{\partial \xi^\mu}b_{\lambda\beta}\mathbf{n} \\
&= -a^{\lambda\mu}\mathbf{t}_\lambda\nabla_\beta\nabla_\mu U_n - a^{\lambda\mu}\frac{\partial U_n}{\partial \xi^\mu}b_{\lambda\beta}\mathbf{n},
\end{aligned} \tag{A.6}$$

where we have used equation A.38 for the partial derivative of the inverse metric tensor. For the right hand side, we have

$$\begin{aligned}
-\frac{\partial}{\partial t}(b_{\alpha\beta}a^{\alpha\lambda}\mathbf{t}_\lambda) &= -\frac{\partial}{\partial t}(b_{\alpha\beta})a^{\alpha\lambda}\mathbf{t}_\lambda - b_{\alpha\beta}(2U_n b^{\alpha\lambda})\mathbf{t}_\lambda - b_{\alpha\beta}a^{\alpha\lambda}\left(\frac{\partial U_n}{\partial \xi^\lambda}\mathbf{n} - U_n b^{\mu}_{\lambda}\mathbf{t}_\mu\right) \\
&= -\frac{\partial}{\partial t}(b_{\alpha\beta})a^{\alpha\lambda}\mathbf{t}_\lambda - 2U_n b_{\alpha\beta}b^{\alpha\lambda}\mathbf{t}_\lambda - a^{\alpha\lambda}\frac{\partial U_n}{\partial u^\lambda}b_{\alpha\beta}\mathbf{n} + U_n b_{\alpha\beta}b^{\alpha\mu}\mathbf{t}_\mu \\
&= -\frac{\partial}{\partial t}(b_{\alpha\beta})a^{\alpha\lambda}\mathbf{t}_\lambda - U_n b_{\alpha\beta}b^{\alpha\lambda}\mathbf{t}_\lambda - a^{\alpha\lambda}\frac{\partial U_n}{\partial u^\lambda}b_{\alpha\beta}\mathbf{n}.
\end{aligned} \tag{A.7}$$

Comparing equation A.6 with equation A.7, we see that that normal components cancel,

leaving

$$\begin{aligned} -a^{\alpha\lambda}\mathbf{t}_\lambda\nabla_\beta\nabla_\alpha U_n &= -\frac{\partial}{\partial t}(b_{\alpha\beta})a^{\alpha\lambda}\mathbf{t}_\lambda - U_n b_{\alpha\beta}b^{\alpha\lambda}\mathbf{t}_\lambda \\ \Rightarrow \frac{\partial}{\partial t}(b_{\alpha\beta})a^{\alpha\lambda}\mathbf{t}_\lambda &= (\nabla_\beta\nabla_\alpha U_n - U_n b_{\mu\beta}b^\mu_\alpha)a^{\alpha\lambda}\mathbf{t}_\lambda \\ \Rightarrow \frac{\partial}{\partial t}(b_{\alpha\beta}) &= \nabla_\beta\nabla_\alpha U_n - U_n b_{\mu\beta}b^\mu_\alpha. \end{aligned} \tag{A.8}$$

With all of these identities, we are able to calculate the time derivative of the mean curvature, $H = \frac{1}{2}a^{\alpha\beta}b_{\alpha\beta}$. We have

$$\begin{aligned} \frac{\partial H}{\partial t} &= \frac{1}{2}\left(\frac{\partial}{\partial t}(a^{\alpha\beta})b_{\alpha\beta} + a^{\alpha\beta}\frac{\partial}{\partial t}(b_{\alpha\beta})\right) \\ &= \frac{1}{2}\left(2U_n b^{\alpha\beta}b_{\alpha\beta} + a^{\alpha\beta}(\nabla_\beta\nabla_\alpha U_n - U_n b_{\mu\beta}b^\mu_\alpha)\right) \\ &= \frac{1}{2}\left(2U_n b^{\alpha\beta}b_{\alpha\beta} + a^{\alpha\beta}\nabla_\beta\nabla_\alpha U_n - U_n b_{\mu\beta}b^{\mu\beta}\right) \\ &= \frac{1}{2}\left(U_n b^{\alpha\beta}b_{\alpha\beta} + a^{\alpha\beta}\nabla_\beta\nabla_\alpha U_n\right) \\ &= \frac{1}{2}(U_n(4H^2 - 2K) + a^{\alpha\beta}\nabla_\beta\nabla_\alpha U_n) \\ &= (2H^2 - K)U_n + \frac{1}{2}a^{\alpha\beta}\nabla_\beta\nabla_\alpha U_n, \end{aligned} \tag{A.9}$$

where we have used the fact given in [2] that $b^{\alpha\beta}b_{\alpha\beta} = 4H^2 - 2K$.

A.1.2 General Coordinates

In general coordinates, we need only calculate the time derivative of the metric tensor. Starting with the tangent vectors, we have

$$\begin{aligned} \frac{\partial}{\partial t}(\mathbf{t}_\alpha) &= \frac{\partial}{\partial t}\left(\frac{\partial \mathbf{r}}{\partial u^\alpha}\right) \\ &= \frac{\partial}{\partial u^\alpha}\left(\frac{\partial \mathbf{r}}{\partial t}\right) \\ &= \frac{\partial}{\partial u^\alpha}\left(U^\lambda\mathbf{t}_\lambda + U_n\mathbf{n}\right) \\ &= \frac{\partial U^\lambda}{\partial u^\alpha}\mathbf{t}_\lambda + \mathbf{U}^\lambda\left(\mathbf{\Gamma}^\gamma_{\alpha\lambda}\mathbf{t}_\gamma + \mathbf{b}_{\alpha\gamma}\mathbf{n}\right) + \frac{\partial \mathbf{U_n}}{\partial \mathbf{u}^\alpha}\mathbf{n} - \mathbf{U_n}\mathbf{b}^\gamma_\alpha\mathbf{t}_\gamma \\ &= \left(\frac{\partial U^\gamma}{\partial u^\alpha} + U^\lambda\Gamma^\gamma_{\alpha\lambda}\right)\mathbf{t}_\gamma + U^\lambda b_{\alpha\lambda}\mathbf{n} + \frac{\partial U_n}{\partial u^\alpha}\mathbf{n} - U_n b^\gamma_\alpha\mathbf{t}_\gamma \\ &= \left(\nabla_\alpha U^\gamma - U_n b^\lambda_\alpha\right)\mathbf{t}_\gamma + \left(\frac{\partial U_n}{\partial u^\alpha} + U^\gamma b_{\alpha\gamma}\right)\mathbf{n}. \end{aligned} \tag{A.10}$$

This gives

$$\begin{aligned}\frac{\partial}{\partial t}a_{\alpha\beta} &= \frac{\partial}{\partial t}\mathbf{t}_\alpha \cdot \mathbf{t}_\beta + \mathbf{t}_\alpha \cdot \frac{\partial}{\partial t}\mathbf{t}_\beta \\ &= \left(\nabla_\alpha U^\gamma - U_n b_\alpha^\gamma\right) a_{\beta\gamma} + \left(\nabla_\beta U^\gamma - U_n b_\beta^\gamma\right) a_{\alpha\gamma} \\ &= \nabla_\alpha U_\beta + \nabla_\beta U_\alpha - 2b_{\alpha\beta}U_n.\end{aligned} \tag{A.11}$$

A.2 Rate of Strain Tensor

We derive the rate of strain tensor following arguments [2]. In convected coordinates,

$$S_{\Gamma\Delta} = \frac{1}{2}\frac{d}{dt}a_{\Gamma\Delta}, \tag{A.12}$$

where the derivative is the material derivative following a particle. We wish to find $S_{\alpha\beta}$, the components of the rate of strain tensor expressed in terms of general coordinates. Using the transformation rule A.45 for covariant tensor components,

$$\begin{aligned}\frac{d}{dt}a_{\Gamma\Delta} &= \frac{d}{dt}\left(\frac{\partial u^\alpha}{\partial u^\Gamma}\frac{\partial u^\beta}{\partial u^\Delta}a_{\alpha\beta}\right) \\ &= \frac{d}{dt}\left(\frac{\partial u^\alpha}{\partial u^\Gamma}\right)\frac{\partial u^\beta}{\partial u^\Delta}a_{\alpha\beta} + \frac{\partial u^\alpha}{\partial u^\Gamma}\frac{d}{dt}\left(\frac{\partial u^\beta}{\partial u^\Delta}\right)a_{\alpha\beta} + \frac{\partial u^\alpha}{\partial u^\Gamma}\frac{\partial u^\beta}{\partial u^\Delta}\frac{d}{dt}a_{\alpha\beta}.\end{aligned} \tag{A.13}$$

Since $\frac{d}{dt}$ is a derivative with fixed $\{u^\Gamma\}$, we can swap orders of integration to get

$$\frac{d}{dt}\left(\frac{\partial u^\alpha}{\partial u^\Gamma}\right) = \frac{\partial}{\partial u^\Gamma}\frac{du^\alpha}{dt} = \frac{\partial v^\alpha}{\partial u^\Gamma} = \frac{\partial v^\alpha}{\partial u^\gamma}\frac{\partial u^\gamma}{\partial u^\Gamma}. \tag{A.14}$$

Thus we have

$$\frac{d}{dt}a_{\Gamma\Delta} = \frac{\partial v^\alpha}{\partial u^\gamma}\frac{\partial u^\gamma}{\partial u^\Gamma}\frac{\partial u^\beta}{\partial u^\Delta}a_{\alpha\beta} + \frac{\partial u^\alpha}{\partial u^\Gamma}\frac{\partial v^\beta}{\partial u^\gamma}\frac{\partial u^\gamma}{\partial u^\Delta}a_{\alpha\beta} + \frac{\partial u^\alpha}{\partial u^\Gamma}\frac{\partial u^\beta}{\partial u^\Delta}\frac{d}{dt}a_{\alpha\beta}, \tag{A.15}$$

which upon permuting the repeated indices, can be written as

$$\frac{d}{dt}a_{\Gamma\Delta} = \frac{\partial u^\alpha}{\partial u^\Gamma}\frac{\partial u^\beta}{\partial u^\Delta}\left(\frac{\partial v^\gamma}{\partial u^\alpha}a_{\gamma\beta} + \frac{\partial v^\gamma}{\partial u^\beta}a_{\alpha\gamma} + \frac{\partial}{\partial t}a_{\alpha\beta} + v^\gamma\frac{\partial}{\partial u^\gamma}a_{\alpha\beta}\right), \tag{A.16}$$

where we have expanded the material derivative of $a_{\alpha\beta}$. Now Since

$$S_{\Gamma\Delta} = \frac{1}{2}\frac{\partial u^\alpha}{\partial u^\Gamma}\frac{\partial u^\beta}{\partial u^\Delta}\left(\frac{\partial v^\gamma}{\partial u^\alpha}a_{\gamma\beta} + \frac{\partial v^\gamma}{\partial u^\beta}a_{\alpha\gamma} + \frac{\partial}{\partial t}a_{\alpha\beta} + v^\gamma\frac{\partial}{\partial u^\gamma}a_{\alpha\beta}\right), \tag{A.17}$$

it follows that $S_{\Gamma\Delta}$, expressed in fixed coordinates, is given by

$$S_{\alpha\beta} = \frac{1}{2}\left(\frac{\partial v^\gamma}{\partial u^\alpha}a_{\gamma\beta} + \frac{\partial v^\gamma}{\partial u^\beta}a_{\alpha\gamma} + \frac{\partial}{\partial t}a_{\alpha\beta} + v^\gamma\frac{\partial}{\partial u^\gamma}a_{\alpha\beta}\right). \tag{A.18}$$

This expression can be cleaned up significantly. We use the definition of the covariant derivative to replace $\frac{\partial v^\gamma}{\partial u^\alpha}$ and $\frac{\partial v^\gamma}{\partial u^\beta}$ with $\nabla_\alpha v^\gamma - v^\nu\Gamma^\gamma_{\nu\alpha}$ and $\nabla v^\gamma - v^\nu\Gamma^\gamma_{\nu\beta}$, respectively. Further, we use the fact that the covariant derivative of $a_{\alpha\beta}$ is zero to replace $\frac{\partial}{\partial u^\gamma}a_{\alpha\beta}$ with $a_{\alpha\nu}\Gamma^\nu_{\beta\gamma} + a_{\nu\beta}\Gamma^\nu_{\alpha\gamma}$. Upon simplification, all the terms with Christoffel symbolys cancel, yielding

$$S_{\alpha\beta} = \frac{1}{2}\left(\nabla_\alpha v_\beta + \nabla_\beta v_\alpha + \frac{\partial}{\partial t} a_{\alpha\beta}\right). \tag{A.19}$$

Recall that the form of $\frac{\partial}{\partial t} a_{\alpha\beta}$ depends on the type of coordinates. Thus

$$S_{\alpha\beta} = \frac{1}{2}\left(\nabla_\alpha v_\beta + \nabla_\beta v_\alpha - 2b_{\alpha\beta} U_n\right), \tag{A.20}$$

in surface-fixed coordinates, and

$$S_{\alpha\beta} = \frac{1}{2}\left(\nabla_\alpha v_\beta + \nabla_\beta v_\alpha + \nabla_\alpha U_\beta + \nabla_\beta U_\alpha - 2b_{\alpha\beta} U_n\right) \tag{A.21}$$

in general coordinates.

A.3 Areal Dilation

Recall that an area element is given by $\sqrt{a} du^1 du^2$ where a is the determinant of the metric tensor. Thus $\frac{1}{\sqrt{a}} \frac{\partial}{\partial t} \sqrt{a} = \frac{1}{2a} \frac{\partial a}{\partial t}$ can be thought of as a relative change in area. Because the metric tensor is only second order, it has a simple form given by

$$a = a_{11} a_{22} - a_{12} a_{21}. \tag{A.22}$$

Taking the time derivative on both sides, using the fact that the components of the inverse of a second order tensor have a simple form, and using the symmetry of $a^{\alpha\beta}$, we have

$$\begin{aligned} \frac{da}{dt} &= \frac{da_{11}}{dt} a_{22} + a_{11} \frac{da_{22}}{dt} - \frac{da_{12}}{dt} a_{21} - a_{12} \frac{da_{21}}{dt} \\ &= a\left(a^{11} \frac{da_{11}}{dt} + a^{22} \frac{da_{22}}{dt} + a^{12} \frac{da_{12}}{dt} + a^{21} \frac{da_{21}}{dt}\right) \\ &= a a^{\alpha\beta} \frac{d}{dt} a_{\alpha\beta}. \end{aligned} \tag{A.23}$$

This relationship holds true in surface fixed, convected, and general coordinates.

Using the transformation rule A.43 for $a^{\Gamma\Delta} = \frac{\partial u^\Gamma}{\partial u^\lambda} \frac{\partial u^\Delta}{\partial u^\mu} a^{\lambda\mu}$ and equation A.16, we have

$$\begin{aligned} \frac{1}{2a'} \frac{da'}{dt} &= \frac{1}{2} a^{\Gamma\Delta} \frac{d}{dt} a_{\Gamma\Delta} \\ &= \frac{1}{2} a^{\lambda\mu} \frac{\partial u^\Gamma}{\partial u^\lambda} \frac{\partial u^\Delta}{\partial u^\mu} \frac{\partial u^\alpha}{\partial u^\Gamma} \frac{\partial u^\beta}{\partial u^\Delta} \left(\nabla_\alpha v_\beta + \nabla_\beta v_\alpha + \frac{\partial}{\partial t} a_{\alpha\beta}\right) \\ &= \frac{1}{2} a^{\lambda\mu} \delta^\alpha_\lambda \delta^\beta_\mu \left(\nabla_\alpha v_\beta + \nabla_\beta v_\alpha + \frac{\partial}{\partial t} a_{\alpha\beta}\right) \\ &= \frac{1}{2} a^{\alpha\beta} \left(\nabla_\alpha v_\beta + \nabla_\beta v_\alpha + \frac{\partial}{\partial t} a_{\alpha\beta}\right). \end{aligned} \tag{A.24}$$

Thus we have

$$\frac{1}{2a'} \frac{da'}{dt} = \nabla_\alpha v^\alpha - 2HU_n, \tag{A.25}$$

in surface-fixed coordinates and

$$\frac{1}{2a'}\frac{da'}{dt} = \nabla_\alpha v^\alpha + \nabla_\alpha U^\alpha - 2HU_n \tag{A.26}$$

in general coordinates.

A.4 Viscous Dissipation Variation

The total rate of viscous dissipation is given by

$$\begin{aligned}\Phi = \frac{1}{2}\int d\xi^1 d\xi^2 \sqrt{a}\Big[&{}_sT^{\alpha\beta}{}_sS_{\alpha\beta}\theta_s + {}_gT^{\alpha\beta}{}_gS_{\alpha\beta}\theta_g \\ &+\theta_s\theta_g\xi a^{\alpha\beta}(v_\alpha - w_\alpha)(v_\beta - w_\beta)\Big].\end{aligned} \tag{A.27}$$

To find the first variation with respect to velocity, we first replace each velocity with that same velocity plus a variation, for example $v_\alpha \to v_\alpha + p\delta v_\alpha$ where p is a positive real number. The variation δv_α must be admissible, meaning that it must meet certain criteria such as smoothness or boundary conditions. These criteria are situation dependent. We then calculate the derivative of the result with respect to p at $p = 0$.

Consider the dissipation in the sphingolipid phase. This is identical to the glycerolipid phase except that v is replaced with w, and the viscosity constants may be different. Define

$$Q^{\alpha\beta\lambda\mu} = \eta a^{\alpha\beta}a^{\lambda\mu} + \epsilon(a^{\alpha\lambda}a^{\beta\mu} + a^{\alpha\mu}a^{\beta\lambda} - a^{\alpha\beta}a^{\lambda\mu}). \tag{A.28}$$

Then $T^{\alpha\beta}S_{\alpha\beta}$ can be written

$$T^{\alpha\beta}S_{\alpha\beta} = Q^{\alpha\beta\lambda\mu}S_{\lambda\mu}S_{\alpha\beta}. \tag{A.29}$$

Notice that $Q^{\alpha\beta\lambda\mu}S_{\alpha\beta} = T^{\lambda\mu}$ and $Q^{\alpha\beta\lambda\mu}S_{\lambda\mu} = T^{\alpha\beta}$. For the first variation of the sphingolipid viscous dissipation, we have

$$\begin{aligned}&\frac{1}{8}\int d\xi^1 d\xi^2 \sqrt{a}\theta_s \Big\{Q^{\alpha\beta\lambda\mu}\left[\nabla_\lambda v_\mu + \nabla_\mu v_\lambda - 2b_{\lambda\mu}U_n\right]\left[\nabla_\alpha(\delta v_\beta) + \nabla_\beta(\delta v_\alpha)\right. \\ &\left.-2b_{\alpha\beta}\delta U_n\right] + Q^{\alpha\beta\lambda\mu}\left[\nabla_\lambda(\delta v_\mu) + \nabla_\mu(\delta v_\lambda) - 2b_{\lambda\mu}\delta U_n\right]\left[\nabla_\alpha v_\beta + \nabla_\beta v_\alpha - 2b_{\alpha\beta}U_n\right]\Big\} \\ &= \frac{1}{4}\int d\xi^1 d\xi^2 \sqrt{a}\theta_s \Big\{T^{\alpha\beta}\left[\nabla_\alpha(\delta v_\beta) + \nabla_\beta(\delta v_\alpha) - 2b_{\alpha\beta}\delta U_n\right] \\ &+T^{\lambda\mu}\left[\nabla_\lambda(\delta v_\mu) + \nabla_\mu(\delta v_\lambda) - 2b_{\lambda\mu}\delta U_n\right]\Big\} \\ &= \int d\xi^1 d\xi^2 \sqrt{a}\theta_s \Big\{T^{\alpha\beta}\left[\nabla_\alpha(\delta v_\beta) - b_{\alpha\beta}\delta U_n\right]\Big\} \\ &= \int d\xi^1 d\xi^2 \sqrt{a}\theta_s \Big\{-\nabla_\alpha(T^{\alpha\beta})\delta v_\beta - T^{\alpha\beta}b_{\alpha\beta}\delta U_n\Big\} + \text{boundary terms},\end{aligned} \tag{A.30}$$

noindent where we have used the fact that $T^{\alpha\beta}$ is symmetric, and have used integration by parts to move the derivative from δv_β to $T^{\alpha\beta}$ as shown in section A.6. The boundary terms that possibly arise when integrating by parts are dealt with in the specific situations

addressed in this dissertation.

It is easy to see that variations of

$$\frac{1}{2}\int d\xi^1 d\xi^2 \sqrt{a}\theta_s\theta_g\xi a^{\alpha\beta}(v_\alpha - w_\alpha)(v_\beta - w_\beta) \tag{A.31}$$

will result in

$$\int d\xi^1 d\xi^2 \sqrt{a}\theta_s\theta_g\xi a^{\alpha\beta}(v_\alpha - w_\alpha)(\delta v_\beta - \delta w_\beta). \tag{A.32}$$

Combining the contributions from sphingolipid viscosity, glycerolipid viscosity, and drag results in equation 2.47.

A.5 Christoffel Symbols and Identities

The Christoffel symbols of the first kind are denoted $\Gamma_{\alpha\beta\gamma}$ and are defined in terms of partial derivatives of the metric tensor as

$$\Gamma_{\alpha\beta\gamma} = \frac{1}{2}\left(\frac{\partial a_{\gamma\beta}}{\partial u^\alpha} + \frac{\partial a_{\gamma\alpha}}{\partial u^\beta} - \frac{\partial a_{\alpha\beta}}{\partial u^\gamma}\right). \tag{A.33}$$

Notice that the Christoffel symbols of the first kind are symmetric in their first two indices. Christoffel symbols of the second kind, which appear in the covariant derivative, are defined

$$\Gamma^\delta_{\alpha\beta} = a^{\delta\gamma}\Gamma_{\alpha\beta\gamma}. \tag{A.34}$$

Notice that Christoffel symbols of the second kind are symmetric in their bottom two indices. In the literature, the term Christoffel symbol is often meant to mean the Christoffel symbol of the second kind.

From equation A.33, we see that partial derivatives of the metric tensor can be expressed in terms of Christoffel symbols,

$$\frac{\partial a_{\alpha\beta}}{\partial u^\gamma} = \Gamma_{\gamma\alpha\beta} + \Gamma_{\gamma\beta\alpha} = a_{\beta\nu}\Gamma^\nu_{\gamma\alpha} + a_{\alpha\nu}\Gamma^\nu_{\gamma\beta}. \tag{A.35}$$

This equation is useful for computing partial derivatives of the determinant of the metric tensor.

Using an argument very similar to the one shown in equation A.23 and using equation A.35, we have

$$\begin{aligned}\frac{\partial a}{\partial u^\gamma} &= a a^{\alpha\beta}\frac{\partial a_{\alpha\beta}}{\partial u^\gamma} \\ &= a a^{\alpha\beta}\left(a_{\beta\nu}\Gamma^\nu_{\gamma\alpha} + a_{\alpha\nu}\Gamma^\nu_{\gamma\beta}\right) \\ &= a\left(\delta^\alpha_\nu\Gamma^\nu_{\gamma\alpha} + \delta^\beta{}_\nu\Gamma^\nu_{\gamma\beta}\right) \\ &= a\left(\Gamma^\alpha_{\gamma\alpha} + \Gamma^\beta_{\gamma\beta}\right) \\ &= 2a\Gamma^\alpha_{\gamma\alpha}.\end{aligned} \tag{A.36}$$

Thus

$$\frac{1}{\sqrt{a}}\frac{\partial\sqrt{a}}{\partial u^\gamma} = \Gamma^\alpha_{\gamma\alpha}. \tag{A.37}$$

This equation is important when carrying out integration by parts.

To find the time derivative of the mean curvature, it is necessary to calculate partial derivatives of the inverse metric tensor. Using $a^{\alpha\mu}a_{\mu\gamma} = \delta^\gamma_\alpha$ and equation A.35, it follows that

$$\begin{aligned}\frac{\partial}{\partial u^\lambda}(a^{\alpha\mu})a_{\mu\gamma} &= -a^{\alpha\mu}\frac{\partial}{\partial u^\lambda}(a_{\mu\gamma}) \\ \Rightarrow \frac{\partial}{\partial u^\lambda}(a^{\alpha\mu})a_{\mu\gamma} &= -a^{\alpha\mu}\left(\Gamma_{\lambda\mu\gamma} + \Gamma_{\lambda\gamma\mu}\right) \\ \Rightarrow \frac{\partial}{\partial u^\lambda}(a^{\alpha\mu})a_{\mu\gamma} &= -a^{\alpha\mu}\Gamma_{\lambda\mu\gamma} - \Gamma^\alpha_{\lambda\gamma} \\ \Rightarrow \frac{\partial}{\partial u^\lambda}(a^{\alpha\mu})a_{\mu\gamma}a^{\gamma\beta} &= -a^{\alpha\mu}\Gamma^\beta_{\lambda\mu} - a^{\gamma\beta}\Gamma^\alpha_{\lambda\gamma} \\ \Rightarrow \frac{\partial}{\partial u^\lambda}(a^{\alpha\beta}) &= -a^{\alpha\mu}\Gamma^\beta_{\lambda\mu} - a^{\mu\beta}\Gamma^\alpha_{\lambda\mu}.\end{aligned} \tag{A.38}$$

A.6 Integration by Parts

In this appendix, we show the details of one integration by parts. Other integrations used in the manuscript are not shown explicitly, but involve similar machinations. Consider the expression

$$\int du^1 du^2\sqrt{a}\; T^{\alpha\beta}\nabla_a v_\beta. \tag{A.39}$$

Carrying out integration parts (and using a comma to denote partial derivative where convenient) yields

$$\begin{aligned}&\int du^1 du^2\sqrt{a}\; T^{\alpha\beta}\nabla_a v_\beta \\ &= \int du^1 du^2\sqrt{a}\; T^{\alpha\beta}\left(\frac{\partial v_\beta}{\partial u^\alpha} - v_\nu\Gamma^\nu_{\alpha\beta}\right) \\ &= -\int du^1 du^2\sqrt{a}\left[\left(\frac{(\sqrt{a}T^{\alpha\beta})_{,\alpha}}{\sqrt{a}}\right)v_\beta + T^{\alpha\beta}v_\nu\Gamma^\nu_{\alpha\beta}\right] + \text{ boundary terms (b.t.)}\end{aligned}$$

$$
\begin{aligned}
&= -\int du^1 du^2 \sqrt{a}\left[\left(T^{\alpha\beta}{}_{,\alpha} + T^{\alpha\beta}\Gamma^{\nu}_{\nu\alpha}\right) v_\beta + T^{\alpha\beta} v_\nu \Gamma^{\nu}_{\alpha\beta}\right] + \text{ b.t.} \\
&= -\int du^1 du^2 \sqrt{a}\left[\left(T^{\alpha\beta}{}_{,\alpha} + T^{\nu\beta}\Gamma^{\alpha}_{\alpha\nu} + T^{\alpha\nu}\Gamma^{\beta}_{\nu\alpha} - T^{\alpha\nu}\Gamma^{\beta}_{\nu\alpha}\right) v_\beta + T^{\alpha\beta} v_\nu \Gamma^{\nu}_{\alpha\beta}\right] + \text{ b.t.} \quad \text{(A.40)} \\
&= -\int du^1 du^2 \sqrt{a}\ \nabla_\alpha (T^{\alpha\beta}) v_\beta + \text{ b.t.},
\end{aligned}
$$

where we have permuted indices to use the fact that $T^{\alpha\nu}\Gamma^{\beta}_{\nu\alpha} v_\beta = T^{\alpha\beta} v_\nu \Gamma^{\nu}_{\alpha\beta}$.

A.7 Coordinate Transformations

Let $\{u^\alpha\}, \alpha = 1, 2$ be some set of coordinates and $\{\bar{u}^\alpha\}, \alpha = 1, 2$ be some other set of coordinates. Suppose the two coordinates are related via

$$
u^\alpha = u^\alpha(\bar{u}^1, \bar{u}^2) \text{ and } \bar{u}^\alpha = \bar{u}^\alpha(u^1, u^2). \tag{A.41}
$$

Consider the tangent vector $\mathbf{w}$. Using contravariant components, we have

$$
\begin{aligned}
w^\alpha \mathbf{t}_\alpha &= w^\alpha \frac{\partial \mathbf{r}}{\partial u^\alpha} \\
&= w^\alpha \frac{\partial \mathbf{r}}{\partial \bar{u}^\gamma} \frac{\partial \bar{u}^\gamma}{\partial u^\alpha} \\
&= w^\alpha \frac{\partial \bar{u}^\gamma}{\partial u^\alpha} \bar{\mathbf{t}}_\gamma \\
&= \bar{w}^\gamma \bar{\mathbf{t}}_\gamma,
\end{aligned} \tag{A.42}
$$

where

$$
\bar{w}^\gamma = \frac{\partial \bar{u}^\gamma}{\partial u^\alpha} w^\alpha. \tag{A.43}
$$

Equation A.43 gives the contravariant transformation rule. Using covariant components,

$$
\begin{aligned}
w_\beta \mathbf{t}^\beta &= w_\beta a^{\beta\gamma} \mathbf{t}_\gamma \\
&= w_\beta \frac{\partial u^\beta}{\partial \bar{u}^\lambda} \frac{\partial u^\gamma}{\partial \bar{u}^\mu} \bar{a}^{\lambda\mu} \frac{\partial \mathbf{r}}{\partial \bar{u}^\eta} \frac{\partial \bar{u}^\eta}{\partial u^\gamma} \\
&= w_\beta \frac{\partial u^\beta}{\partial \bar{u}^\lambda} \frac{\partial u^\gamma}{\partial \bar{u}^\mu} \frac{\partial \bar{u}^\eta}{\partial u^\gamma} \bar{a}^{\lambda\mu} \bar{\mathbf{t}}_\eta \\
&= w_\beta \frac{\partial u^\beta}{\partial \bar{u}^\lambda} \delta^\eta_\mu \bar{a}^{\lambda\mu} \bar{\mathbf{t}}_\eta \\
&= w_\beta \frac{\partial u^\beta}{\partial \bar{u}^\lambda} \bar{\mathbf{t}}^\lambda \\
&= \bar{w}_\lambda \bar{\mathbf{t}}^\lambda,
\end{aligned} \tag{A.44}
$$

where

$$
\bar{w}_\lambda = w_\beta \frac{\partial u^\beta}{\partial \bar{u}^\lambda}. \tag{A.45}
$$

Equation A.45 gives the covariant transformation rule.

The covariant and contravariant transformation rules can be combined together (as was done in equation A.44) to give transformation rules for higher order covariant, contravariant, and mixed tensors.

APPENDIX B

CALCULATIONS TO SUPPLEMENT CHAPTER 3

B.1 Monge Parametrization

In this section, we present many of the background calculations necessary to derive the Monge Parametrization form of the two phase fluid equations. We show most calculations for the sphingolipid phase. Similar results exist for the glycerolipid phase.

B.1.1 Christoffel Symbols and Covariant Derivatives

Using equation A.33, we calculate the Christoffel symbols of the first kind to be

$$\Gamma_{\alpha\beta x} = h_x \begin{pmatrix} h_{xx} & h_{xy} \\ h_{xy} & h_{yy} \end{pmatrix} \tag{B.1}$$

and

$$\Gamma_{\alpha\beta y} = h_y \begin{pmatrix} h_{xx} & h_{xy} \\ h_{xy} & h_{yy} \end{pmatrix}. \tag{B.2}$$

Using equation A.34, we find that the Christoffel symbols of the second kind are

$$\Gamma^x_{\alpha\beta} = \frac{h_x}{a} \begin{pmatrix} h_{xx} & h_{xy} \\ h_{xy} & h_{yy} \end{pmatrix} \tag{B.3}$$

and

$$\Gamma^y_{\alpha\beta} = \frac{h_y}{a} \begin{pmatrix} h_{xx} & h_{xy} \\ h_{xy} & h_{yy} \end{pmatrix}. \tag{B.4}$$

Using the Christoffel symbols of the second kind, we calculate the components of the covariant derivative of contravariant vector components to be

$$\nabla_\alpha v^\beta = \begin{pmatrix} \frac{\partial v^x}{\partial x} + \frac{h_x}{a}(v^x h_{xx} + v^y h_{xy}) & \frac{\partial v^y}{\partial x} + \frac{h_y}{a}(v^x h_{xx} + v^y h_{xy}) \\ \frac{\partial v^x}{\partial y} + \frac{h_x}{a}(v^x h_{xy} + v^y h_{yy}) & \frac{\partial v^y}{\partial y} + \frac{h_y}{a}(v^x h_{xy} + v^y h_{yy}) \end{pmatrix}. \tag{B.5}$$

B.1.2 Surface Dilation

Using equations 3.13–3.15, we can calculate

$$\begin{aligned}\nabla_\alpha U^\alpha = &\frac{h_{xx}h_t + h_x h_{xt} + h_{yy}h_t + h_y h_{yt}}{a} \\ &- \frac{h_x h_t(h_x h_{xx} + h_y h_{xy}) + h_y h_t(h_x h_{xy} + h_y h_{yy})}{a^2}\end{aligned} \tag{B.6}$$

and

$$2HU_n = \frac{h_{xx}(1+h_y^2) + h_{yy}(1+h_x^2) - 2h_x h_y h_{xy}}{a^2} h_t \tag{B.7}$$

so that

$$\nabla_\alpha U^\alpha - 2HU_n = \frac{h_x h_{xt} + h_y h_{yt}}{a}. \tag{B.8}$$

It follows that the surface dilation is given by

$$\begin{aligned}a^{\alpha\beta}S_{\alpha\beta} &= \nabla_\alpha v^\alpha + \nabla_\alpha U^\alpha - 2HU_n \\ &= \frac{\partial v^x}{\partial x} + \frac{h_x}{a}(v^x h_{xx} + v^y h_{xy} + h_{xt}) + \frac{\partial v^y}{\partial y} + \frac{h_y}{a}(v^x h_{xy} + v^y h_{yy} + h_{yt}) \\ &= d_v.\end{aligned} \tag{B.9}$$

B.1.3 Tangential Force Balance Terms

B.1.3.1 Divergence of the Stress Tensor

The stress tensor is given by

$$\begin{aligned}T^{\alpha\beta} &= \eta a^{\alpha\beta}a^{\lambda\mu}S_{\lambda\mu} + \epsilon\left(a^{\alpha\lambda}a^{\beta\mu} + a^{\alpha\mu}a^{\beta\lambda} - a^{\alpha\beta}a^{\lambda\mu}\right)S_{\lambda\mu} \\ &= (\eta+\epsilon)a^{\alpha\beta}a^{\lambda\mu}S_{\lambda\mu} + 2\epsilon\left(S^{\alpha\beta} - a^{\alpha\beta}a^{\lambda\mu}S_{\lambda\mu}\right),\end{aligned} \tag{B.10}$$

where

$$S^{\alpha\beta} = \frac{1}{2}\left(a^{\alpha\lambda}\nabla_\lambda v^\beta + a^{\beta\mu}\nabla_\mu v^\alpha + a^{\alpha\lambda}\nabla_\lambda v^\beta + a^{\beta\mu}\nabla_\mu v^\alpha - 2b^{\alpha\beta}U_n\right). \tag{B.11}$$

We can calculate the components of $S^{\alpha\beta}$ to be

$$\begin{aligned}S^{xx} = &\frac{1+h_y^2}{a}\left(\frac{\partial v^x}{\partial x} + \frac{h_x}{a}\left(v^x h_{xx} + v^y h_{yy} + h_{xt}\right)\right) \\ &- \frac{h_x h_y}{a}\left(\frac{\partial v^y}{\partial y} + \frac{h_x}{a}\left(v^x h_{xy} + v^y h_{yy} + h_{yt}\right)\right),\end{aligned} \tag{B.12}$$

$$
\begin{aligned}
S^{xy} = S^{yx} = \frac{1}{2}\Bigg[& \frac{1+h_y^2}{a}\left(\frac{\partial v^y}{\partial x} + \frac{h_y}{a}\left(v^x h_{xx} + v^y h_{xh} + h_{xt}\right)\right) \\
& + \frac{1+h_x^2}{a}\left(\frac{\partial v^x}{\partial y} + \frac{h_x}{a}\left(v^x h_{xy} + v^y h_{yy} + h_{yt}\right)\right) \\
& - \frac{h_x h_y}{a}\left(\frac{\partial v^x}{\partial x} + \frac{h_x}{a}\left(v^x h_{xx} + v^y h_{xy} + h_{xt}\right)\right. \\
& \left. + \frac{\partial v^y}{\partial y} + \frac{h_y}{a}\left(v^x h_{xy} + v^y h_{yy} + h_{yt}\right)\right)\Bigg],
\end{aligned}
\tag{B.13}
$$

and

$$
\begin{aligned}
S^{yy} = & \frac{1+h_x^2}{a}\left(\frac{\partial v^y}{\partial y} + \frac{h_y}{a}\left(v^x h_{xy} + v^y h_{yy} + h_{yt}\right)\right) \\
& - \frac{h_x h_y}{a}\left(\frac{\partial v^y}{\partial x} + \frac{h_y}{a}\left(v^x h_{xx} + v^y h_{xy} + h_{xt}\right)\right).
\end{aligned}
\tag{B.14}
$$

This yields the components of $T^{\alpha\beta}$:

$$
\begin{aligned}
T^{xx} = & \frac{(\eta+\epsilon)(1+h_y^2)}{a} d_v \\
& - \frac{2\epsilon}{a}\left(h_x h_y \frac{\partial v^x}{\partial y} + (1+h_y^2)\frac{\partial v^y}{\partial y} + h_y h_{xy} v^x + h_y h_{yy} v^y + h_y h_{yt}\right),
\end{aligned}
\tag{B.15}
$$

$$
\begin{aligned}
T^{xy} = T^{yx} = & -\frac{(\eta+\epsilon)h_x h_y}{a} d_v \\
& + \frac{\epsilon}{a}\Bigg[h_x h_y\left(\frac{\partial v^x}{\partial x} + \frac{\partial v^y}{\partial y}\right) + (1+h_x^2)\frac{\partial v^x}{\partial y} + (1+h_y^2)\frac{\partial v^y}{\partial x} \\
& + (h_y h_{xx} + h_x h_{xy})v^x + (h_x h_{yy} + h_y h_{xy})v^y + h_y h_{xt} + h_x h_{yt}\Bigg],
\end{aligned}
\tag{B.16}
$$

and

$$
\begin{aligned}
T^{yy} = & \frac{(\eta+\epsilon)(1+h_x^2)}{a} d_v \\
& - \frac{2\epsilon}{a}\left(h_x h_y \frac{\partial v^y}{\partial x} + (1+h_x^2)\frac{\partial v^x}{\partial x} + h_x h_{xx} v^x + h_x h_{xy} v^y + h_x h_{xt}\right).
\end{aligned}
\tag{B.17}
$$

Using equation 2.17, we have

$$
\begin{aligned}
\nabla_\alpha T^{\alpha x} = & \frac{\partial}{\partial x} T^{xx} + \frac{\partial}{\partial y} T^{xy} \\
& + \frac{1}{a}\left[T^{xx}(2h_x h_{xx} + h_y h_{xy}) + T^{xy}(3h_x h_{xy} + h_y h_{yy}) + T^{yy} h_x h_{yy}\right]
\end{aligned}
\tag{B.18}
$$

and

$$
\begin{aligned}
\nabla_\alpha T^{\alpha y} = & \frac{\partial}{\partial x} T^{xy} + \frac{\partial}{\partial y} T^{yy} \\
& + \frac{1}{a}\left[T^{xx} h_y h_{xx} + T^{xy}(h_x h_{xx} + 3h_y h_{xy}) + T^{yy}(h_x h_{xy} + 2h_y h_{yy})\right].
\end{aligned}
\tag{B.19}
$$

Define

$$\tilde{T}^{\alpha\beta} = aT^{\alpha\beta}. \tag{B.20}$$

The terms that appear in the tangential force balance equations can be expressed as

$$\begin{aligned}\nabla_\alpha(T^{\alpha x}\theta_s) = &\frac{1}{a}\frac{\partial}{\partial x}\left(\tilde{T}^{xx}\theta_s\right) + \frac{1}{a}\frac{\partial}{\partial y}\left(\tilde{T}^{xy}\theta_s\right) \\ &- \frac{\theta_s}{a^2}\left(\tilde{T}^{xx}h_y h_{xy} - \tilde{T}^{xy}(h_x h_{xy} - h_y h_{yy}) - \tilde{T}^{yy}h_x h_{yy}\right)\end{aligned} \tag{B.21}$$

and

$$\begin{aligned}\nabla_\alpha\left(\tilde{T}^{\alpha y}\right) = &\frac{1}{a}\frac{\partial}{\partial x}\left(\tilde{T}^{xy}\theta_s\right) + \frac{1}{a}\frac{\partial}{\partial y}\left(\tilde{T}^{yy}\theta_s\right) \\ &+ \frac{\theta_s}{a^2}\left(\tilde{T}^{xx}h_y h_{xx} - \tilde{T}^{xy}(h_x h_{xx} - h_y h_{xy}) - \tilde{T}^{yy}h_x h_{xy}\right).\end{aligned} \tag{B.22}$$

B.1.3.2 Surface Laplacian

The surface Laplacian appears in both the tangential and normal force balance equations. Suppose g is some scalar function. We calculate the surface Laplacian of g to be

$$\begin{aligned}a^{\alpha\beta}\nabla_\alpha\nabla_\beta g = \frac{1}{a}\big\{&(1+h_y^2)g_{xx} - 2h_x h_y g_{xy} + (1+h_x^2)g_{yy} \\ &+ (g_x h_x + g_y h_y)\left[(1+h_y^2)h_{xx} - 2h_x h_y h_{xy} + (1+h_x^2)h_{yy}\right]\big\}.\end{aligned} \tag{B.23}$$

B.1.4 Normal Force Balance Terms

B.1.4.1 Contraction of Stress and Curvature Tensors

The contraction of the stress and curvature tensors that appears in the normal force balance equation is given by

$$\begin{aligned}T^{\alpha\beta}b_{\alpha\beta} &= \left[(\eta+\epsilon)a^{\alpha\beta}a^{\lambda\mu}S_{\lambda\mu} + 2\epsilon\left(S^{\alpha\beta} - a^{\alpha\beta}a^{\lambda\mu}S_{\lambda\mu}\right)\right]b_{\alpha\beta} \\ &= (\eta+\epsilon)(2H)\left(a^{\lambda\mu}S_{\lambda\mu}\right) + 2\epsilon\left[S^{\alpha\beta}b_{\alpha\beta} - (2H)\left(a^{\lambda\mu}S_{\lambda\mu}\right)\right].\end{aligned} \tag{B.24}$$

We calculate that $S^{\alpha\beta}b_{\alpha\beta}$ is given by

$$\begin{aligned}S^{\alpha\beta}b_{\alpha\beta} = \frac{1}{a^{3/2}}\Bigg\{&\left[h_{xx}(1+h_y^2) - h_x h_y h_{xy}\right]\left[\frac{\partial v^x}{\partial x} + \frac{h_x}{a}\left(v^x h_{xx} + v^y h_{xy} + h_{xt}\right)\right] \\ &+ \left[h_{xy}(1+h_y^2) - h_x h_y h_{yy}\right]\left[\frac{\partial v^y}{\partial x} + \frac{h_y}{a}\left(v^x h_{xx} + v^y h_{xy} + h_{xt}\right)\right] \\ &+ \left[h_{xy}(1+h_x^2) - h_x h_y h_{xx}\right]\left[\frac{\partial v^x}{\partial y} + \frac{h_x}{a}\left(v^x h_{xy} + v^y h_{yy} + h_{yt}\right)\right] \\ &+ \left[h_{yy}(1+h_x^2) - h_x h_y h_{xy}\right]\left[\frac{\partial v^y}{\partial y} + \frac{h_y}{a}\left(v^x h_{xy} + v^y h_{yy} + h_{yt}\right)\right]\Bigg\}\end{aligned} \tag{B.25}$$

so that

$$
\begin{aligned}
&S^{\alpha\beta}b_{\alpha\beta} - 2Ha^{\lambda\mu}S_{\lambda\mu} \\
&= \frac{1}{a^{3/2}}\left\{\left[h_{xy}(1+h_y^2) - h_x h_y h_{yy}\right]\left[\frac{\partial v^y}{\partial x} + \frac{h_y}{a}\left(v^x h_{xx} + v^y h_{xy} + h_{xt}\right)\right]\right. \\
&\left. + \left[h_{xy}(1+h_x^2) - h_x h_y h_{xx}\right]\left[\frac{\partial v^x}{\partial y} + \frac{h_x}{a}\left(v^x h_{xy} + v^y h_{yy} + h_{yt}\right)\right]\right\}
\end{aligned} \tag{B.26}
$$

and

$$
\begin{aligned}
T^{\alpha\beta}b_{\alpha\beta} &= (\eta+\epsilon)(2H)d_v \\
&+ \frac{2\epsilon}{a^{3/2}}\left\{\left[h_{xy}(1+h_y^2) - h_x h_y h_{yy}\right]\left[\frac{\partial v^y}{\partial x} + \frac{h_y}{a}\left(v^x h_{xx} + v^y h_{xy} + h_{xt}\right)\right]\right. \\
&\left. + \left[h_{xy}(1+h_x^2) - h_x h_y h_{xx}\right]\left[\frac{\partial v^x}{\partial y} + \frac{h_x}{a}\left(v^x h_{xy} + v^y h_{yy} + h_{yt}\right)\right]\right\}.
\end{aligned} \tag{B.27}
$$

B.1.4.2 Cahn–Hilliard Penalty Terms

The Cahn–Hilliard penalty term for a scalar function g is given by

$$
a^{\alpha\beta}\nabla_\alpha g \nabla_\beta g = \frac{1}{a}\left[\left(1+h_y^2\right)\left(\frac{\partial g}{\partial x}\right)^2 - 2h_x h_y \frac{\partial g}{\partial x}\frac{\partial g}{\partial y} + \left(1+h_x^2\right)\left(\frac{\partial g}{\partial y}\right)^2\right]. \tag{B.28}
$$

B.2 Axisymmetric Parametrization

In this section, we present many of the background calculations necessary to derive and analyze the axisymmetric parametrization form of the two phase fluid equations. We show most calculations for the sphingolipid phase. Similar results exist for the glycerolipid phase.

B.2.1 Christoffel Symbols and Covariant Derivatives

Using equation A.33, we calculate the Christoffel symbols of the first kind to be

$$
\Gamma_{uuu} = pp', \tag{B.29}
$$

$$
\Gamma_{u\theta\theta} = \Gamma_{\theta u\theta} = xx', \tag{B.30}
$$

$$
\Gamma_{\theta\theta u} = -xx', \tag{B.31}
$$

and

$$
\Gamma_{uu\theta} = \Gamma_{u\theta u} = \Gamma_{\theta uu} = \Gamma_{\theta\theta\theta} = 0, \tag{B.32}
$$

where the prime notation indicates a derivative with respect to u.

Using equation A.34, the Christoffel symbols of the second kind are given by

$$\Gamma^{u}_{\alpha\beta} = \begin{pmatrix} \frac{p'}{p} & 0 \\ 0 & -\frac{xx'}{p^2} \end{pmatrix} \tag{B.33}$$

and

$$\Gamma^{\theta}_{\alpha\beta} = \begin{pmatrix} 0 & \frac{x'}{x} \\ \frac{x'}{x} & 0 \end{pmatrix}. \tag{B.34}$$

Using these definitions, and under the assumption that $\frac{\partial v^\alpha}{\partial \theta} = 0$, we calculate the covariant derivative of contravariant vector components to be

$$\nabla_\alpha v^\beta = \begin{pmatrix} \frac{(v^u p)'}{p} & \frac{(v^\theta x)'}{x} \\ -\frac{v^\theta x x'}{p^2} & \frac{v^u x'}{x} \end{pmatrix}. \tag{B.35}$$

B.2.2 Surface Dilation

We calculate

$$\nabla_\alpha v^\alpha = v^{u\prime} + v^u \left(\frac{p'}{p} + \frac{x'}{x} \right), \tag{B.36}$$

so the local surface dilation is given by

$$\begin{aligned} a^{\alpha\beta} S_{\alpha\beta} &= \nabla_\alpha v^\alpha - 2HU_n \\ &= v^{u\prime} + v^u \left(\frac{p'}{p} + \frac{x'}{x} \right) - \left(\frac{q}{p^3} + \frac{z'}{px} \right) U_n \\ &= d_v. \end{aligned} \tag{B.37}$$

B.2.3 Tangential Force Balance Terms

B.2.3.1 Divergence of the Stress Tensor

The stress tensor is defined as

$$\begin{aligned} T^{\alpha\beta} &= \eta a^{\alpha\beta} a^{\lambda\mu} S_{\lambda\mu} + \epsilon (a^{\alpha\lambda} a^{\beta\mu} + a^{\alpha\mu} a^{\beta\lambda} - a^{\alpha\beta} a^{\lambda\mu}) S_{\lambda\mu} \\ &= (\eta + \epsilon) a^{\alpha\beta} a^{\lambda\mu} S_{\lambda\mu} + 2\epsilon (s^{\alpha\beta} - a^{\alpha\beta} a^{\lambda\mu}) S_{\lambda\mu}, \end{aligned} \tag{B.38}$$

where

$$S^{\alpha\beta} = \frac{1}{2} \left(a^{\alpha\lambda} \nabla_\lambda v^\beta + a^{\beta\mu} \nabla_\mu v^\alpha - 2 b^{\alpha\beta} U_n \right). \tag{B.39}$$

Using the definitions of $\nabla_\alpha v^\beta, a^{\alpha\beta}$, and $b^{\alpha\beta}$, we find that

$$S^{\alpha\beta} = \begin{pmatrix} \dfrac{(v^u p)'}{p^3} - \dfrac{q}{p^5} U_n & \dfrac{v^{\theta'}}{2p^2} \\ \dfrac{v^{\theta'}}{2p^2} & \dfrac{v^u x'}{x^3} - \dfrac{z'}{px^3} U_n \end{pmatrix}. \tag{B.40}$$

This yields the components of $T^{\alpha\beta}$ to be

$$T^{uu} = \frac{\eta + \epsilon}{p^2} d_v - \frac{2\epsilon}{p^2} \left(v^u \frac{x'}{x} - \frac{z'}{px} U_n \right), \tag{B.41}$$

$$T^{u\theta} = T^{\theta u} = \frac{\epsilon}{p^2} v^{\theta'}, \tag{B.42}$$

and

$$T^{\theta\theta} = \frac{\eta + \epsilon}{x^2} d_v - \frac{2\epsilon}{x^2} \left(v^{u\prime} + v^u \frac{p'}{p} - \frac{q}{p^3} U_n \right). \tag{B.43}$$

Using equation 2.17, we have

$$\nabla_\alpha T^{\alpha\beta} = \frac{\partial}{\partial u} T^{u\beta} + T^{u\beta} \left(\frac{p'}{p} + \frac{x'}{x} \right) + T^{uu} \Gamma^\beta_{uu} + 2T^{u\theta} \Gamma^\beta_{u\theta} + T^{\theta\theta} \Gamma^\beta_{\theta\theta}, \tag{B.44}$$

so then

$$\begin{aligned} \nabla_\alpha T^{\alpha u} =& \frac{\eta + \epsilon}{p^2} d_v' \\ &+ \frac{2\epsilon}{p^2} \left[-v^u \left(\frac{p}{x} \right) \left(\frac{x'}{p} \right)' + \left(\frac{1}{x} \right) \left(\frac{z' U_n}{p} \right)' - \frac{q x'}{p^3 x} U_n \right] \end{aligned} \tag{B.45}$$

and

$$\nabla_\alpha T^{\alpha\theta} = \frac{\epsilon}{p^2} \left[v^{\theta\prime\prime} + v^{\theta'} \left(\frac{3x'}{x} - \frac{p'}{p} \right) \right]. \tag{B.46}$$

The terms that appear in the tangential force balance equations can be expressed as

$$\begin{aligned} \nabla_\alpha \left(T^{\alpha\beta} \theta_s \right) =& \frac{\eta + \epsilon}{p^2} \left\{ \theta_s d_v \right\}' \\ &+ \frac{2\epsilon}{p^2} \left[-v^u \left(\frac{p}{x} \right) \left(\frac{x' \theta_s}{p} \right)' + \left(\frac{1}{x} \right) \left(\frac{z' \theta_s U_n}{p} \right)' - \frac{\theta_s q x'}{p^3 x} U_n \right] \end{aligned} \tag{B.47}$$

and

$$\nabla_\alpha \left(T^{\alpha\theta} \theta_s \right) = \frac{\epsilon}{p^2} \left\{ \left[\theta_s v^{\theta'} \right]' + \theta_s v^{\theta'} \left(\frac{3x'}{x} - \frac{p'}{p} \right) \right\}. \tag{B.48}$$

B.2.3.2 Surface Laplacian

The surface Laplacian appears in both the tangential and normal force balance equations. Suppose g is some scalar function. We calculate the surface Laplacan of g to be

$$a^{\alpha\beta} \nabla_\alpha \nabla_\beta g = \frac{1}{p^2} \left(g'' - g' \left(\frac{p'}{p} - \frac{x'}{x} \right) \right). \tag{B.49}$$

B.2.4 Normal Force Balance Components

B.2.4.1 Contraction of Stress and Curvature Tensors

The contraction of the stress and curvature tensors that appears in the normal force balance equation is given by

$$\begin{aligned} T^{\alpha\beta}b_{\alpha\beta} &= T^{uu}b_{uu} + T^{\theta\theta}b_{\theta\theta} \\ &= (\eta+\epsilon)(2H)d_v \\ &- \frac{2\epsilon}{p^2}\left[v^u\left(\frac{qx'}{px}\right) + \left(\frac{z'}{x}\right)(pv^u)' - \frac{2qz'}{p^2x}U_n\right]. \end{aligned} \tag{B.50}$$

B.2.4.2 Cahn–Hilliard Penalty terms

The Cahn–Hilliard penalty term for a scalar function g is given by

$$a^{\alpha\beta}\nabla_\alpha g \nabla_\beta g = \frac{1}{p^2}\left(g'\right)^2. \tag{B.51}$$

B.2.5 Simplifications to the First Order System

After substituting the perturbations 3.100–3.109 into the full system 3.70–3.78, we use the following identities to arrive at the system 3.110–3.116:

$$\frac{x_0''}{x_0} = \frac{-p_0\pi/L\sin(\pi u/L)}{p_0L/\pi\sin(\pi u/L)} = -\left(\frac{\pi}{L}\right)^2, \tag{B.52}$$

$$\frac{z_0''}{p_0x_0} = \frac{p_0\pi/L\cos(\pi u/L)}{p_0^2L/\pi\sin(\pi u/L)} = \frac{\pi^2}{L^2p_0}\cot\left(\frac{\pi}{L}u\right), \tag{B.53}$$

$$\frac{z_0'}{p_0x_0} = \frac{p_0\sin(\pi u/L)}{p_0^2L/\pi\sin(\pi u/L)} = \frac{\pi}{Lp_0} = H_0, \tag{B.54}$$

$$\frac{q_0x_0'}{p_0^3x_0} = \frac{p_0^3\pi/L\cos(\pi u/L)}{p_0^4L/\pi\sin(\pi u/L)} = \frac{\pi^2}{L^2p_0}\cot\left(\frac{\pi}{L}u\right), \tag{B.55}$$

$$\frac{q_0x_0'}{p_0x_0} = \frac{p_0^3\pi/L\cos(\pi u/L)}{p_0^2L/\pi\sin(\pi u/L)} = \frac{p_0\pi^2}{L^2}\cot\left(\frac{\pi}{L}u\right), \tag{B.56}$$

$$\frac{p_0z_0'}{x_0} = \frac{p_0^2\sin(\pi u/L)}{p_0L/\pi\sin(\pi u/L)} = \frac{p_0\pi}{L}, \tag{B.57}$$

$$\frac{q_0z_0'}{p_0^2x_0} = \frac{p_0^3\pi/L\sin(\pi u/L)}{p_0^3L/\pi\sin(\pi u/L)} = \left(\frac{\pi}{L}\right)^2, \tag{B.58}$$

and

$$\frac{x_0'}{x_0} = \frac{p_0 \cos(\pi u/L)}{p_0 L/\pi \sin(\pi u/L)} = \frac{\pi}{L} \cot\left(\frac{\pi}{L} u\right). \tag{B.59}$$

Further, in terms of principle curvature C_1 and C_2, we have $H = \frac{1}{2}(C_1 + C_2)$ and $K = C_1 C_2$. Letting $C_1 = C_{1_0} + \lambda C_{1_1}$ and $C_2 = C_{2_0} + \lambda C_{2_1}$, the expression $2H_0H_1 - K_1$ is given by

$$\begin{aligned} 2H_0H_1 - K_1 &= \frac{1}{2}\left(C_{1_0} + C_{2_0}\right)\left(C_{1_1} + C_{2_1}\right) - \left(C_{1_0}C_{2_1} + C_{2_0}C_{1_1}\right) \\ &= \frac{1}{2}\left(C_{1_0} - C_{2_0}\right)\left(C_{1_1} - C_{2_1}\right). \end{aligned} \tag{B.60}$$

Now, if the equilibrium shape is a sphere, $C_{1_0} = C_{2_0}$ so that $2H_0H_1 - K_1 = 0$. Thus the expression $(4H_0H_1 - K_1)f_{H_0}$, which appears in the normal force balance equation upon substitution of the perturbed steady state values, can be replaced with $2H_0H_1 f_{H_0}$.

REFERENCES

[1] T. C. Anglin and J. C. Conboy, *Lateral pressure dependence of the phospholipid transmembrane diffusion rate in planar-supported lipid bilayers*, Biophys. J., 95 (2008), pp. 186–193.

[2] R. Aris, *Vectors, Tensors, and the Basic Equations of Fluid Mechanics*, Courier Dover Publications, Mineola, NY, 1989.

[3] M. Arroyo and A. DeSimone, *Relaxation dynamics of fluid membranes*, Phys. Rev. E, 79 (2009), p. 031915.

[4] M. Babst, *MVB vesicle formation: ESCRT-dependent, ESCRT-independent and everything in between*, Curr. Opin. Cell Biol., 23 (2011), pp. 452–457.

[5] L. A. Bagatolli, J. H. Ipsen, A. C. Simonsen, and O. G. Mouritsen, *An outlook on organization of lipids in membranes: Searching for a realistic connection with the organization of biological membranes*, Prog. Lipid Res., 49 (2010), pp. 378–389.

[6] T. Baumgart, S. Hess, and W. Webb, *Imaging coexisting fluid domains in biomembrane models coupling curvature and line tension*, Nature, 425 (2003), pp. 821–824.

[7] G. V. Beznoussenko and A. A. Mironov, *Models of intracellular transport and evolution of the Golgi complex*, Anat. Rec., 268 (2002), pp. 226–238.

[8] K. L. Brown and J. C. Conboy, *Electrostatic induction of lipid asymmetry*, J. Am. Chem. Soc., 133 (2011), pp. 8794–8797.

[9] J. W. Cahn, *Phase separation by spinodal decomposition in isotropic systems*, J. Chem. Phys., 42 (1965), p. 93.

[10] W. Cai and T. C. Lubensky, *Hydrodynamics and dynamic fluctuations of fluid membranes*, Phys. Rev. E, 52 (1995), p. 4251.

[11] P. B. Canham, *The minimum energy of bending as a possible explanation of the biconcave shape of the human red blood cell*, J. Theor. Biol., 26 (1970), pp. 61–81.

[12] J. Derganc, *Curvature-driven lateral segregation of membrane constituents in Golgi cisternae*, Phys. Biol., 4 (2007), pp. 317–324.

[13] M. Deserno, *Notes on differential geometry*, 2004. http://www.cmu.edu/biolphys/deserno/pdf/diff_geom.pdf.

[14] K. A. Dill and S. Bromberg, *Molecular driving forces: Statistical Thermodynamics in Chemistry and Biology*, Garland Science, New York, NY, 2003.

[15] M. Doi, *Introduction to Polymer Physics*, Oxford University Press, Oxford, UK, 1995.

[16] M. Doi, *Onsager's variational principle in soft matter*, J. Phys.: Condens. Matter, 23 (2011), p. 284118.

[17] C. J. Durning and K. N. Morman, *Nonlinear swelling of polymer gels*, J. Chem. Phys., 98 (1993), p. 4275.

[18] K. Farsad and P. D. Camilli, *Mechanisms of membrane deformation*, Curr. Opin. Cell Biol., 15 (2003), pp. 372–381.

[19] P. C. Fife, *Models for phase separation and their mathematics*, Electron J. Diff. Eqns., 48 (2000), pp. 1–26.

[20] A. H. Futerman and Y. A. Hannun, *The complex life of simple sphingolipids*, EMBO Rep., 5 (2004), pp. 777–782.

[21] A. H. Futerman and H. Riezman, *The ins and outs of sphingolipid synthesis*, Trends Cell Biol., 15 (2005), pp. 312–318.

[22] D. T. Gillespie, *Markov Processes: An Introduction for Physical Scientist*, Gulf Professional Publishing, Houston, TX, 1992.

[23] B. Glick and V. Malhotra, *The curious status of the Golgi apparatus*, Cell, 95 (1998), pp. 883–889.

[24] F. M. Goñi, A. Alonso, L. A. Bagatolli, R. E. Brown, D. Marsh, M. Prieto, and J. L. Thewalt, *Phase diagrams of lipid mixtures relevant to the study of membrane rafts*, Biochim. Biophys. Acta, Mol. Cell Biol. Lipids, 1781 (2008), pp. 665–684.

[25] T. R. Graham and M. M. Kozlov, *Interplay of proteins and lipids in generating membrane curvature*, Curr. Opin. Cell Biol., 22 (2010), pp. 430–436.

[26] M. Heinrich, A. Tian, C. Esposito, and T. Baumgart, *Dynamic sorting of lipids and proteins in membrane tubes with a moving phase boundary*, Proc. Natl. Acad. Sci., 107 (2010), pp. 7208–7213.

[27] W. Helfrich, *Elastic properties of lipid bilayers: Theory and possible experiments*, Z. Naturforsch., 28 (1973), pp. 693–703.

[28] J. Holthuis, T. Pomorski, R. Raggers, H. Sprong, and G. van Meer, *The organizing potential of sphingolipids in intracellular membrane transport*, Physiol. Rev., 81 (2001), pp. 1689–1723.

[29] D. Hu, P. Zhang, and W. E, *Continuum theory of a moving membrane*, Phys. Rev. E, 75 (2007), p. 041605.

[30] J. H. Hurley and P. I. Hanson, *Membrane budding and scission by the ESCRT machinery: it's all in the neck*, Nat. Rev. Mol. Cell Biol., 11 (2010), pp. 556–566.

[31] H. Jiang and T. Powers, *Curvature-driven lipid sorting in a membrane tubule*, Phys. Rev. Lett., 101 (2008), p. 018103.

[32] J. P. Keener, *Principles of Applied Mathematics : Transformation and Approximation*, Westview Press, Boulder, CO, 2000.

[33] J. P. Keener, S. Sircar, and A. L. Fogelson, *Kinetics of swelling gels*, SIAM J. Appl. Math., 71 (2011), p. 854.

[34] J. P. Keener and J. Sneyd, *Mathematical Physiology: I: Cellular Physiology*, vol. 1, Springer Verlag, New York, NY, 2008.

[35] M. A. Kol, A. I. P. M. de Kroon, J. A. Killian, and B. De Kruijff, *Transbilayer movement of phospholipids in biogenic membranes*, Biochem., 43 (2004), pp. 2673–2681.

[36] D. Lee, J.-Y. Huh, D. Jeong, J. Shin, A. Yun, and J. Kim, *Physical, mathematical, and numerical derivations of the Cahn–Hilliard equation*, Compu. Mater. Sci., 81 (2014), pp. 216–225.

[37] P. A. Leventis and S. Grinstein, *The distribution and function of phosphatidylserine in cellular membranes*, Annu. Rev. Biophys., 39 (2010), pp. 407–427.

[38] R. J. Leveque, *Finite Volume Methods for Hyperbolic Problems*, Cambridge Texts in Applied Mathematics, Cambridge University Press, Cambridge, UK, 2002.

[39] R. Lipowsky, *Budding of membranes induced by intramembrane domains*, J. Phys. II, 2 (1992), pp. 1825–1840.

[40] J. Liu and J. C. Conboy, *Direct measurement of the transbilayer movement of phospholipids by sum-frequency vibrational spectroscopy*, J. Am. Chem. Soc., 126 (2004), pp. 8376–8377.

[41] ——, *1,2-diacyl-phosphatidylcholine flip-flop measured directly by sum-frequency vibrational spectroscopy*, Biophys. J., 89 (2005), pp. 2522–2532.

[42] J. S. Lowengrub, A. Rätz, and A. Voigt, *Phase-field modeling of the dynamics of multicomponent vesicles: Spinodal decomposition, coarsening, budding, and fission*, Phys. Rev. E, 79 (2009), p. 031926.

[43] D. Marsh, *Elastic curvature constants of lipid monolayers and bilayers*, Chem. Phys. Lipids, 144 (2006), pp. 146–159.

[44] H. Matsuo, *Role of LBPA and Alix in multivesicular liposome formation and endosome organization*, Science, 303 (2004), pp. 531–534.

[45] H. M. McConnell and R. D. Kornberg, *Inside-outside transitions of phospholipids in vesicle membranes*, Biochem., 10 (1971), pp. 1111–1120.

[46] L. Miao, M. A. Lomholt, and J. Kleis, *Dynamics of shape fluctuations of quasi-spherical vesicles revisited*, Eur. Phys. J. E, 9 (2002), pp. 143–160.

[47] H. Pelham, *Getting stuck in the Golgi*, Traffic, 1 (2000), pp. 191–192.

[48] R. Phillips, J. Kondev, and J. Theriot, *Physical Biology of the Cell*, Garland Science, New York, NY, 2008.

[49] T. R. Powers, *Dynamics of filaments and membranes in a viscous fluid*, Rev. Mod. Phys., 82 (2010), pp. 1607–1631.

[50] M. Rahimi and M. Arroyo, *Shape dynamics, lipid hydrodynamics, and the complex viscoelasticity of bilayer membranes*, Phys. Rev. E, 86 (2012), p. 011932.

[51] P. Rangamani, A. Agrawal, K. K. Mandadapu, G. Oster, and D. J. Steigmann, *Interaction between surface shape and intra-surface viscous flow on lipid membranes*, Biomech. Model. Mechanobiol., 12 (2012), pp. 833–845.

[52] C. C. Scott and J. Gruenberg, *Ion flux and the function of endosomes and lysosomes: pH is just the start*, BioEssays, 33 (2010), pp. 103–110.

[53] L. E. Scriven, *Dynamics of a fluid interface equation of motion for newtonian surface fluids*, Chem. Eng. Sci., 12 (1960), pp. 98–108.

[54] U. Seifert, *Curvature-induced lateral phase segregation in two-component vesicles*, Phys. Rev. Lett., 70 (1993), pp. 1335–1338.

[55] U. Seifert, *Configurations of fluid membranes and vesicles*, Adv. Phys., 46 (1997), pp. 13–137.

[56] ——, *Fluid membranes in hydrodynamic flow fields: Formalism and an application to fluctuating quasispherical vesicles in shear flow*, Eur. Phys. J. B, 8 (1999), pp. 405–415.

[57] U. Seifert, K. Berndl, and R. Lipowsky, *Shape transformations of vesicles: Phase diagram for spontaneous-curvature and bilayer-coupling models*, Phys. Rev. A, 44 (1991), p. 1182.

[58] K. Simons and E. Ikonen, *Functional rafts in cell membranes*, Nature, 387 (1997), pp. 569–572.

[59] S. J. Singer and G. L. Nicolson, *The fluid mosaic model of the structure of cell membranes*, Science, New Series, 175 (1972), pp. 720–731.

[60] S. Sircar, J. P. Keener, and A. L. Fogelson, *The effect of divalent vs. monovalent ions on the swelling of mucin-like polyelectrolyte gels: Governing equations and equilibrium analysis*, J. Chem. Phys., 138 (2013), p. 014901.

[61] B. Sorre, A. Callan-Jones, J. Manneville, P. Nassoy, J. Joanny, J. Prost, B. Goud, and P. Bassereau, *Curvature-driven lipid sorting needs proximity to a demixing point and is aided by proteins*, Proc. Natl. Acad. Sci., 106 (2009), p. 5622.

[62] S. Stuffers, C. Sem Wegner, H. Stenmark, and A. Brech, *Multivesicular endosome biogenesis in the absence of ESCRTs*, Traffic, 10 (2009), pp. 925–937.

[63] M. A. Surma, C. Klose, and K. Simons, *Lipid-dependent protein sorting at the trans-Golgi network*, Biochim. Biophys. Acta, Mol. Cell Biol. Lipids, 1821 (2012), pp. 1059–1067.

[64] G. van Meer, *Dynamic transbilayer lipid asymmetry*, Cold Spring Harbor Perspect. Biol., 3 (2011), pp. a004671–a004671.

[65] G. van Meer, D. R. Voelker, and G. W. Feigenson, *Membrane lipids: Where they are and how they behave*, Nat. Rev. Mol. Cell Biol., 9 (2008), pp. 112–124.

[66] M. R. Villarreal, *Phospholipids aqueous solution structures*, 2007. http://upload.wikimedia.org/wikipedia/commons/c/c6/Phospholipids_aqueous_solution_structures.svg#.

[67] G. Voeltz and W. Prinz, *Sheets, ribbons and tubules—How organelles get their shape*, Nat. Rev. Mol. Cell Biol., 8 (2007), pp. 258–264.

[68] C. Wang, Y. Li, and Z. Hu, *Swelling kinetics of polymer gels*, Macromolecules, 30 (1997), pp. 4727–4732.

[69] C. W. Wolgemuth, A. Mogilner, and G. Oster, *The hydration dynamics of polyelectrolyte gels with applications to cell motility and drug delivery*, Eur. Biophys. J., 33 (2004), pp. 146–158.

[70] G. B. Wright, R. D. Guy, J. Du, and A. L. Fogelson, *A high-resolution finite-difference method for simulating two-fluid, viscoelastic gel dynamics*, J. Non-Newtonian Fluid Mech., 166 (2011), pp. 1137–1157.

[71] G. B. Wright, R. D. Guy, and A. L. Fogelson, *An efficient and robust method for simulating two-phase gel dynamics*, SIAM J. Sci. Comput., 30 (2008), p. 2535.

[72] F. Youhei, *Dynamics of the lipid-bilayer membrane taking a vesicle shape*, Phys. A, 203 (1994), pp. 214–242.

[73] O.-Y. Zhong-Can and W. Helfrich, *Bending energy of vesicle membranes: General expressions for the first, second, and third variation of the shape energy and applications to spheres and cylinders*, Phys. Rev. A, 39 (1989), p. 5280.

[74] J. Zimmerberg and M. M. Kozlov, *How proteins produce cellular membrane curvature*, Nat. Rev. Mol. Cell Biol., 7 (2005), pp. 9–19.